University of South Carolina
Scholar Commons

Theses and Dissertations

2017

The Development Of Novel Hybridized Hyaluronic Acid Biomaterials For Applications In Tissue Engineering And Controlled Drug Delivery

Panita Maturavongsadit
University of South Carolina

Follow this and additional works at: https://scholarcommons.sc.edu/etd

Part of the Chemistry Commons

Recommended Citation
Maturavongsadit, P.(2017). *The Development Of Novel Hybridized Hyaluronic Acid Biomaterials For Applications In Tissue Engineering And Controlled Drug Delivery.* (Doctoral dissertation). Retrieved from https://scholarcommons.sc.edu/etd/4380

This Open Access Dissertation is brought to you by Scholar Commons. It has been accepted for inclusion in Theses and Dissertations by an authorized administrator of Scholar Commons. For more information, please contact dillarda@mailbox.sc.edu.

www.manaraa.com

THE DEVELOPMENT OF NOVEL HYBRIDIZED HYALURONIC ACID BIOMATERIALS FOR APPLICATIONS IN TISSUE ENGINEERING AND CONTROLLED DRUG DELIVERY

by

Panita Maturavongsadit

Bachelor of Science
Chulalongkorn University, 2012

Submitted in Partial Fulfillment of the Requirements

For the Degree of Doctor of Philosophy in

Chemistry

College of Arts and Sciences

University of South Carolina

2017

Accepted by:

Qian Wang, Major Professor

Thomas M. Makris, Committee Member

Chuanbing Tang, Committee Member

Peisheng Xu, Committee Member

Cheryl L. Addy, Vice Provost and Dean of the Graduate School

المنارة للاستشارات

www.manaraa.com

© Copyright by Panita Maturavongsadit, 2017
All Rights Reserved.

المنارة للاستشارات
www.manaraa.com

DEDICATION

This dissertation is dedicated to my lovely parents, Songsak and Suwan Maturavongsadit, for their kindness, devotion, and endless support. They have been a source of encouragement and inspiration to me throughout my life.

المنارة للاستشارات
www.manaraa.com

ACKNOWLEDGEMENTS

This dissertation is the outcome of experiences I have encountered at USC from many remarkable individuals who I have supported and helped me so much throughout pursuing Ph.D. I would like to firstly thank my enthusiastic supervisor, Dr. Qian Wang, for giving me so many wonderful opportunities, for encouraging my research and for allowing me to grow as a research scientist. Your advice on both research as well as on my career have been priceless. I would also like to thank my committee members, Dr. Thomas M. Makris, Dr. Chuanbing Tang, Dr. Peisheng Xu and Dr. Rekha Patel for not only serving as my committee members, but also my brilliant mentors. I would especially like to thank my all collaborative advisors, including Dr. Xiangdong Bi from Charleston Southern University, Dr. Qiao Lin from Columbia University (New York), and Dr. Taixing Cui from University of South Carolina School of Medicine for allowing me to learn and broaden my skills, experience and knowledge in your research. All of you have shaped my work standards during the Ph.D.

Very special thanks to our previous group members, including Dr. Jittima Amie Luckanagul, Dr. Kamolrat Gift Metavarayuth, and Dr. Nikki Sitasuwan, for sharing your expertise, as well as constructive discussion and suggestions for my research. Without your help and support, I could not imagine how tough my life would be during my first year of studying Ph.D. I also would like to thank Amanda Wagner and Monchupa Kingsak, for your contribution in the graphene hybridized HA hydrogel project and titanium nanotube

المنارة للاستشارات
www.manaraa.com

array project. Additionally, I would like to thank all of current members, including Lin Lu, Yanmei Xu, and Libo Zhang, for sharing all the knowledge and wonderful time during pursuing Ph.D.

I am also grateful to all of the facility supports from Dr. Peisheng Xu's, Dr. Chuanbing Tang's, Dr. Brian C. Benicewicz's, Dr. Morgan Stefik's, Dr. Andrew B. Greytak's, Dr. Aaron K. Vannucci's, Dr. Taixing Cui's, Dr. John J. Lavigne's research labs, and the Electron Microscopy center at the University of South Carolina. It would have been impossible for me to complete my research without your supports and equipment.

Finally, I would like to express my very profound gratitude to my family. Words cannot express how grateful I am to my father, mother, and sisters for all of their endless love and support. A special thanks to my friends in Columbia, such as Preecha Kittikhunnathum, Trisha Sittisonthorn, and Greysi Adam, who have supported me along the way and made my time here a lot more fun. At the end, I would like express appreciation to my beloved fiancé, Nathan M. Trenor, who has been my best friend and great loved, supported, encouraged, entertained, and helped me get through the stressful periods in the most positive way.

المنارة للاستشارات
www.manaraa.com

ABSTRACT

This thesis is focused on the development of novel hybridized biomaterials for applications in tissue engineering and controlled drug delivery. Two types of materials used in my research are biopolymers and nanomaterials. Hyaluronic acid (HA), a natural polymer commonly found in extracellular matrix (ECM), was the primary polymer used in my research due to biocompatibility, biodegradability and the ease of manipulation to offer a wide range of physical and mechanical properties. Meanwhile, the nanomaterials, including Tobacco mosaic virus (TMV), gold nanorods and graphene, provide attractive properties, such as a nanoscale topography, biochemistry, high surface area, and special chemical and electrical properties. These properties could promote cell response, and allow the nanomaterials to react with a myriad of biological small molecules. Hence, in this thesis, we aimed to integrate these two types of materials to create a new type of biomaterials, and provide ideal properties that can leverage the tissue regeneration and targeted drug delivery for various treatment applications.

Previously, our research group has found the intriguing effect of TMV on bone differentiation of mesenchymal stem cells (MSCs). We demonstrated that TMV could promote MSC osteogenesis via upregulating bone morphogenetic protein-2 (BMP-2) gene expression, a common gene used to enhance cartilage differentiation. This discovery combined with the clinical demand for cartilage tissue repair, which is limited by the minimum self-healing capacity of cartilage, inspired us to design a hybrid TMV scaffold

المنارة للاستشارات
www.manaraa.com

in a simple injectable form, using thiol-ene "click" chemistry, to promote the MSC differentiation to cartilage. We demonstrated that cysteine-inserted TMV mutants (TMV1cys), containing thiol functional groups, could successfully crosslink to methacrylated hyaluronic acid (MeHA) polymers by thiol–ene "click" chemistry and form hydrogels under physiological conditions. The resulting hydrogels promoted *in vitro* chondrogenesis of MSCs by upregulating BMP-2 and enhancing collagen accumulation. In addition, incorporation of RGD-inserted TMV mutants (TMV-RGD1) in the HA hydrogels further promoted the *in vitro* chondrogenesis of BMSCs. Meanwhile, incorporation of gold nanorods, which provide similar size and shape as TMV, HA hydrogels showed no impact on the *in vitro* chondrogenesis. These results implied that the influences of nanoscale topography and biochemistry provided by TMV and TMV-RGD play critical roles in directing encapsulated MSC chondrogenesis.

To better mediate new cartilage tissue formation, the physical and mechanical properties of the HA hydrogels were further optimized by varying the structures of thiol-tailored crosslinker molecules using dithiothreitol (DTT), 4-arm polyethylene glycol (PEG), and a multi-arm polyamidoamine (PAMAM) dendrimer. Chondrogenesis and osteogenesis of MSCs were highly enhanced in 4-arm PEG-crosslinked HA hydrogels, as measured by chondrogenic markers, glycosaminoglycan (GAG) and collagen accumulation, and osteogenic markers, alkaline phosphatase activity, and calcium deposition. It implied that the differentiation performance of MSCs directly correlated to the mechanical stiffness, permeability, pore size, porosity and chemistry of crosslinkers. The 4-arm PEG-crosslinked HA hydrogels seemingly mimicked the architecture of real cartilage and bone closer than other hydrogels.

المنارة للاستشارات
www.manaraa.com

Aside from the application in tissue engineering, we developed a graphene oxide (GO)-hybridized HA-based hydrogel for perivascular drug delivery. The nanoscale GO was used as a novel nanocarrier for controlled drug delivery, owing to its high loading capacity of drugs resulting from the aromatic structure. HA serves as a biodegradable macroscale polymeric scaffold, making the prepared GO nanocarriers localized and stable in different microenvironments. The nanocarrier was firstly synthesized by attaching Senexin A (SNX), a kinase inhibitor and a possible anti-tumor drug, to GO via strong π–π interaction, followed by the *in situ* encapsulation of GO-SNX with HA-based hydrogel. The results of *in vitro* testing indicate high loading of SNX onto GO, and subsequent slow release of SNX within the therapeutic window. The slow release of SNX closed correlates to the loading-ratio of GO to SNX. With the *in vitro* results, we have demonstrated that the SNX loaded-GO hybridized HA hydrogel could be successfully attached to the decellularized scaffolds and form hydrogels under physiological condition. The hybridized materials provided a good biocompatibility and no impact on the proliferation and migration of vessel smooth muscle cells (VSMCs). More importantly, it could inhibit the dedifferentiation of VSMCs in the same manner as the SNX treatment.

المنارة للاستشارات
www.manaraa.com

TABLE OF CONTENTS

DEDICATION iii

ACKNOWLEDGEMENTS iv

ABSTRACT vi

LIST OF TABLES xii

LIST OF FIGURES xiii

CHAPTER 1 THE DEVELOPMENT OF *IN SITU* HYBRIDIZED BIONANOPARTICLE-HYALURONIC ACID HYDROGELS AS CELL SCAFFOLDS FOR TISSUE ENGINEERING 1

1.1 INTRODUCTION 1

1.2 RESULTS AND DISCUSSION 6

1.3 CONCLUSIONS 15

1.4 MATERIALS AND METHODS 16

1.5 REFERENCES 23

CHAPTER 2 THE *IN VITRO* MESENCHYMAL STEM CELL CHONDROGENESIS IN THE *IN SITU* HYBRIDIZED ROD-LIKE NANOPARTICLE-HYALURONIC ACID HYDROGELS 31

2.1 INTRODUCTION 31

2.2 RESULTS AND DISCUSSION 33

2.3 CONCLUSIONS 48

2.4 MATERIALS AND METHODS 48

2.5 REFERENCES 56

CHAPTER 3 THE OPTIMIZATION OF PHYSICAL AND MECHANICAL PROPERTIES OF THE THIOL–ENE "CLICK" HA HYDROGELS THROUGH CHEMISTRIES OF CROSS-LINKERS FOR OSTEOCHONDRAL REGENERATION APPLICATIONS 64

المنارة للاستشارات
www.manaraa.com

3.1 INTRODUCTION 64

3.2 RESULTS AND DISCUSSION.....68

3.3 CONCLUSIONS 80

3.4 MATERIALS AND METHODS 80

3.5 REFERENCES.....87

CHAPTER 4 THE *IN VITRO* MESENCHYMAL STEM CELL CHONDROGENESIS AND OSTEOGENESIS IN DIFFERENT THIOL–ENE "CLICK" HA HYDROGELS 94

4.1 INTRODUCTION 94

4.2 RESULTS AND DISCUSSION.....96

4.3 CONCLUSIONS 106

4.4 MATERIALS AND METHODS 106

4.5 REFERENCES 111

CHAPTER 5 THE DEVELOPMENT OF HYBRIDIZED-GRAPHENE HA HYDROGELS AS CONTROLLED PERIVASCULAR DRUG DELIVERIES FOR VESSEL GRAFT REGENERATION ...117

5.1 INTRODUCTION 117

5.2 RESULTS AND DISCUSSION.....120

5.3 CONCLUSIONS 136

5.4 MATERIALS AND METHODS 137

5.5 REFERENCES 145

APPENDIX A – COPYRIGHT CLEARANCE FOR CHAPTER 1 AND 2 153

APPENDIX B – COPYRIGHT CLEARANCE FOR FIGURE 1.2.....154

APPENDIX C – COPYRIGHT CLEARANCE FOR FIGURE 1.3.....155

APPENDIX D – COPYRIGHT CLEARANCE FOR CHAPTER 3 AND 4 156

APPENDIX E – COPYRIGHT CLEARANCE FOR FIGURE 3.2 157

المنارة للاستشارات
www.manaraa.com

APPENDIX F – THE DEVELOPMENT OF GRAPHENE-FET NANOSENSOR FOR SMALL-MOLECULE DETECTION 158

المنارة للاستشارات
www.manaraa.com

LIST OF TABLES

Table 1.1 Percent degree of methacrylation of different macromer size HA when reacting with various molar ratio of methacrylic anhydride 16

Table 1.2 Formulation of the TMV-based HA hydrogel and the controlled HA hydrogel 17

Table 2.1 Formulation of HA, TMV1Cys-based HA, and TMV-RGD1-based HA hydrogels.....38

Table 2.2 Formulation of HA, wide-type TMV-based HA, and GNR-based HA hydrogels.....42

Table 3.1 Summary of the thiol-ene "click" HA hydrogel formulations.....70

Table 4.1 Summary of the impact physical properties of the thiol–ene "click" HA hydrogels on BMSC differentiation.....104

Table 5.1 The gelation time of different Senexin A-loaded graphene HA hydrogels, which were determined by tilting method. The values expressed are means (n = 4) ± SD 124

Table 5.2 Correlation coefficient (R^2), rate constant (K), and release exponent (n) values obtained by fitting the data of the release of SNX from different hydrogel formulations into PBS at pH 7.4.....129

المنارة للاستشارات
www.manaraa.com

LIST OF FIGURES

Figure 1.1 TMV structure 2

Figure 1.2 The promotion of *in vitro* BMSC osteogenesis by the TMV coated on 2D substrates.....3

Figure 1.3 The promotion of *in vitro* BMSC osteogenesis and *in vivo* bone regeneration by the TMV and TMV-RGD1 embedded macroporous alginate hydrogels (TMV-PAH, RGD-PAH) 4

Figure 1.4 Transmission electron micrograph of TMV1cys.....7

Figure 1.5 Schematic illustration of the synthesis of TMV-based HA hydrogels 7

Figure 1.6 ^{1}H NMR spectra of methacrylated HA with approximate 40% degree of modification 8

Figure 1.7 Illustration of the *in situ* hydrogel formation 8

Figure 1.8 Interaction of TMV1cys and its structural integrity in HA hydrogel.....9

Figure 1.9 Atomic force microscopy height image of the TMV1cys-based HA hydrogel.....10

Figure 1.10 Cross-section and surface SEM micrographs of the TMV-based HA hydrogel after freeze-drying.....11

Figure 1.11 (A) Permeability of the hydrogels in terms of molecular retention using dye retention study. (B) Swelling ratios of the hydrogels after gelation and immersion into PBS. The weight change due to water absorption was monitored over time. (C) The stability of the hydrogels.....13

Figure 1.12 (A) Gelation behavior of the hydrogels was observed via oscillation time sweep at 25 °C, 2% strain and 10 rad/s frequency. (B) The average gelation time of the hydrogels.....14

Figure 1.13 Metabolic activity of BMSCs encapsulated in the hydrogels after 1, 7, 14, and 21 days of culturing in complete primary media 15

Figure 1.14 Fluorescence spectroscopy calibration with linear fitting curve and equation for quantification of fluorescein amine isomer I.....20

المنارة للاستشارات
www.manaraa.com

Figure 2.1 RT-qPCR analysis of BMP-2 expression in the BMSCs encapsulated in the hydrogels under chondrogenic conditions for 8 h, 2, and 7 days. 35

Figure 2.2 The results of *in vitro* chondrogenesis of MSCs in the *in situ* TMV1cys-based HA hydrogels. 37

Figure 2.3 The results of *in vitro* chondrogenesis of MSCs in the *in situ* TMV-RGD1-based HA hydrogels compared to the *in situ* TMV1cys-based HA hydrogels. 40

Figure 2.4 Transmission electron micrograph of wide-type TMVs (A) and GNRs (B)....42

Figure 2.5 Physical properties of the *in situ* GNR-based HA hydrogels compared to HA and TMV-based HA hydrogels 44

Figure 2.6 Celltiter-Blue assay of viable MSCs encapsulated in the hydrogels after 7 days of culturing in primary media. 45

Figure 2.7 The results of *in vitro* chondrogenesis of MSCs in the *in situ* GNR-based HA hydrogels compared to the *in situ* HA and TMV-based HA hydrogels.....47

Figure 3.1 Schematic representation of different strategies utilized to improve the mechanical properties of hydrogels. 65

Figure 3.2 *In vitro* cell proliferation and differentiation on the biochemical-modified PAMAM dendrimers. 67

Figure 3.3 Schematic illustrating the formation of the thiol–ene "click" HA hydrogels. .69

Figure 3.4 ^{1}H NMR spectra of the thiol-tailored G2-PAMAM with approximate 100% degree of modification (16 thiol groups on the structure) 70

Figure 3.5 ^{1}H NMR spectra of the thiol-tailored G3-PAMAM with approximate 100% degree of modification (32 thiol groups on the structure) 71

Figure 3.6 Exterior and cross-section SEM micrographs of the thiol–ene "click" HA hydrogels after freeze-drying 73

Figure 3.7 Mechanical properties and gelation time of the thiol–ene "click" HA hydrogels. 74

Figure 3.8 Swelling properties of the thiol–ene "click" HA hydrogels 77

Figure 3.9 Permeability of the thiol–ene "click" HA hydrogels.....78

Figure 3.10 Degradation of the thiol–ene "click" HA hydrogels. 79

Figure 3.11 Fluorescence spectroscopy calibration with linear fitting curve and equation for quantification of BSA proteins at concentration of 0-25 µg/mL (A), and 50-1000 µg/mL (B) 85

المنارة للاستشارات
www.manaraa.com

Figure 3.12 UV-Vis spectroscopy calibration with linear fitting curve and equation for quantification of HA at concentration of 0-1 mg/mL 86

Figure 4.1 Schematic illustration of the research design for the study of the effect of cross-linker types on the chondrogenic and osteogenic differentiation by encapsulated BMSCs in the thiol–ene "click" HA hydrogels. 95

Figure 4.2 BMSC viability after culturing in complete growth media, and GAG accumulation of differentiated BMSCs in the hydrogels after culturing in chondrogenic media. 97

Figure 4.3 Negative controls of histochemical staining for GAG and immunohistostaining for type II and I collagen 98

Figure 4.4 Type II and I collagen accumulation of differentiated BMSCs in the hydrogels after culturing in chondrogenic media. 101

Figure 4.5 Osteogenesis performance of differentiated BMSCs in the hydrogels after culturing in osteogenic media. 105

Figure 5.1 Schematic illustration of the experimental research of hybridized-graphene HA hydrogels as controlled perivascular drug deliveries for vessel graft regeneration 119

Figure 5.2 Characterization of the synthesized graphene oxide 121

Figure 5.3 Preparation and characterization of Senexin A-loaded graphene oxide 122

Figure 5.4 Schematic illustrating the synthesis of Senexin A-loaded graphene HA hydrogels via thiol–ene "click" reaction 123

Figure 5.5 Physical and mechanical properties of Senexin A-loaded graphene HA hydrogels. 125

Figure 5.6 The attachment of Senexin A-loaded graphene HA hydrogels to the decellularized scaffolds in PBS after gelling (A) and 1 day (B) 125

Figure 5.7. *In vitro* SNX release profiles of Senexin A-loaded graphene (GO-SNX) HA hydrogels. 127

Figure 5.8 *In vitro* SNX release profiles of GO-SNX (4:1) HA hydrogels. 127

Figure 5.9 Fitting of the data for SNX release from the SNX loaded HA hydrogels (SNX-HA) and GO-SNX HA hydrogels having different loading ratio of GO:SNX (1:3, 1:1, and 4:1) into PBS (pH 7.4) to the zero order (A) and first order kinetics (B) 130

Figure 5.10 Fitting of the data for SNX release from the SNX loaded HA hydrogels (SNX-HA) and GO-SNX HA hydrogels having different loading ratio of GO:SNX (1:3, 1:1, and

المنارة للاستشارات
www.manaraa.com

4:1) into PBS (pH 7.4) to the Higuchi release model (A) and Korsmeyer-Peppas release model (B) 131

Figure 5.11 *In vitro* cytocompatibility and efficacy of Senexin A-loaded graphene HA hydrogels.....133

Figure 5.12 Western blot analysis showed the expression of smooth muscle-specific SM22, alpha-smooth muscle actin (α-SMA) GAPDH and β-actin protein in VSMCs after treatment in serum-free medium for 48 h and later in complete medium without or with HA (3 mg/mL) or 0.5M DTT (2 µL/mL) or GO (1 mg/mL) for 24 h, *n* = 3 135

المنارة للاستشارات
www.manaraa.com

CHAPTER 1

THE DEVELOPMENT OF *IN SITU* HYBRIDIZED BIONANOPARTICLE-HYALURONIC ACID HYDROGELS AS CELL SCAFFOLDS FOR TISSUE ENGINEERING[1]

1.1 INTRODUCTION

The pursuit to cartilage tissue engineering is prompted by the limitation of current clinical methods to repair the defected cartilage[1] as well as the limitation in self-healing capacity of cartilage.[2-4] The basic principle of cartilage tissue engineering is isolation of appropriate cells that are proliferated in a 3D scaffold, subsequently implanted into the site of injury, and regenerated the defected cartilage tissue. Bone marrow derived stem cells (BMSCs) are promising cell sources for cartilage tissue engineering since they can be easily isolated, cultured, and differentiated into matrix-producing chondrocytes.[5-7] Importantly, the use of BMSCs can lessen the limitations of using autologous chondrocytes which are donor-site morbidity and limited matrix production after cell expansion.[8,9] However, promoting stem cell chondrogenesis is still a key to accomplish a successful cartilage repair.

Recently, we reported that the use of Tobacco mosaic virus (TMV) and other plant virus particles as cell-supporting materials could rapidly induce BMSCs toward osteogenic

[1] Portions of this chapter were adapted with permission from Maturavongsadit, P.; Luckanagul, J. A.; Metavarayuth, K.; Zhao, X.; Chen, L.; Lin, Y.; Wang, Q. *Biomacromolecules* **2016,** *17*, 1930-1938. Copyright (2016) American Chemical Society (Appendix A).

المنارة للاستشارات
www.manaraa.com

differentiation.[10-14] TMV is a rod-like plant virus that is 300 nm in length, with an average diameter of 18 nm, and consists of 2130 identical coat protein subunits assembled in a helical manner around single-stranded RNA (Figure 1.1). Its surface chemistry can be tailored through chemical or genetic modification.[15,16] For example, a TMV mutant genetically engineered to express a coat protein cysteine residue, TMV1cys, has been broadly used in the different applications.[17,18] Our previous studies demonstrated that the TMV coated on two-dimensional (2D) substrates could enhance osteogenesis of BMSCs through an upregulation of bone morphogenetic protein-2 (BMP-2) expression, a key morphogenetic protein involved in bone and cartilage formation (Figure 1.2).[13] TMV was also incorporated in a 3D alginate-based hydrogel system which aimed to mimic a native bone microenvironment. It was found that the TMV embedded macroporous alginate hydrogel could enhance osteogenesis *in vitro* and *in vivo* (Figure 1.3).[19,20] The results from these earlier studies confirmed that TMV plays a critical role in accelerating the osteogenesis process of BMSCs in both 2D and 3D environments; however, it is still unknown whether similar events can be translated to chondrogenesis in 3D scaffolds.

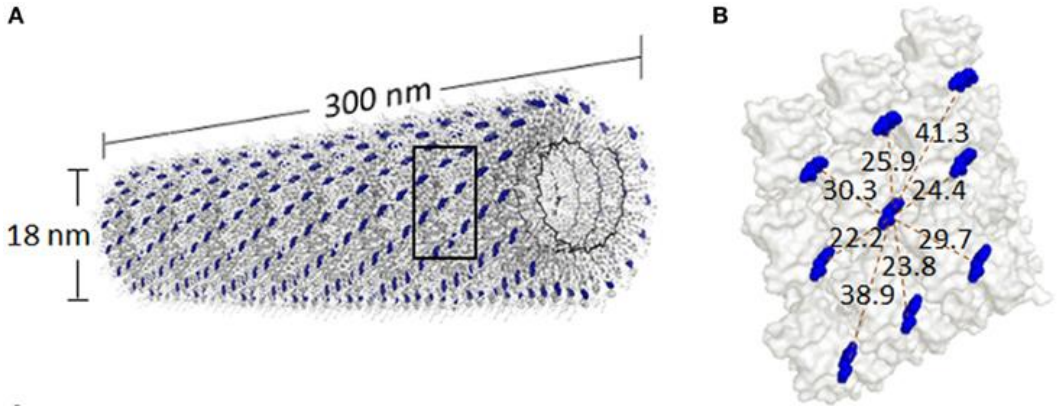

Figure 1.1. TMV structure. (A) Computer reconstructed image showing TMV structure using PyMOL with coordinates from Protein Data Bank. The single stranded RNA inside TMV particle is represented by the black helix. The tyrosine 139 (Y139) residues of individual TMV coat proteins subunits are colored in blue while all other amino acid

المنارة للاستشارات
www.manaraa.com

residues are washed out in gray. (B) An enlarged portion of TMV coat protein [from the boxed area in (A)], showing possible distances (dashed red lines, measured in Angstroms) among the blue Y139. Reprinted from Sitasuwan, P.; Lee, A. L.; Li, K.; Nguyen, H. G.; Wang, Q. *RGD-conjugated rod-like viral nanoparticles on 2D scaffold improve bone differentiation of mesenchymal stem cells* **2014**, 2:31. Copyright (2014) Sitasuwan, Lee, Li, Nguyen and Wang, Open Access. Published by Creative Commons Attribution License.

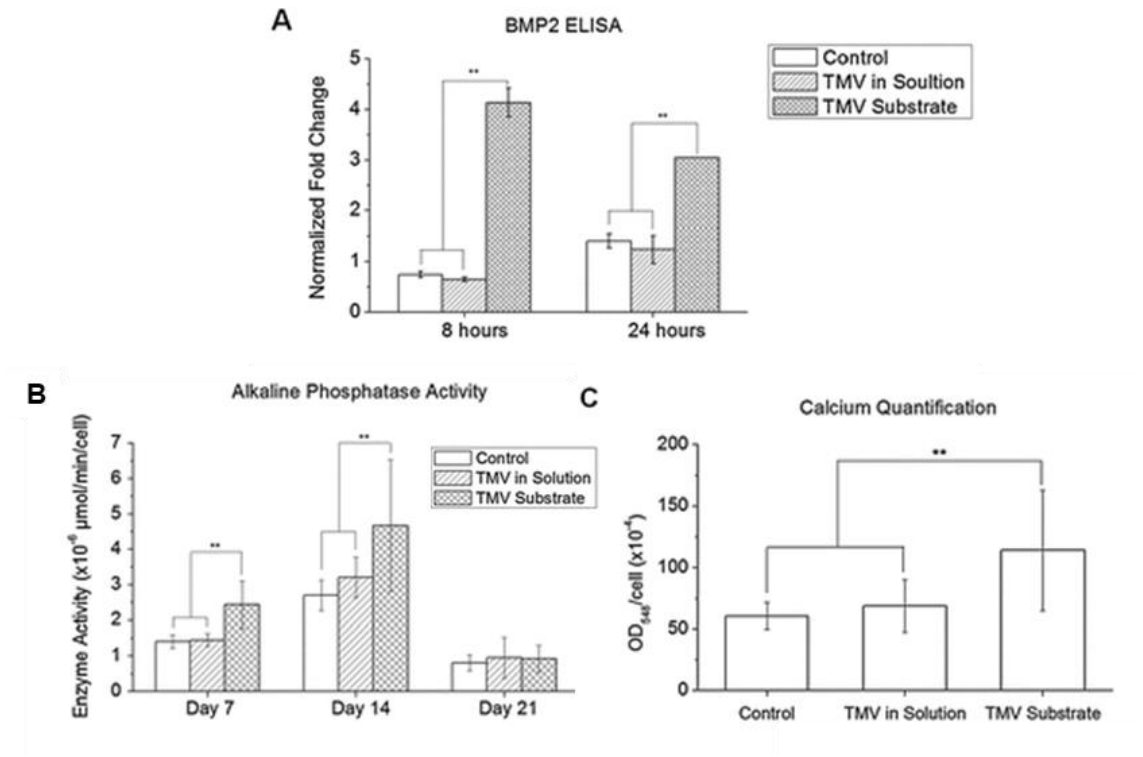

Figure 1.2. The promotion of *in vitro* BMSC osteogenesis by the TMV coated on 2D substrates. (A) Quantification of BMP2 protein expression at 8 and 24 hours normalized to the cell number by ELISA. The values are expressed as fold change compared to cells on tissue culture plate (TCP) before osteoinduction. The error bars denote ±1 S.D. ** $p < 0.05$ based on ANOVA. (A) Alkaline phosphatase activity of cells under three different conditions. (C) Absorbance at 548 nm normalized to the cell number to indicate a relative amount of calcium deposit at day 14 stained by alizarin red solution (**$p < 0.05$ based ANOVA). The error bars denote ±S.D. Reprinted with permission from Sitasuwan, P.; Lee, L. A.; Bo, P.; Davis, E. N.; Lin, Y.; Wang, Q. A Plant Virus Substrate Induces Early Upregulation of BMP2 for Rapid Bone Formation. *Integrative biology : quantitative biosciences from nano to macro* **2012,** *4*, 651-660. Copyright (2012) Royal Society of Chemistry (Appendix B).

المنارة للاستشارات
www.manaraa.com

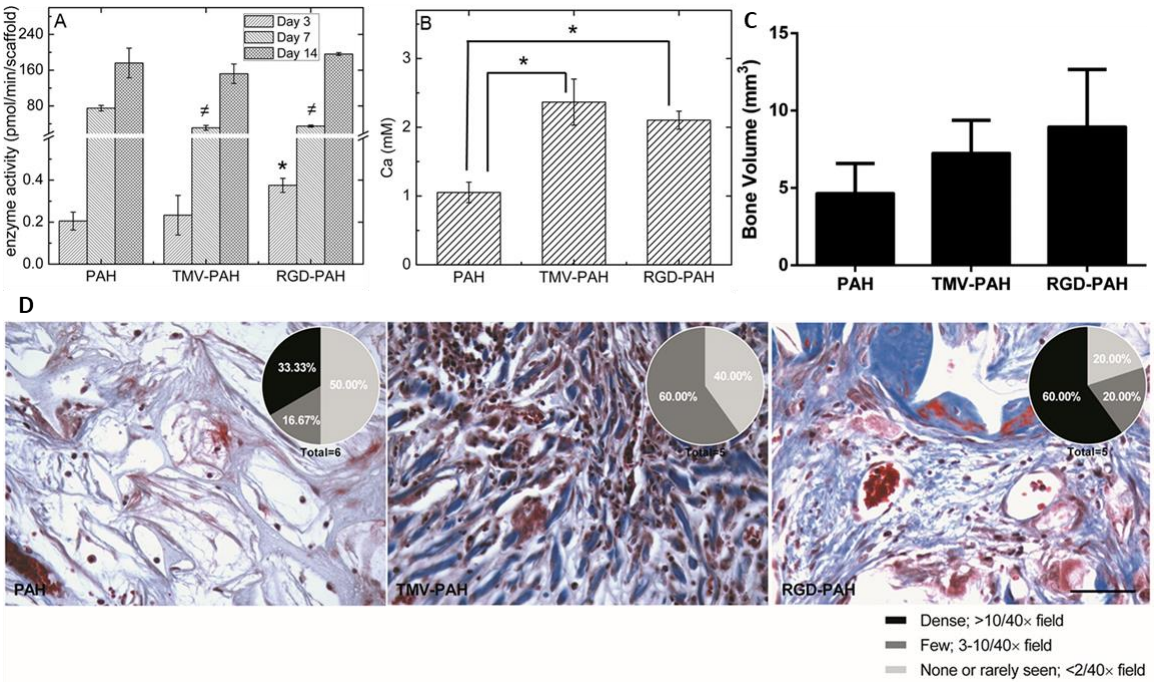

Figure 1.3. The promotion of *in vitro* BMSC osteogenesis and *in vivo* bone regeneration by the TMV and TMV-RGD1 embedded macroporous alginate hydrogels (TMV-PAH, RGD-PAH). (A) *In vitro* ALP activity assay was performed on days 3, 7, and 14 of osteogenic culture. Values expressed are mean (n = 3) ± S.D., ≠*paired equal variance Student t test, $p < 0.05$. (B) Calcium deposition quantified by ICP-OES on day 6 after background subtraction from control samples with no cells. Values expressed are mean (n = 3) ± SEM, *paired equal variance Student t test, $p < 0.05$. Reprinted with permission from Luckanagul, J.; Lee, L. A.; Nguyen, Q. L.; Sitasuwan, P.; Yang, X.; Shazly, T.; Wang, Q. Porous Alginate Hydrogel Functionalized with Virus as Three-Dimensional Scaffolds for Bone Differentiation. *Biomacromolecules* **2012,** *13*, 3949-3958. Copyright (2012) American Chemical Society (Appendix C). (C) Bone regeneration in critical size defect areas with porous hydrogel bone substitutes. The bone volume regenerated in each type of hydrogel was quantified using microcomputed tomography (microCT). Values expressed are the means (n = 6 for PAH and n = 5 for TMV-PAH and RGD-PAH) ± SEM. (D) Histological analysis of regenerated bone at defect sites filled with hydrogel implants after 10 weeks of implantation. The sections were stained with Masson's trichrome and imaged with 100× magnification. The regenerated bone was characterized by the presence of a collagen-rich matrix stained blue. The inset pie charts represent the number of rats that developed different degrees of bone regeneration at the defect site. Reprinted with permission from Luckanagul, J. A.; Metavarayuth, K.; Feng, S.; Maneesaay, P.; Clark, A. Y.; Yang, X.; García, A. J.; Wang, Q. Tobacco Mosaic Virus Functionalized Alginate Hydrogel Scaffolds for Bone Regeneration in Rats with Cranial Defect. *ACS Biomaterials Science & Engineering* **2016,** *2*, 606-615. Copyright (2016) American Chemical Society (Appendix C).

المنارة للاستشارات
www.manaraa.com

In situ-forming hydrogels have been recognized as promising biomaterials in cartilage-repairing applications[21] because it is possible to inject pre-gel solutions into cartilage damage through minimally invasive surgical procedures and fill irregular shape defects before gelation.[22,23] Among various starting materials, hyaluronic acid (HA) is one building block of particular interest because it is biocompatible, biodegradable, and functional in the synovial fluid of cartilage.[24] HA binds specifically to the proteins in the extracellular matrix (ECM), on the cell surface, and within the cell, and hence play a role in stabilizing cartilage matrix,[25,26] cell motility,[27,28] function of growth factor,[29] and inflammation.[30] Clinically, HA is commonly used as a viscosupplementation for treatment of knee osteoarthritis (OA), in which HA is injected into the knee joint for the alleviation of joint pain and improvement of joint function.[31-33] More importantly, HA hydrogels have been developed that could be formed, *in situ*, under physiological conditions, and the structure of HA can be chemically modified through its hydroxyl or carboxyl group to alter the properties of the resulting materials.[34,35]

Taken together, the goal of this study is to develop the *in situ* TMV-based HA hydrogels for cartilage tissue engineering applications. HA was firstly modified with methacrylic anhydride under basic conditions to form methacrylated HA (MeHA). TMV1cys was used to crosslink into the *in situ* MeHA hydrogels via thiol–ene coupling reaction. Physical properties of the TMV-based HA hydrogels were characterized and compared to the unhybridized HA hydrogels. Cytocompatibility was observed when the BMSCs were cultured in the TMV-based HA hydrogels.

المنارة للاستشارات
www.manaraa.com

1.2 RESULTS AND DISCUSSION

1.2.1 Synthesis of TMV-Based HA Hydrogels

Before fabrication of the hydrogels, the stabilities of the purified TMV1cys were confirmed by TEM analyses (Figure 1.4). As shown in Figure 1.5, HA macromers (47 kDa MW) were firstly modified with methacrylates to enable cross-linking via thiol–ene reaction to form hydrogels. The modification was performed by a simple one-step reaction with methacrylic anhydride. An excess of methacrylic anhydride with respect to HA was used because of the limited solubility and potential hydrolysis reaction of methacrylic anhydride in an aqueous medium.[36,37] The higher molecular weight HA provided a higher viscosity of the HA solution which reduced the reaction rate. We found that the 47 kDa HA was practical for the experiment since it gave optimum viscosity and modularity in a wide range of percent degree of methacrylation. In the report by Chung *et al.*, they also supported the use of relatively small HA macromer (approximate 50 kDa) to fabricate hydrogels for continued development of cartilage since it most resembled the properties of native cartilage when compared to the hydrogels from the larger HA (tested up to 1100 kDa).[38,39] The 1:6 molar ratio of HA monomer and methacrylic anhydride consistently generated 40–50% degree of modification of HA backbones, as determined by ^{1}H NMR (Figure 1.6). TMV1cys, providing cysteine residues on its coat proteins,[40] was covalently conjugated to methacrylated HA backbone via a Michael addition reaction. DTT was then cross-linked to the methacrylated HA functionalized with TMV1cys solution to create the hydrogel via the same thiol–ene reaction, which can be completed in an aqueous medium at physiological temperature and pH in the presence of proteins or cells;[41-43] therefore, it

المنارة للاستشارات
www.manaraa.com

can be used for *in vivo* applications. The illustration and physical appearance of the *in situ* TMV-based HA hydrogels are shown in Figure 1.7.

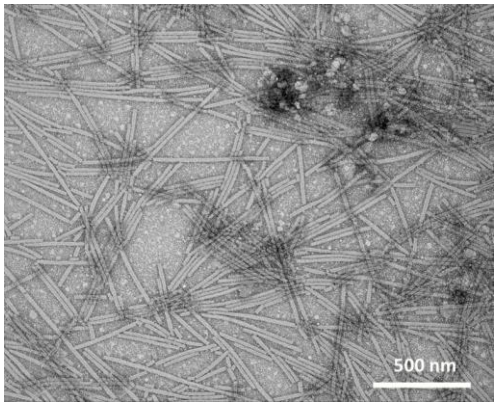

Figure 1.4. Transmission electron micrograph of TMV1cys.

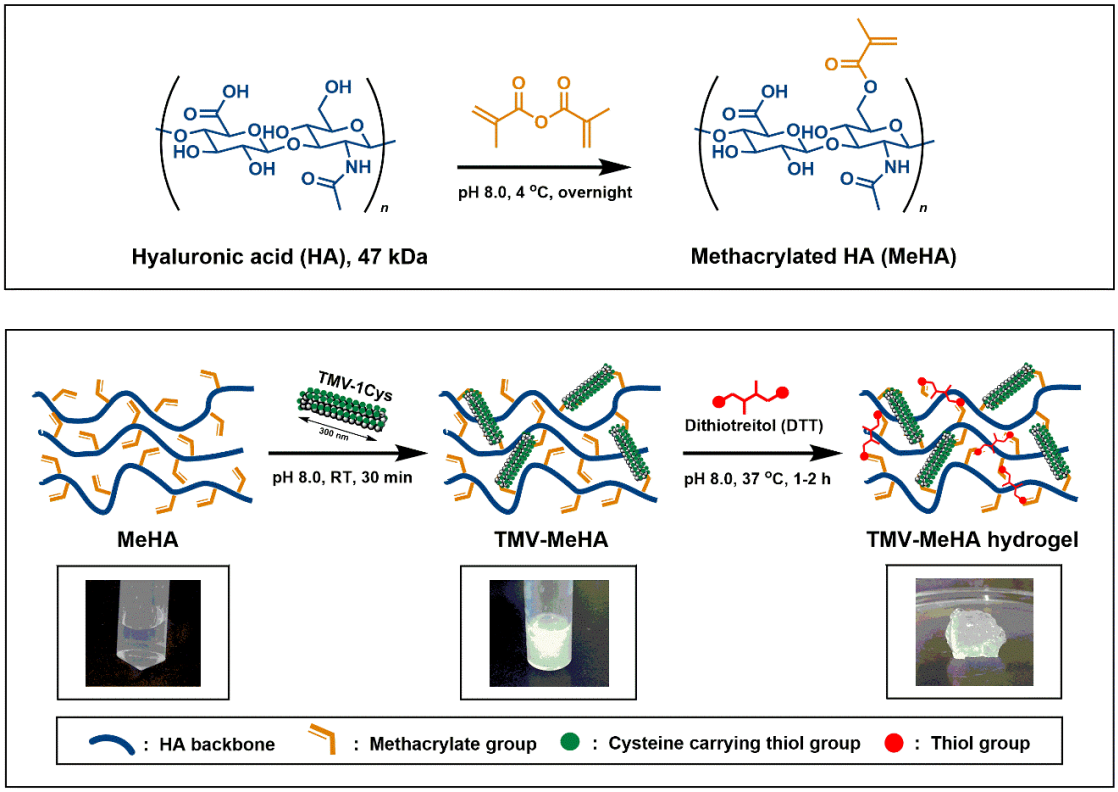

Figure 1.5. Schematic illustration of the synthesis of TMV-based HA hydrogels (A) HA modification with methacrylic anhydride to form the methacrylated HA (MeHA); (B) Synthesis of the TMV-based HA hydrogel.

المنارة للاستشارات
www.manaraa.com

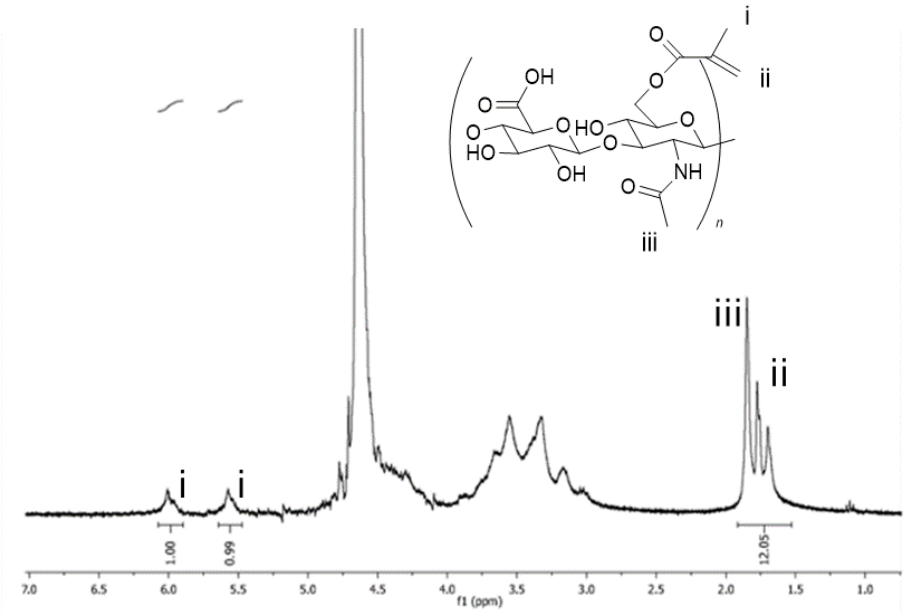

Figure 1.6. ^{1}H NMR spectra of methacrylated HA with approximate 40% degree of modification.

Figure 1.7. Illustration of the *in situ* hydrogel formation. (A) The pre-hydrogel mixture with TMV1cys (left) and without TMV1cys (right). (B) Injectable simulation of pre-hydrogel mixture through needle 20G. (C) The TMV1cys-based HA hydrogel (left) and HA hydrogel (right) after gelation for 2 h.

1.2.2 Structure of TMV-Based HA Hydrogels

MALDI-TOF MS was used to confirm the cross-linking between TMV1cys and the MeHA backbone after the formation of the hydrogel. The TMV-Cys-HA hydrogel was digested using hyaluronidase (HAase), which could randomly cleave β-*N*-acetylhexosamine-[1 → 4]glycosidic bonds in HA before it was processed to run MALDI-TOF MS analysis. Figure 1.8A demonstrated that the TMV-Cys-HA hydrogel obtained

المنارة للاستشارات
www.manaraa.com

pronounced peaks at 19652 *m*/*z* in addition to the peak of original TMV1cys coat protein (around 17630 *m*/*z*). The mass difference subtracted from the TMV1cys peak was calculated, and the possible structure of the TMV1cys-based HA hydrogel was proposed in Figure 1.8B. It showed that TMV1cys covalently interacted with the backbone of polymer. However, the degree of HA conjugation to the TMV1cys was hardly quantified since the weight percentage of TMV1cys comparing to HA polymer and other components in the hydrogel system is very small.

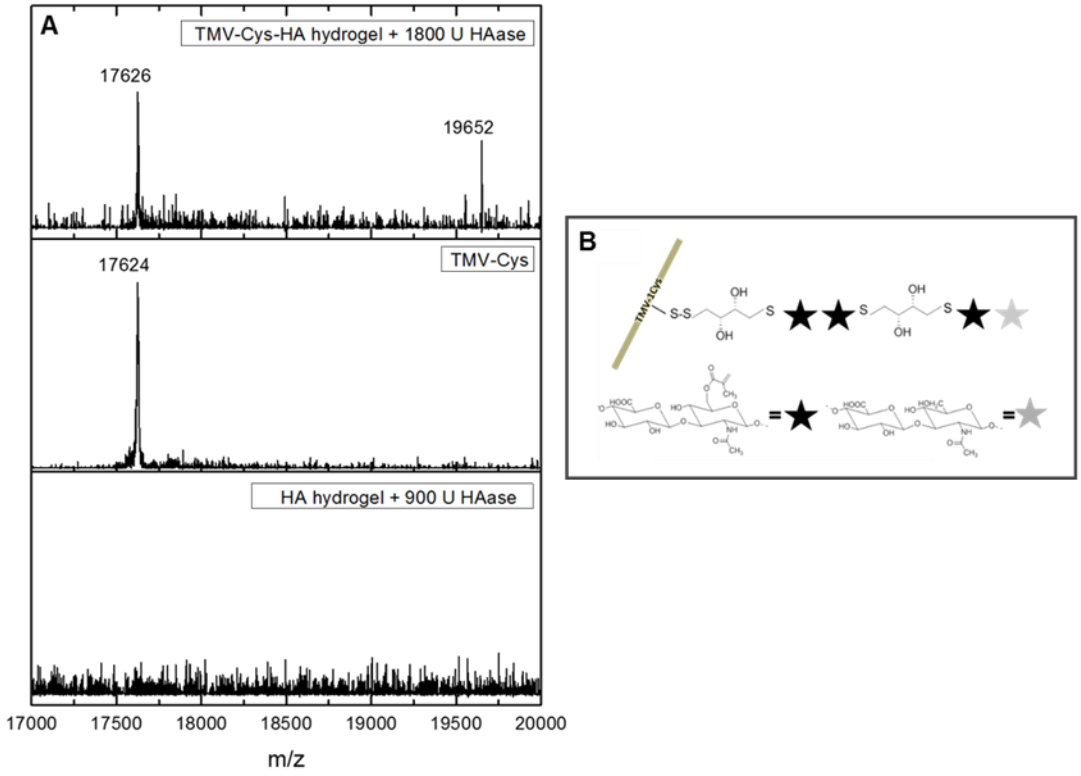

Figure 1.8. Interaction of TMV1cys and its structural integrity in HA hydrogel. (A) MALDI-TOF spectra compared the m/z profiles of TMV1cys-based hydrogel after enzyme digestion of HA backbone (top panel) with the virus alone (middle panel) and with the control HA hydrogel (last panel). (B) The proposed structure of TMV1cys-based HA hydrogel from MALDI-TOF analysis, the TMV1cys covalently interacted with the polymer backbone.

المنارة للاستشارات
www.manaraa.com

The existence of TMV1cys particles in the MeHA hydrogel was confirmed by AFM images. Figure 1.9A showed the height profile of TMV1cys particles on the silicon wafer substrate coated with the TMV-Cys-HA hydrogel, which had the same appearance with wild-type TMV observed by AFM. Additionally, Figure 1.9B revealed that intact TMV1cys particles still remained in the TMV-Cys-HA hydrogel after keeping more than 6 months at room temperature.

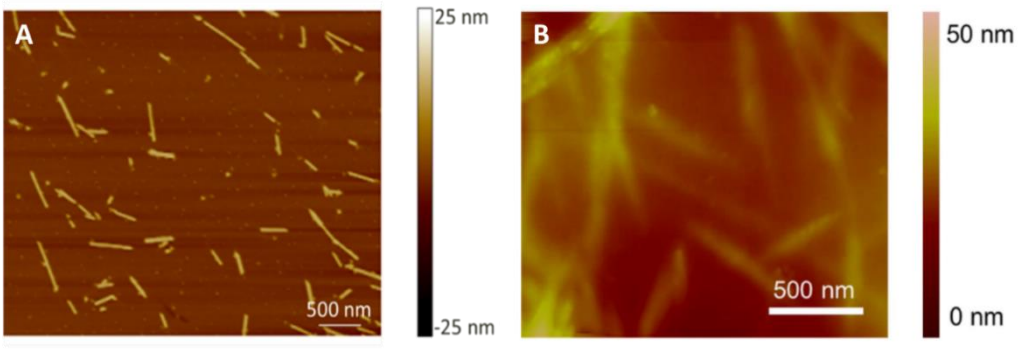

Figure 1.9. Atomic force microscopy height image of the TMV1cys-based HA hydrogel, showing the presence of TMV1cys intact particles in the hydrogel right after gelling (A), and after storage for approximate 6 months (B).

The microstructure of the freeze-dried TMV-Cys-HA hydrogels was characterized by SEM (Figure 1.10). The cross-section SEM images of the TMV-Cys-HA hydrogels revealed 20–100 μm range of pore size with high porosity and interconnectivity. Furthermore, a thin layer of compacted outer edge was observed in the cross-section of the hydrogels. HA hydrogels obtained a similar pore architecture but less porosity and interconnectivity with a thicker layer of compacted outer edge. The exterior surfaces of both hydrogels were a dense, rough, and folded architecture with submicron-sized pores (<2 μm). High degrees of porosity and pore interconnectivity played a critical role in initial cells or substances penetration, uniform cells distribution, further cell–cell interactions,

المنارة للاستشارات
www.manaraa.com

mass transfer of nutrients and metabolites, and tissue growth.[44,45] For example, scaffolds with large pore sizes of 115–335 μm were appropriate for the cartilaginous tissue formation.[44,46] Meanwhile, small pore sizes may help maintain chondrocyte phenotypes, since chondrocytes are more likely to differentiate when the pore size is about 30 times the cell diameter, which is approximately 10–15 μm.[45]

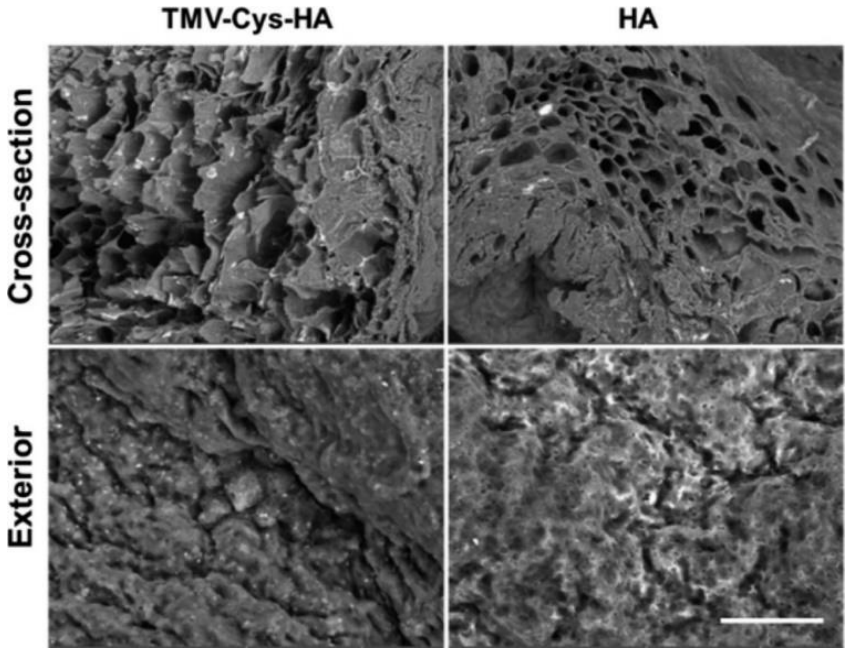

Figure 1.10. Cross-section and surface SEM micrographs of the TMV-based HA hydrogel after freeze-drying. Scale bar is 200 μm for all images.

1.2.3 Permeability of TMV-Based HA Hydrogels

The permeability of the hydrogels was observed by the fluorescent dye retention study. The amount of dye diffused into the pre-saturated hydrogel was calculated from the reduction of fluorescent dye amount measured from fluorescence intensity differences of the medium over time. Figure 1.11A showed that both hydrogels could absorb the dye in a similar manner, reaching equilibrium within 1 h. At the equilibrium, the TMV-Cys-HA

المنارة للاستشارات
www.manaraa.com

hydrogels accommodated slightly more dye (~3.3 μg/mL) than the value calculated for the HA hydrogels (~2.2 μg/mL). The swelling ratios revealed the ability of the hydrogels to absorb water. As shown in Figure 1.11B, the swelling ratio of the TMV-Cys-HA hydrogel was slightly higher than the control HA hydrogel at early time points and became insignificantly different at later time points. Both hydrogels could absorb water up to 3.5-fold of their initial weight. No weight loss in both hydrogels was observed within 21 days in PBS (Figure 1.11C). We additionally observed a significantly lower mechanical strength in the TMV-Cys-HA hydrogels compared to the HA hydrogels. The differences in permeability, swelling rate, and mechanical strength between these two hydrogels could possibly be attributed to the higher porosity and pore interconnectivity of the TMV-Cys-HA hydrogels. Karande *et al.* have reviewed that when the pores are highly interconnected, an increase in porosity leads to an increase in permeability.[47] Furthermore, many studies have shown that increased porosity and interconnectivity of the hydrogels could improve the swelling rate of the hydrogels because of enlarging the contact area between the hydrogels and fluid.[48-50] In addition, the increased porosity and interconnectivity of the hydrogels may lead to a reduction in the solid content of the hydrogels, resulting in a lower storage modulus.[51] In our case, the swelling ratio of both TMV-Cys-HA and HA hydrogels were insignificantly different at later time points, absorbing water up to 3.5-fold their initial weight, indicating that both hydrogels exhibited the extreme hydrophilic properties similar to tissue environment and the capability to uptake medium for cell culture. From the stability test, no weight loss was observed from both hydrogels during 21 days, indicating that they could support the entire cell culture experiments and were suitable for tissue engineering applications.

المنارة للاستشارات
www.manaraa.com

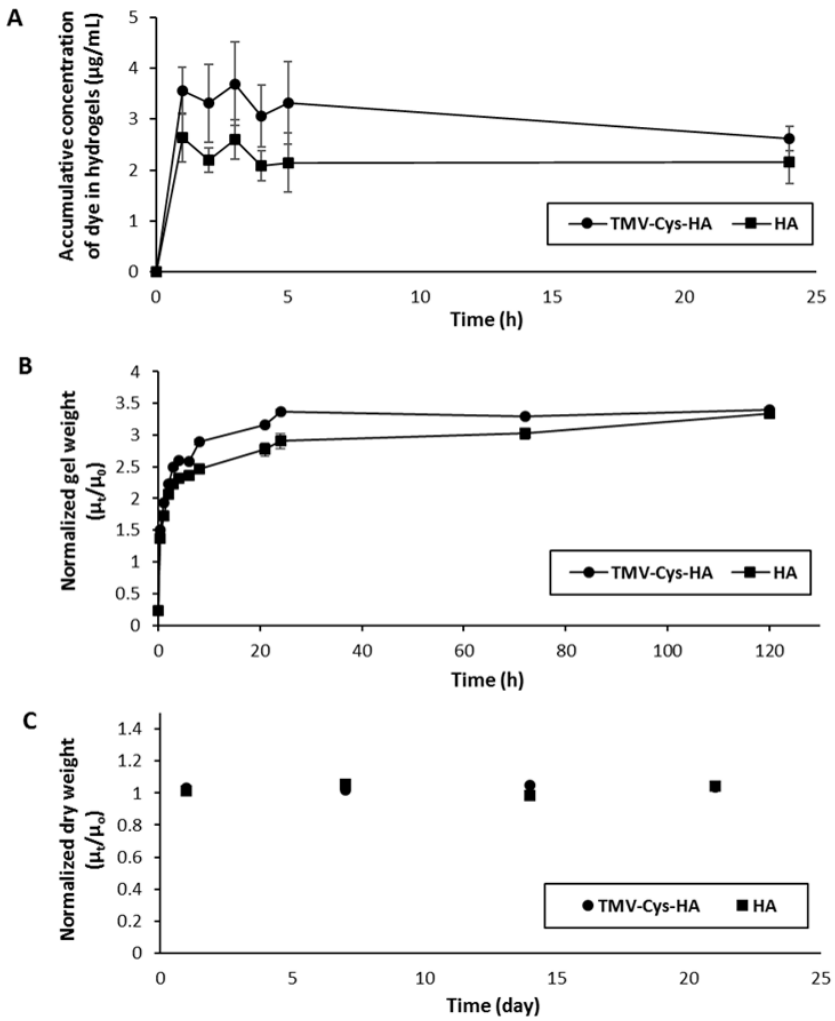

Figure 1.11. (A) Permeability of the hydrogels in terms of molecular retention using dye retention study. (B) Swelling ratios of the hydrogels after gelation and immersion into PBS. The weight change due to water absorption was monitored over time. (C) The stability of the hydrogels. The weight loss was observed over time. The values expressed are means ± SD, n = 3.

1.2.4 Gelation Time of TMV-Based HA Hydrogels

The gelation time is another crucial factor for the development of injectable hydrogels in terms of therapeutic applications. In the study, the gelation time of the hydrogels was determined by observing the solution–gel phase transition. We found that the solution–gel phase transition in the TMV-Cys-HA hydrogels appeared much earlier

المنارة للاستشارات
www.manaraa.com

than that in the HA hydrogels. The average gelation time of the TMV-Cys-HA and HA hydrogels were 15 min and 2 h, respectively (Figure 1.12). It is possible that prior the addition of DTT, TMV1cys cross-linked to the methacrylated HA backbone via Michael addition reaction, helping to increase the rate of hydrogel formation. However, the gelation time of the hydrogels also relied on the basicity of the medium.[52,53] We observed that when primary media or PBS buffer was used and the pH was set to 7.3 and 8, the gelation time of the HA hydrogels was an average within 6 and 2 h, respectively. This is consistent to the study by Pritchard et al. showing that the gelation time of thiol–acrylate poly(ethylene glycol) hydrogels followed an exponential dependence on pH of buffer.[53]

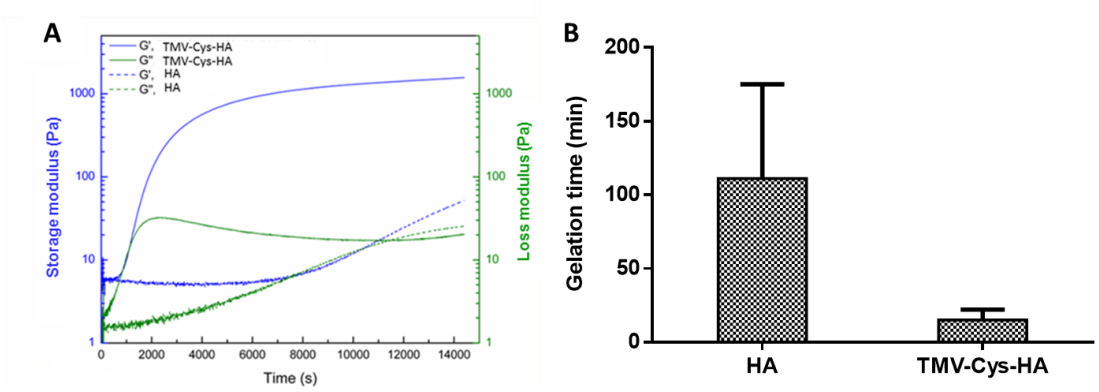

Figure 1.12. (A) Gelation behavior of the hydrogels was observed via oscillation time sweep at 25 °C, 2% strain and 10 rad/s frequency. (B) The average gelation time of the hydrogels. The horizontal bars are means ± SD with each data expressed in dot plots (n = 3); *$p < 0.05$.

1.2.5 Biocompatibility of TMV-Based HA Hydrogels

The cytotoxicity of the hydrogels was examined by CellTiter-Blue (CTB) cell viability assay (Figure 1.13). The metabolic rate was normalized by BMSCs encapsulated in the hydrogels after 1 day. Both hydrogels could support cell viability over 21 days of culture. The metabolic rate of viable cells in the TMV-Cys-HA hydrogels slightly

المنارة للاستشارات
www.manaraa.com

decreased from day 1 to day 7, and slightly increased at later time points. In contrast, the metabolic rate of viable cells in the HA hydrogels slightly increased from day 1 to day 14, and slightly decreased at later stage. A possible explanation is that the TMV incorporated HA hydrogels played a role in cellular differentiation which could occur slowly even without chondrogenic induction supplements, resulting in a slower metabolic rate of the cells in early culture days.[13]

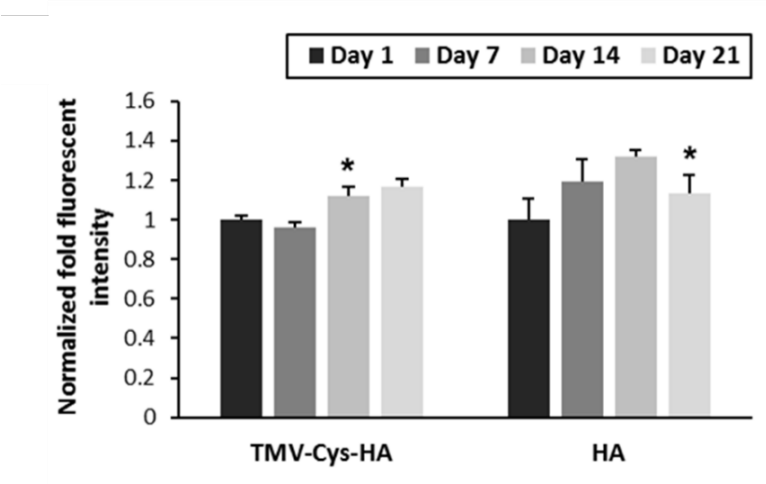

Figure 1.13. Metabolic activity of BMSCs encapsulated in the hydrogels after 1, 7, 14, and 21 days of culturing in complete primary media. The values expressed are means ± SD, n = 3 with two repeated experiments. *Paired equal variance Student t test, $p < 0.05$.

1.3 CONCLUSIONS

In situ TMV-based HA hydrogels were successfully prepared via Michael addition reaction under physiological condition. The resulting hydrogels obtained macropore structures enabling an exchange of nutrients and other biochemical cues. The gelation time was improved after addition of TMV1cys. The hydrogel was compatible for BMSCs culture. This study is considered to be a foundation of the development of injectable

المنارة للاستشارات
www.manaraa.com

hydrogels incorporated with TMV particles which is applicable for cartilage tissue engineering and regenerative medicine.

1.4 MATERIALS AND METHODS

1.4.1 Modification of HA and Synthesis of TMV-Based HA Hydrogels

MeHA was synthesized following the literature protocols.[54,55] Briefly, HA of molecular weight 47 kDa (Dali) was dissolved at 1 wt % in potassium phosphate buffer, pH 8, and methacrylic anhydride (Alfa Aesar) of different folds molar excess (relative to the HA disaccharide repeat unit), as listed in Table 1.1, was added dropwise to the solution at 0 °C. The pH of the two-phase reaction mixture was adjusted to 8.0 with 5 M NaOH aq., and the reaction continued for 24 h at 4 °C with frequent readjustment of the solution pH. The product was dialyzed against milli-Q water for at least 48 h, followed by centrifugation to remove the precipitate, which was then flash frozen in liquid nitrogen, and lyophilized, resulting in powder that was analyzed by degree of modification by ^{1}H NMR.

Table 1.1. Percent degree of methacrylation of different macromer size HA when reacting with various molar ratio of methacrylic anhydride.

MW of HA	**HA monomer: Methacrylic anhydride molar ratio**			
	1:3	1:6	1:10	1:12
47 kDa	~ 10%	~ 40-50%	100%	100%
310 kDa	N/A	~ 30%	N/A	~ 75%
1 MDa	N/A	Not detectable	N/A	N/A

N/A data not available

TMV1cys was created following the literature protocols.[40,56] Briefly, the addition of a single cysteine residue within the TMV coat protein was created by the insertion of a

المنارة للاستشارات
www.manaraa.com

TGT codon at the third position within the coat protein open reading frame using a PCR-based mutagenesis procedure. *Nicotiana tabacum*, cv Xanthi, a systemic TMV host, was inoculated with infectious RNA transcripts generated from the TMV1cys cDNA clone. Virus was harvested after 20 days of inoculation and purified according to previously reported methods.[57,58]

To form the TMV-based HA hydrogels (hereafter denoted as TMV-Cys-HA), MeHA polymers with 40–50% degree of modification were dissolved in a phosphate buffer saline solution (PBS) at 5 wt % concentration, and TMV1cys in potassium phosphate buffer was added to make a final concentration of 0.1 wt %. A cross-linking agent, dithiotreitol (DTT), was then added at a molar ratio of thiol/ene = 1:4. For comparison purposes, the HA hydrogels were also synthesized by the same procedure, except adding the TMV1cys solution (as shown in Table 1.2).

Table 1.2. Formulation of the TMV-based HA hydrogel and the controlled HA hydrogel.

Formulation	40-50% DM MeHA	TMV1cys	0.5 M DTT (molar ratio)	Solvent, pH system
TMV-Cys-HA	5%	0.1%	4Ene:1SH	PBS, pH 7.4
HA	5%	-	4Ene:1SH	PBS, pH 7.4

1.4.2 Structure Analysis of TMV-Based HA Hydrogels

Matrix-assisted laser desorption ionization–time of flight (MALDI-TOF) analysis was performed on the TMV-Cys-HA hydrogel. The preformed TMV-Cys-HA hydrogel (100 μL) was digested using 1800 U Hyaluronidase (HAase) in 1 mL of PBS (Type IV–S from bovine testes, Sigma) for 2 days. The controls included (1) the purified TMV1cys in

المنارة للاستشارات
www.manaraa.com

10 mM potassium phosphate buffer, pH 7; and (2) the HA hydrogel without the virus digested with 900 U HAase in 200 μL of PBS. Each sample was prepared by mixing the virus (0.5 mg/mL, 1 μL) or digested hydrogels solution (1 μL) with 9 μL of matrix solution (saturated sinapic acid in 70% acetonitrile, 0.1% trifluoroacetic acid). A total of 1 μL of the mixture was spotted on a MALDI plate, air-dried, and analyzed by MALDI-TOF mass spectrometry (Bruker Ultraflex MALDI-TOF/TOF).

Atomic force microscopy (AFM) was performed on the TMV-Cys-HA hydrogels. After gelation, the hydrogel was spin-coated on the silicon wafer. The hydrogel-coated wafer was then dried and subjected to AFM imaging. To study the stability of TMV1cys in the hydrogel, the TMV-Cys-HA hydrogels after keeping more than 6 months were digested using 1800 U HAase in 1 mL of PBS for 1 day. The digested hydrogel solution was coated on the silicon wafer, then dried, and subjected to AFM imaging. The TMV1cys in the hydrogel was characterized by tapping-mode AFM images using a NanoScope IIIA MultiMode AFM (Veeco). Si tips with a resonance frequency of approximately 300 kHz, a spring constant of about 40 N m^{-1}, and a scan rate of 1.0 Hz were used.

Environmental scanning electron microscopy (ESEM) images of the TMV-Cys-HA and HA hydrogels were obtained by VEGA3 TESCAN electron microscope. The freeze-dried samples were cross-sectioned and mounted on aluminum stubs with carbon tape. Samples were observed under a low vacuum with 20 kV of electron acceleration and a 9.95–13.16 mm of working distance.

المنارة للاستشارات
www.manaraa.com

1.4.3 Gelation Time Testing

Oscillatory shear rheology was performed using a DHR-3 rheometer (TA Instruments) with 12 mm diameter parallel-plate geometry and temperature-controlled Peltier plate. The TMV-Cys-HA and HA hydrogels were cross-linked *in situ* between the rheometer plates in a close chamber, protecting hydrogels from dehydration. The measurement in oscillatory time sweep mode (2% strain amplitude, 10 rad/s) immediately started after the freshly prepared prehydrogel mixture was loaded on the Peltier plate. Typically, 200 μL of the hydrogel solution was used with a gap width of 1 mm between the plates.

1.4.4 Retention Study

After the hydrogels (150 μL) were fabricated by afore mentioned methods, each hydrogel was soaked into 5 μg/mL fluoresceinamine isomer I (Sigma) in PBS (400 μL). The amount of dye diffused into the hydrogel was calculated from the left-over dye detected from the medium. Dye amounts were transformed from fluorescence intensity measured at 490/520 nm (Ex/Em) by SpectraMax M2Multi-Mode microplate reader (Molecular Devices). The standard curve was generated from different dye concentrations in the range of 1–10 μg/mL plotted over fluorescence intensities (Figure 1.14). The amounts of dye retention were then calculated into concentrations of dye diffused into the hydrogels, as shown in the following equation:

$$\text{Diffused dye concentration} = \frac{\text{amount of dye in hydrogel } (\mu g)}{\text{hydrogel volume (mL)}}$$

المنارة للاستشارات
www.manaraa.com

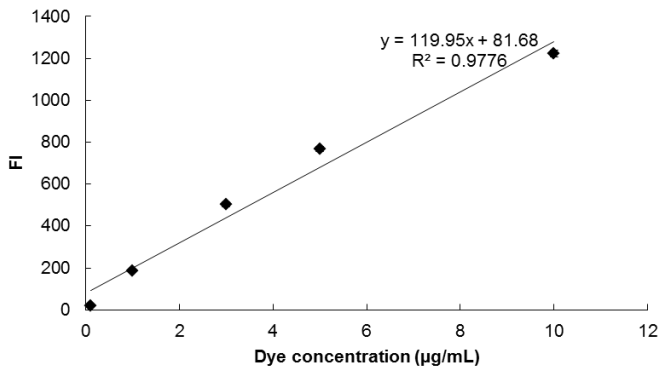

Figure 1.14. Fluorescence spectroscopy calibration with linear fitting curve and equation for quantification of fluorescein amine isomer I.

1.4.5 Swelling Ratio and Stability Analysis

Swelling property of each hydrogel was determined by the final weight divided by the initial weight of the hydrogel. The initial weights (~250 mg) of hydrogels were recorded (μ_0). Hydrogels were immersed in 1 mL of PBS at room temperature, and then the weights after immersion over time were recorded (μ_t). Surrounding water was drained and blotted out with Whatman filter paper from hydrogels before weighing. The swelling ratios were calculated from μ_t/μ_0.

For the stability test, the hydrogels (250 µL) were incubated with 1 mL of PBS at room temperature. The hydrogel mass reduction at each time point was monitored. The hydrogels were collected and lyophilized for at least 24 h before the dry weight was measured. The dry weight at the starting point was measured as γ_0 (~16 mg). The dry weight measured at different time point was symbolized γ_t. Normalized hydrogel dry weight was calculated as γ_t/γ_0.

المنارة للاستشارات
www.manaraa.com

1.4.6 Bone Marrow Stem Cells (BMSCs) Isolation and Maintenance

Primary BMSCs were isolated from the bone marrow of young adult 160–180 g male Sprague–Dawley rats (Charles River Laboratories). The procedures were performed in accordance with the guidelines for animal experimentation by the Institutional Animal Care and Use Committee, School of Medicine, University of South Carolina. Cells were maintained in complete primary media (Dulbecco's Modified Eagle's Medium (DMEM) supplemented with 10% fetal bovine serum (FBS)), kept at 37 °C in a CO_2 incubator with 5% CO_2/95% air, and passaged no more than seven times after isolation.

1.4.7 In Situ Cell Encapsulation and Culture

The hydrogels were prepared previously described except that the preparation occurred under sterile condition and prewarmed complete DMEM media was used to dissolve the polymer. TMV1cys was filtered to remove any pathogens before mixing. All other components including 5 M NaOH and 0.2 M DTT in PBS were also filtered with 0.2 μm PES membranes. BMSCs passage 3 or 4 were harvested from the tissue culture plate after reaching 80% confluency. The cells were then mixed with the mixture of prewarmed hydrogel in DMEM media at concentration of 10^6 cells/mL right after addition of DTT. The cells–hydrogel mixture (150 μL) was then pipetted into each Transwell (Corning) that was inserted and anchored in a 24-well tissue culture plate and incubated at 37 °C in a CO_2 incubator with 5% CO_2/95% air. After 6 h of initial incubation, complete primary media (800 μL) was added into each well. The media was exchanged every 2 days for the entire experimental period.

المنارة للاستشارات
www.manaraa.com

1.4.8 Cell Viability Assay

CellTiter-Blue (CTB) cell viability assay (Promega) was performed after days 1, 7, 14, and 21 of culturing BMSCs in the hydrogels. The culture media in each well was replaced by 300 mL of prewarmed media containing 15% CTB and incubated for 20 h at 37 °C and 5% CO_2. The media containing CTB without cells was used as negative controls. The media containing metabolite of CTB was measured for fluorescence intensity at 560/590 nm (Ex/Em) using SpectraMax M2Multi-Mode microplate reader (Molecular Devices).

المنارة للاستشارات
www.manaraa.com

1.5 REFERENCES

(1) Bedi, A.; Feeley, B. T.; Williams, R. J., 3rd. Management of Articular Cartilage Defects of the Knee. *J. Bone Joint Surg. Am.* **2010,** *92*, 994-1009.

(2) Liu, S. Q.; Tian, Q.; Hedrick, J. L.; Po Hui, J. H.; Ee, P. L.; Yang, Y. Y. Biomimetic Hydrogels for Chondrogenic Differentiation of Human Mesenchymal Stem Cells to Neocartilage. *Biomaterials* **2010,** *31*, 7298-7307.

(3) Kock, L.; van Donkelaar, C. C.; Ito, K. Tissue Engineering of Functional Articular Cartilage: The Current Status. *Cell Tissue Res.* **2012,** *347*, 613-627.

(4) Ahmed, T. A.; Hincke, M. T. Strategies for Articular Cartilage Lesion Repair and Functional Restoration. *Tissue engineering. Part B, Reviews* **2010,** *16*, 305-329.

(5) Sekiya, I.; Vuoristo, J. T.; Larson, B. L.; Prockop, D. J. In Vitro Cartilage Formation by Human Adult Stem Cells from Bone Marrow Stroma Defines the Sequence of Cellular and Molecular Events During Chondrogenesis. *Proc. Natl. Acad. Sci. U. S. A.* **2002,** *99*, 4397-4402.

(6) Mackay, A. M.; Beck, S. C.; Murphy, J. M.; Barry, F. P.; Chichester, C. O.; Pittenger, M. F. Chondrogenic Differentiation of Cultured Human Mesenchymal Stem Cells from Marrow. *Tissue Eng.* **1998,** *4*, 415-428.

(7) Boeuf, S.; Richter, W. Chondrogenesis of Mesenchymal Stem Cells: Role of Tissue Source and Inducing Factors. *Stem cell research & therapy* **2010,** *1*, 31.

(8) Gilbert, J. E. Current Treatment Options for the Restoration of Articular Cartilage. *Am. J. Knee Surg.* **1998,** *11*, 42-46.

المنارة للاستشارات
www.manaraa.com

(9) Lee, C. R.; Grodzinsky, A. J.; Hsu, H. P.; Martin, S. D.; Spector, M. Effects of Harvest and Selected Cartilage Repair Procedures on the Physical and Biochemical Properties of Articular Cartilage in the Canine Knee. *J. Orthop. Res.* **2000,** *18*, 790-799.

(10) Kaur, G.; Valarmathi, M. T.; Potts, J. D.; Wang, Q. The Promotion of Osteoblastic Differentiation of Rat Bone Marrow Stromal Cells by a Polyvalent Plant Mosaic Virus. *Biomaterials* **2008,** *29*, 4074-4081.

(11) Kaur, G.; Wang, C.; Sun, J.; Wang, Q. The Synergistic Effects of Multivalent Ligand Display and Nanotopography on Osteogenic Differentiation of Rat Bone Marrow Stem Cells. *Biomaterials* **2010,** *31*, 5813-5824.

(12) Lee, L. A.; Muhammad, S. M.; Nguyen, Q. L.; Sitasuwan, P.; Horvath, G.; Wang, Q. Multivalent Ligand Displayed on Plant Virus Induces Rapid Onset of Bone Differentiation. *Mol Pharm* **2012,** *9*, 2121-2125.

(13) Sitasuwan, P.; Lee, L. A.; Bo, P.; Davis, E. N.; Lin, Y.; Wang, Q. A Plant Virus Substrate Induces Early Upregulation of Bmp2 for Rapid Bone Formation. *Integrative biology : quantitative biosciences from nano to macro* **2012,** *4*, 651-660.

(14) Sitasuwan, P.; Lee, L. A.; Li, K.; Nguyen, H. G.; Wang, Q. Rgd-Conjugated Rod-Like Viral Nanoparticles on 2d Scaffold Improve Bone Differentiation of Mesenchymal Stem Cells. *Frontiers in chemistry* **2014,** *2*, 31.

(15) Bruckman, M. A.; Kaur, G.; Lee, L. A.; Xie, F.; Sepulveda, J.; Breitenkamp, R.; Zhang, X.; Joralemon, M.; Russell, T. P.; Emrick, T.; Wang, Q. Surface Modification of Tobacco Mosaic Virus with "Click" Chemistry. *ChemBioChem* **2008,** *9*, 519-523.

(16) Schlick, T. L.; Ding, Z.; Kovacs, E. W.; Francis, M. B. Dual-Surface Modification of the Tobacco Mosaic Virus. *J. Am. Chem. Soc.* **2005,** *127*, 3718-3723.

المنارة للاستشارات
www.manaraa.com

(17) Lee, S. Y.; Royston, E.; Culver, J. N.; Harris, M. T. Improved Metal Cluster Deposition on a Genetically Engineered Tobacco Mosaic Virus Template. *Nanotechnology* **2005,** *16*, S435-441.

(18) Lee, S. Y.; Choi, J.; Royston, E.; Janes, D. B.; Culver, J. N.; Harris, M. T. Deposition of Platinum Clusters on Surface-Modified Tobacco Mosaic Virus. *Journal of nanoscience and nanotechnology* **2006,** *6*, 974-981.

(19) Luckanagul, J.; Lee, L. A.; Nguyen, Q. L.; Sitasuwan, P.; Yang, X.; Shazly, T.; Wang, Q. Porous Alginate Hydrogel Functionalized with Virus as Three-Dimensional Scaffolds for Bone Differentiation. *Biomacromolecules* **2012,** *13*, 3949-3958.

(20) Luckanagul, J. A.; Metavarayuth, K.; Feng, S.; Maneesaay, P.; Clark, A. Y.; Yang, X.; García, A. J.; Wang, Q. Tobacco Mosaic Virus Functionalized Alginate Hydrogel Scaffolds for Bone Regeneration in Rats with Cranial Defect. *ACS Biomaterials Science & Engineering* **2016,** *2*, 606-615.

(21) Tibbitt, M. W.; Anseth, K. S. Hydrogels as Extracellular Matrix Mimics for 3d Cell Culture. *Biotechnol. Bioeng.* **2009,** *103*, 655-663.

(22) Nguyen, M. K.; Lee, D. S. Injectable Biodegradable Hydrogels. *Macromol Biosci* **2010,** *10*, 563-579.

(23) Amini, A. A.; Nair, L. S. Injectable Hydrogels for Bone and Cartilage Repair. *Biomed Mater* **2012,** *7*, 024105.

(24) Laurent, T. C.; Fraser, J. R. Hyaluronan. *FASEB J.* **1992,** *6*, 2397-2404.

(25) Fraser, J. R.; Laurent, T. C.; Laurent, U. B. Hyaluronan: Its Nature, Distribution, Functions and Turnover. *J. Intern. Med.* **1997,** *242*, 27-33.

المنارة للاستشارات
www.manaraa.com

(26) Dowthwaite, G. P.; Edwards, J. C. W.; Pitsillides, A. A. An Essential Role for the Interaction between Hyaluronan and Hyaluronan Binding Proteins During Joint Development. *J. Histochem. Cytochem.* **1998,** *46*, 641-651.

(27) Hardwick, C.; Hoare, K.; Owens, R.; Hohn, H. P.; Hook, M.; Moore, D.; Cripps, V.; Austen, L.; Nance, D. M.; Turley, E. A. Molecular Cloning of a Novel Hyaluronan Receptor That Mediates Tumor Cell Motility. *J. Cell Biol.* **1992,** *117*, 1343-1350.

(28) Collis, L.; Hall, C.; Lange, L.; Ziebell, M.; Prestwich, R.; Turley, E. A. Rapid Hyaluronan Uptake Is Associated with Enhanced Motility: Implications for an Intracellular Mode of Action. *FEBS Lett.* **1998,** *440*, 444-449.

(29) Cheung, W.-F.; Cruz, T. F.; Turley, E. A. Receptor for Hyaluronan-Mediated Motility (Rhamm), a Hyaladherin That Regulates Cell Responses to Growth Factors. *Biochem. Soc. Trans.* **1999,** *27*, 135-141.

(30) Gerdin, B.; Hällgren, R. Dynamic Role of Hyaluronan (Hya) in Connective Tissue Activation and Inflammation. *J. Intern. Med.* **1997,** *242*, 49-55.

(31) Reid, M. C. Viscosupplementation for Osteoarthritis: A Primer for Primary Care Physicians. *Adv. Ther.* **2013,** *30*, 967-986.

(32) Strand, V.; Conaghan, P. G.; Lohmander, L. S.; Koutsoukos, A. D.; Hurley, F. L.; Bird, H.; Brooks, P.; Day, R.; Puhl, W.; Band, P. A. An Integrated Analysis of Five Double-Blind, Randomized Controlled Trials Evaluating the Safety and Efficacy of a Hyaluronan Product for Intra-Articular Injection in Osteoarthritis of the Knee. *Osteoarthritis Cartilage* **2006,** *14*, 859-866.

(33) Strand, V.; Baraf, H. S. B.; Lavin, P. T.; Lim, S.; Hosokawa, H. A Multicenter, Randomized Controlled Trial Comparing a Single Intra-Articular Injection of Gel-

المنارة للاستشارات
www.manaraa.com

200, a new Cross-Linked Formulation of Hyaluronic Acid, to Phosphate Buffered Saline for Treatment of Osteoarthritis of the Knee. *Osteoarthritis Cartilage* **2012,** *20*, 350-356.

(34) Zheng Shu, X.; Liu, Y.; Palumbo, F. S.; Luo, Y.; Prestwich, G. D. In Situ Crosslinkable Hyaluronan Hydrogels for Tissue Engineering. *Biomaterials* **2004,** *25*, 1339-1348.

(35) Tan, H.; Chu, C. R.; Payne, K. A.; Marra, K. G. Injectable in Situ Forming Biodegradable Chitosan-Hyaluronic Acid Based Hydrogels for Cartilage Tissue Engineering. *Biomaterials* **2009,** *30*, 2499-2506.

(36) van Dijk-Wolthuis, W. N. E.; van Steenbergen, M. J.; Underberg, W. J. M.; Hennink, W. E. Degradation Kinetics of Methacrylated Dextrans in Aqueous Solution. *J. Pharm. Sci.* **1997,** *86*, 413-417.

(37) Oudshoorn, M. H. M.; Rissmann, R.; Bouwstra, J. A.; Hennink, W. E. Synthesis of Methacrylated Hyaluronic Acid with Tailored Degree of Substitution. *Polymer* **2007,** *48*, 1915-1920.

(38) Burdick, J. A.; Prestwich, G. D. Hyaluronic Acid Hydrogels for Biomedical Applications. *Adv. Mater.* **2011,** *23*, H41-H56.

(39) Chung, C.; Mesa, J.; Randolph, M. A.; Yaremchuk, M.; Burdick, J. A. Influence of Gel Properties on Neocartilage Formation by Auricular Chondrocytes Photoencapsulated in Hyaluronic Acid Networks. *J Biomed Mater Res A* **2006,** *77*, 518-525.

(40) Royston, E.; Ghosh, A.; Kofinas, P.; Harris, M. T.; Culver, J. N. Self-Assembly of Virus-Structured High Surface Area Nanomaterials and Their Application as Battery Electrodes. *Langmuir* **2008,** *24*, 906-912.

المنارة للاستشارات
www.manaraa.com

(41) Elbert, D. L.; Pratt, A. B.; Lutolf, M. P.; Halstenberg, S.; Hubbell, J. A. Protein Delivery from Materials Formed by Self-Selective Conjugate Addition Reactions. *Journal of controlled release : official journal of the Controlled Release Society* **2001,** *76*, 11-25.

(42) Khetan, S.; Burdick, J. Cellular Encapsulation in 3d Hydrogels for Tissue Engineering. *Journal of visualized experiments : JoVE* **2009**.

(43) Nair, D. P.; Podgórski, M.; Chatani, S.; Gong, T.; Xi, W.; Fenoli, C. R.; Bowman, C. N. The Thiol-Michael Addition Click Reaction: A Powerful and Widely Used Tool in Materials Chemistry. *Chem. Mater.* **2014,** *26*, 724-744.

(44) Livecchi, A. B.; Tombes, R. M.; LaBerge, M. In Vitro Chondrocyte Collagen Deposition within Porous Hdpe: Substrate Microstructure and Wettability Effects. *J. Biomed. Mater. Res.* **1994,** *28*, 839-850.

(45) Grad, S.; Zhou, L.; Gogolewski, S.; Alini, M. Chondrocytes Seeded onto Poly (L/Dl-Lactide) 80%/20% Porous Scaffolds: A Biochemical Evaluation. *Journal of Biomedical Materials Research Part A* **2003,** *66A*, 571-579.

(46) Miralles, G.; Baudoin, R.; Dumas, D.; Baptiste, D.; Hubert, P.; Stoltz, J. F.; Dellacherie, E.; Mainard, D.; Netter, P.; Payan, E. Sodium Alginate Sponges with or without Sodium Hyaluronate: In Vitro Engineering of Cartilage. *J. Biomed. Mater. Res.* **2001,** *57*, 268-278.

(47) Karande, T.; Ong, J.; Agrawal, C. M. Diffusion in Musculoskeletal Tissue Engineering Scaffolds: Design Issues Related to Porosity, Permeability, Architecture, and Nutrient Mixing. *Ann. Biomed. Eng.* **2004,** *32*, 1728-1743.

(48) Chen, J. U. N.; Park, K. Superporous Hydrogels: Fast Responsive Hydrogel Systems. *Journal of Macromolecular Science, Part A* **1999,** *36*, 917-930.

المنارة للاستشارات
www.manaraa.com

(49) Chen, J.; Park, H.; Park, K. Synthesis of Superporous Hydrogels: Hydrogels with Fast Swelling and Superabsorbent Properties. *J. Biomed. Mater. Res.* **1999,** *44*, 53-62.

(50) Sannino, A.; Netti, P. A.; Madaghiele, M.; Coccoli, V.; Luciani, A.; Maffezzoli, A.; Nicolais, L. Synthesis and Characterization of Macroporous Poly(Ethylene Glycol)-Based Hydrogels for Tissue Engineering Application. *Journal of Biomedical Materials Research Part A* **2006,** *79A*, 229-236.

(51) Spiller, K. L.; Laurencin, S. J.; Charlton, D.; Maher, S. A.; Lowman, A. M. Superporous Hydrogels for Cartilage Repair: Evaluation of the Morphological and Mechanical Properties. *Acta Biomater* **2008,** *4*, 17-25.

(52) Li, G.-Z.; Randev, R. K.; Soeriyadi, A. H.; Rees, G.; Boyer, C.; Tong, Z.; Davis, T. P.; Becer, C. R.; Haddleton, D. M. Investigation into Thiol-(Meth)Acrylate Michael Addition Reactions Using Amine and Phosphine Catalysts. *Polymer Chemistry* **2010,** *1*, 1196-1204.

(53) Pritchard, C. D.; O'Shea, T. M.; Siegwart, D. J.; Calo, E.; Anderson, D. G.; Reynolds, F. M.; Thomas, J. A.; Slotkin, J. R.; Woodard, E. J.; Langer, R. An Injectable Thiol-Acrylate Poly(Ethylene Glycol) Hydrogel for Sustained Release of Methylprednisolone Sodium Succinate. *Biomaterials* **2011,** *32*, 587-597.

(54) Smeds, K. A.; Pfister-Serres, A.; Miki, D.; Dastgheib, K.; Inoue, M.; Hatchell, D. L.; Grinstaff, M. W. Photocrosslinkable Polysaccharides for in Situ Hydrogel Formation. *J. Biomed. Mater. Res.* **2001,** *54*, 115-121.

(55) Marklein, R. A.; Burdick, J. A. Controlling Stem Cell Fate with Material Design. *Adv Mater* **2010,** *22*, 175-189.

المنارة للاستشارات
www.manaraa.com

(56) Yi, H.; Nisar, S.; Lee, S.-Y.; Powers, M. A.; Bentley, W. E.; Payne, G. F.; Ghodssi, R.; Rubloff, G. W.; Harris, M. T.; Culver, J. N. Patterned Assembly of Genetically Modified Viral Nanotemplates Via Nucleic Acid Hybridization. *Nano Lett.* **2005,** *5*, 1931-1936.

(57) Gooding, G. V., Jr.; Hebert, T. T. A Simple Technique for Purification of Tobacco Mosaic Virus in Large Quantities. *Phytopathology* **1967,** *57*, 1285.

(58) Lee, L. A.; Nguyen, Q. L.; Wu, L.; Horvath, G.; Nelson, R. S.; Wang, Q. Mutant Plant Viruses with Cell Binding Motifs Provide Differential Adhesion Strengths and Morphologies. *Biomacromolecules* **2012,** *13*, 422-431.

المنارة للاستشارات
www.manaraa.com

CHAPTER 2

IN VITRO MESENCHYMAL STEM CELL CHONDROGENESIS IN THE *IN SITU* HYBRIDIZED ROD-LIKE NANOPARTICLE-HYALURONIC ACID HYDROGEL[1]

2.1 INTRODUCTION

As mentioned earlier, driving MSC differentiation to the cartilage phenotype in a 3D scaffold is highly challenge to accomplish the cartilage repair by tissue engineering. Various factors, including growth factor supplement, cell–matrix interaction, hypoxia, and mechanical stimulus, have been emphasized as important cues promoting MSC chondrogenesis.[1,2] Particularly, the impacts of the ECM topography and biochemical cue on stem cell fate have been widely studied. The stem cell-ECM interaction *in vivo* encompasses the structural components in nanometer length scales, which in turn regulate stem cell fate along with other physical factors.[3-6] Namely, *in vivo* ECM is composed of hierarchical fibrils that consist of filamentous proteins, such as collagen, elastin, fibronectin, vitronectin, and laminin, presenting adhesive ligands on the structures in spatial organizations and nanoscale dimensions.[7] The surface nanotopography of ECM fibrils plays as a physical cue that can control stem cell behaviors.[8] That is, the cell membrane is augmented with adhesive molecules and protrusive structures in nanoscale

[1] Portions of this chapter were adapted from Maturavongsadit, P.; Luckanagul, J. A.; Metavarayuth, K.; Zhao, X.; Chen, L.; Lin, Y.; Wang, Q. *Biomacromolecules* **2016,** *17*, 1930-1938., with permission of publisher (Appendix A). Copyright (2016) American Chemical Society.

www.manaraa.com

dimensions that function in cellular probing of extracellular nanotopographical features. The cellular probing through nanoscale cell-ECM interaction initiates downstream intracellular mechanotransductive events, leading to cellular behaviors, including cell adhesion, morphology, proliferation, gene expression, and particular differentiation.[9-11] Nanoscale topographical surface and its effect on MSC chondrogenesis have been previously reported.[12-14] However, the results shown have been varying and the topography was studied only on 2D materials. It is important to investigate how specific nanotopographies provided in 3D scaffolds regulate the MSC chondrogenesis.

Another challenge to cartilage tissue engineering with MSCs is how to regulate the differentiation progression. The chondrocytes may be further pushed to hypertrophy, matrix mineralization, and ossification, also known as terminal differentiation,[15-17] lead to osteophyte or bone formation[18] instead of permanent cartilage. To date, it has been debated whether chondrogenically differentiated MSCs are programmed to progress towards terminal differentiation and bone formation.[16,19] Age-related changes in the ECM molecules or activation by inflammatory cytokines are believed to play a role in the progress of terminal differentiation.[20-22] Nevertheless, the exact activation mechanism of chondrocytes into osteophytes is not clearly understood. Type X collagen and MMP13 are the most widely used markers for chondrocyte hypertrophy.[23-25] There are also many genes and proteins have been shown to be associated with chondrocyte hypertrophy, such as osteopontin, osteocalcin, Indian Hedgehog, Runx2, VEGF, transglutaminase-2 and alkaline phosphatase.[26-30] The chondrocyte hypertrophy is ultimately developed to calcium deposition, which appears to be associated with elevated expression of hypertrophy markers.[31]

المنارة للاستشارات
www.manaraa.com

In previous chapter, TMV1cys was selected to incorporate in 3D scaffold materials due to providing nanoscale surface topography, attachment sites for backbone polymers, high stability, and uniformity. We showed a simple method of modification and functionalization of HA scaffold materials with TMV1cys by cross-linking method. Herein, we expected that the covalent incorporation of TMV in 3D hydrogels could support and accelerate chondrogenesis of MSCs. Various types of rod-like nanoparticles, including arginine-glycine-aspartic acid (RGD)-mutant TMV (TMV-RGD1), and gold nanorods (GNRs), were further introduced into the HA-based hydrogels in similar manner to TMV1cys in order to understand the impact of biochemistry and nanoscale topography displayed by rod-like nanoparticles in 3D scaffold materials on MSC chondrogenesis. TMV-RGD1 is TMV that genetically modified to display spatial RGD motifs, cell adhesive sequences, on the surface structure. The GNRs in this study were synthesized to provide similar dimensions to TMV (300 nm of length and 20 nm of diameter) except no surface nanotopographical features. We hypothesized that nanoscale topography and biochemistry displayed by rod-like nanoparticles synergistically promoted chondrogenesis and inhibited hypertrophy, matrix mineralization, and ossification of *in vitro* encapsulated MSCs.

2.2 RESULTS AND DISCUSSION

2.2.1 Effect of the In Situ TMV1cys-Based HA Hydrogels on In Vitro Chondrogenesis of MSCs

TMV, providing nano-topographic surface in the spatial organizations, has been used as an effective scaffolding material that could accelerate bone differentiation of BMSCs in 2D and 3D scaffold materials based on our previous works.[32,33] It could

المنارة للاستشارات
www.manaraa.com

upregulate the BMP-2 gene expression of the cells on 2D materials within 8 h and promote alkaline phosphatase activity and calcium phosphate deposition around the cells in 3D alginate scaffold on day 3 and 6, respectively.[32] One possible interpretation of this study is that the topographical features on TMV play an important role in the accelerated osteogenic differentiation. Cartilage and bone differentiation of stem cells have shown some common potent induction proteins, such as BMP-2, BMP-6, and BMP-7.[34] The result from several studies indicated that BMP-2 was an effective inducer of mesenchymal stem cell differentiation toward chondrocytes.[35,36] It regulates chondrogenic development of mesenchymal progenitors,[37] and stimulates the synthesis of chondrocyte matrix components by human articular chondrocytes *in vitro*.[38,39] In this regard, the development of 3D scaffold materials with TMV was considered to determine enhanced chondrogenesis events of BMSCs.

We firstly investigated the BMP-2 gene expression, which is an indication of early stage chondrogenesis, in the hydrogels after 8 h, 2, and 7 days of chondrogenic culture (Figure 2.1). Gene expression was normalized by BMSCs before encapsulation, and GAPDH was used as a housekeeping gene. BMP-2 was expressed at significantly higher levels in BMSCs encapsulated in the TMV1cys-crosslinked HA hydrogels (hereafter denoted as TMV-Cys-HA) compared to BMSCs encapsulated in the HA hydrogels after 8 h and 7 days. This result agrees with our previous studies by culturing BMSCs on the TMV-based 2D scaffolds. However, at day 2, no significantly higher level of BMP-2 expression was observed for BMSCs in the TMV-Cys-HA hydrogels compared to the HA hydrogels.

المنارة للاستشارات
www.manaraa.com

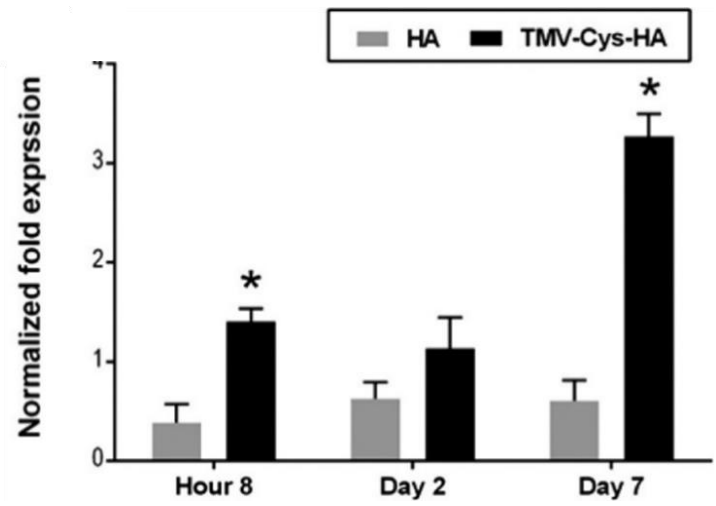

Figure 2.1. RT-qPCR analysis of BMP-2 expression in the BMSCs encapsulated in the hydrogels under chondrogenic conditions for 8 h, 2, and 7 days. The values expressed are means ± SEM, $n = 3$ with three repeated experiments. *Paired equal variance Student t test, $p < 0.05$.

Immunohistostaining analysis for type II collagen, which is a later-stage chondrogenic marker, demonstrated significant differences between the TMV-Cys-HA hydrogels and HA hydrogels over time (14, 21, and 28 days). The differentiated BMSCs encapsulated in the TMV-Cys-HA hydrogels produced concentrated and well-defined chondrogenic extracellular matrix (ECM) in the periphery of the cells as indicated by staining with type II collagen antibody. Especially, after 28 days of culturing, the cells encapsulated in the TMV-Cys-HA constructs produced a strong type II collagen network throughout the hydrogels (Figure 2.2A, C). Sirius-Red staining demonstrated the accumulation of all types and species of collagen present in chondrogenic ECM. In the TMV-Cys-HA hydrogels, the stain was primarily distributed inside and around BMSCs in the samples, and was significantly higher than the stain in the HA hydrogels after 28 days of culture (Figure 2.2B, D). The nondifferentiated BMSCs encapsulated in the TMV-Cys-

المنارة للاستشارات
www.manaraa.com

HA and HA hydrogels at day 0 were used as a negative control which showed no existence of type II collagen and total collagen (Figure 2.2A, B).

The biomechanical property of the BMSCs encapsulated hydrogels was accessed using rheological analysis. The linear equilibrium modulus plateau (G_e) of the hydrogels was calculated from the average of storage modulus (G') over frequency ranging from 0.1 to 10 rad/s at constant strain amplitude of 2%. At day 0, the G_e in the TMV-Cys-HA hydrogels was significantly lower than that in the HA hydrogels. The average G_e of the TMV-Cys-HA and HA hydrogels were 59 and 66 Pa, respectively. Both hydrogels showed a trend of increasing the G_e over 28 days as compared with day 0, 14), indicating that cell-secreted ECM might contribute to the increase in the mechanical property of the hydrogels. A significant increase in the G_e was observed in the TMV-Cys-HA hydrogels compared to the HA hydrogels. Notably, the G_e for the TMV-Cys-HA scaffolds doubled, whereas the G_e for the HA scaffolds increased by 1.3-folds after 28 days of culture (Figure 2.2E). Combined with the results of collagen accumulation, it indicated that the increase in the mechanical property of the hydrogels might be contributed by cell-secreted ECM. One possible mechanism behind the enhanced chondrogenesis event of BMSCs in the TMV-based HA hydrogels likely involves the increase in the level of BMP-2 in the scaffold as a result of the interactions between the cells and TMV nanoparticles.

المنارة للاستشارات
www.manaraa.com

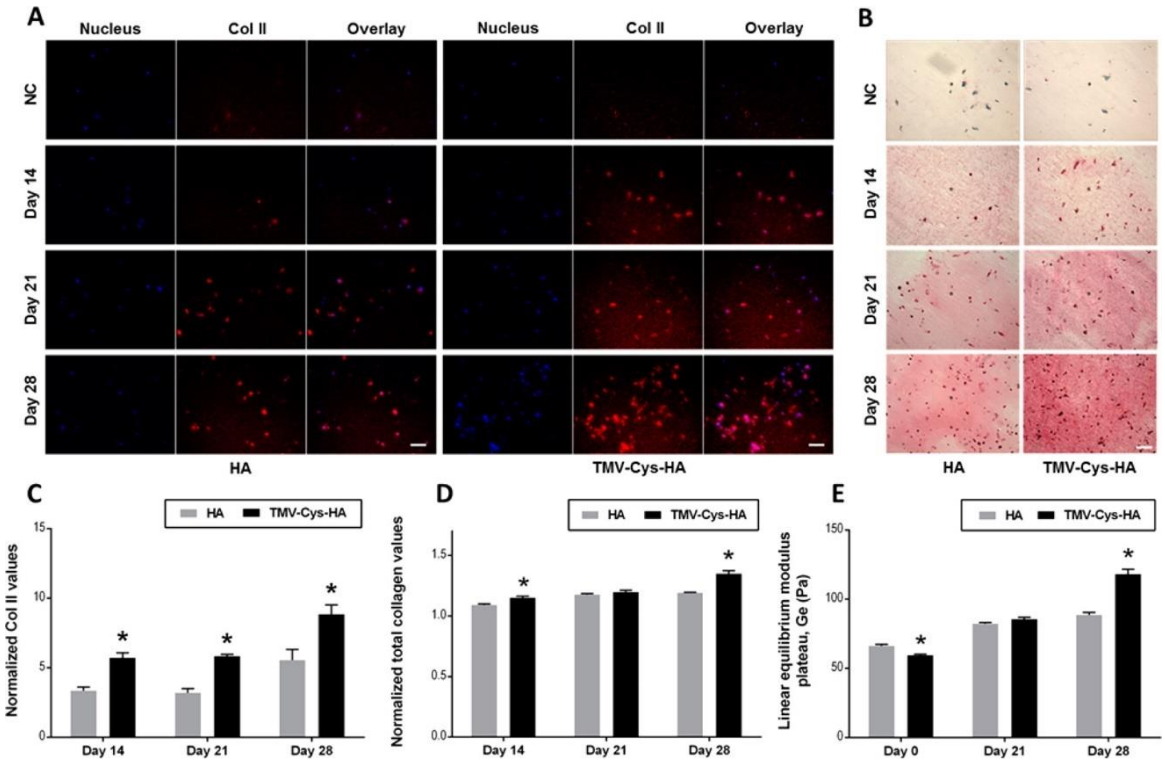

Figure 2.2. The results of *in vitro* chondrogenesis of MSCs in the *in situ* TMV1cys-based HA hydrogels. (A) Confocal images of nondifferentiated and differentiated BMSCs in the hydrogels under chondrogenic conditions stained for nucleus (blue) and type II collagen (red) after 0, 14, 21, and 28 days. All images share the same scale bar: 50 μm. (B) Histochemical staining for total collagen content of nondifferentiated and differentiated BMSCs in the hydrogels under chondrogenic conditions after 0 day, 14, 21, and 28 days. All images share the same scale bar: 50 μm. (C, D) Quantification of the signal intensities of type II collagen and total collagen shown in A and B, respectively. The intensity of type II collagen and total collagen were normalized to the intensity of nucleus signal and non-collagenous protein signal, respectively. Each plot expressed mean ± SEM, $n = 3$ with two repeated experiments. *Paired equal variance Student t test, $p < 0.05$. (E) Biomechanical properties of the BMSCs encapsulated hydrogels after 0, 14, and 28 days in chondrogenic conditions. Each plot expressed mean ± SEM, $n = 3$ with two repeated experiments. *Paired equal variance Student's t test, $p < 0.05$.

2.2.2 Effect of the In Situ TMV-RGD1-Based HA Hydrogels on In Vitro Chondrogenesis of MSCs

The effect of biochemical cues provided by TMV in the *in situ* HA hydrogels on MSC chondrogenesis was further investigated in this study. Previously, we have demonstrated that the incorporated biochemical cues to TMV surfaces could alter cell

المنارة للاستشارات
www.manaraa.com

responses.[40,41] For instance, TMV chemically modified RGD peptide as a 2D TMV-based material showed increased cell binding capacity, further promoted the proliferation and osteogenic differentiation of BMSCs. It was possible that RGD ligand spacing on the surface of TMV was appropriated, 2–4 nm, to offer a polyvalent ligand clustering effect for enhanced cell receptor signaling.[41] Additionally, the coupling of biochemical cues to scaffold polymers was shown to promote cell responses. Poly(amidoamine) (PAMAM) dendrimers modified with bioactive molecules, such as RGD, Tyr-Ile-Gly-Ser-Arg (YIGSR), and Ile-Lys-Val-Ala-Val (IKVAV), as coating polymeric materials demonstrated increased cell viability, cell adhesion, and enhanced neuron differentiation of adrenal pheochromocytoma (PC12) cells.[42] Based on these studies, we sought to incorporate TMV-RGD1, concentration of 0.1% w/v, into *in situ* TMV-Cys-HA to form the new *in situ* TMV-hybridized HA hydrogels (hereafter denoted as TMV-Cys-RGD-HA) that could further alter MSC chondrogenesis. The TMV-Cys-HA at TMV1cys concentration of 0.2% w/v (hereafter denoted as 2X TMV-Cys-HA) was also generated for comparison purpose (the formulations in this study are shown in Table 2.1). The performance of MSC chondrogenesis in these hydrogels was investigated through the accumulation of type II collagen and total collagen, and the mechanical properties.

Table 2.1. Formulation of HA, TMV1cys-based HA, and TMV-RGD1-based HA hydrogels.

Formulation	40-50% DM MeHA	TMV1cys	TMV-RGD1	0.5 M DTT (molar ratio)	Solvent, pH system
HA	5%	-	-	4Ene:1SH	PBS, pH 7.4
TMV-Cys-HA	5%	0.1%	-	4Ene:1SH	PBS, pH 7.4
2X TMV-Cys-HA	5%	0.2%	-	4Ene:1SH	PBS, pH 7.4
TMV-Cys-RGD-HA	5%	0.1%	0.1%	4Ene:1SH	PBS, pH 7.4

المنارة للاستشارات
www.manaraa.com

The analysis of total collagen revealed that the accumulation of collagen in TMV-Cys-RGD-HA was significantly higher than those in HA, TMV-Cys-HA and 2X TMV-Cys-HA after 28 days of culture (Figure 2.3A, B), and no significant enhancement of total collagen deposition was observed in 2X TMV-Cys-HA compare to TMV-Cys-HA. The accumulation of type II collagen in these hydrogels showed significantly different after 14 days of culture; that is, TMV-Cys-RGD-HA and 2X TMV-Cys-HA could significantly promote the type II collagen deposition higher than HA and TMV-Cys-HA. At later time points, TMV-Cys-HA and 2X TMV-Cys-HA however showed no significantly difference in promotion of MSC chondrogenesis. Meanwhile, TMV-Cys-RGD-HA showed most significant enhancement of the accumulation throughout the culturing time (Figure 2.3C, D). Correspondingly, the mechanical property of TMV-Cys-RGD-HA at day 28 showed dramatical increase 5 times from day 0, and significantly higher than other hydrogels, approximately 2.5, 2 and 0.5 times of HA, TMV-Cys-HA, and 2X TMV-Cys-HA, respectively (Figure 2.3E). Based on this finding, it indicated that TMV-RGD1 could synergistically promote MSC chondrogenesis in TMV-Cys-HA better than purely TMV1cys.

The results of TMV-RGD1 in synergistic promotion of MSC chondrogenesis are agreement to many other research groups' reports, which have similarly shown that the incorporated RGD ligands could enhance MSC chondrogenesis. For example, PEG hydrogels modified with RGD ligands demonstrated increased viability and enhanced cartilage specific gene expression and matrix synthesis in the presence of mechanical stimulation.[43] It was also found that combination of cartilaginous ECM molecules to the 3D polymer scaffolds could regulate MSC chondrogenesis.[44-46] The conjugation of type I

المنارة للاستشارات
www.manaraa.com

collagen in PEG scaffolds helped to maintain chondrogenic phenotype and promote cartilage repair.[43] Varying ratios of PEG polymer incorporating to ECM molecules, including HA, and chondroitin sulfate, could produce different quantities of proteoglycan and collagen type II deposition mimic the different zones of native articular cartilage.[46]

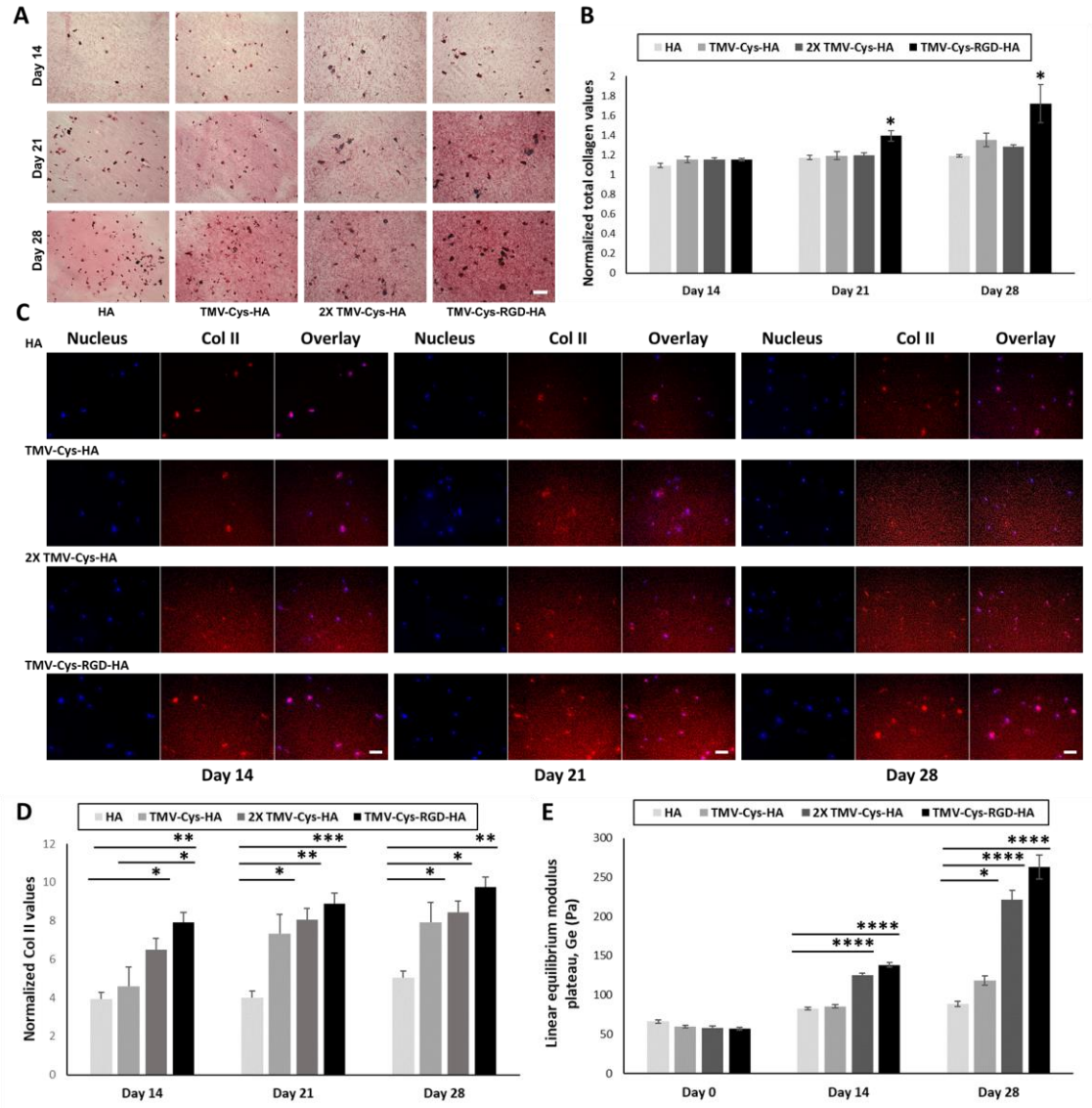

Figure 2.3. The results of *in vitro* chondrogenesis of MSCs in the *in situ* TMV-RGD1-based HA hydrogels compared to the *in situ* TMV1cys-based HA hydrogels. (A) Histochemical staining for total collagen content of differentiated BMSCs in the hydrogels under chondrogenic conditions after 14, 21, and 28 days. All images share the same scale bar: 50 µm. (B) Quantification of the signal intensities of total collagen shown in A. The intensity of total collagen was normalized to the intensity of non-collagenous protein

المنارة للاستشارات
www.manaraa.com

signal. Each plot expressed mean ± SEM, $n = 3$ with one repeated experiments. (C) Confocal images of differentiated BMSCs in the hydrogels under chondrogenic conditions stained for nucleus (blue) and type II collagen (red) after 14, 21, and 28 days. All images share the same scale bar: 50 μm (D) Quantification of the signal intensities of type II collagen shown in C. The intensity of type II collagen was normalized to the intensity of nucleus signal Each plot expressed mean ± SEM, $n = 3$. (E) Biomechanical properties of the BMSCs encapsulated hydrogels after 0, 14, and 28 days in chondrogenic conditions. Each plot expressed mean ± SEM, $n = 3$ with one repeated experiments. Statistics: ANOVA with Tukey's multiple comparisons tests, $*p < 0.05$, $**p < 0.01$, $***p < 0.001$, $****p < 0.0001$.

2.2.3 Effect of the In Situ GNR-Based HA Hydrogels on In Vitro Chondrogenesis of MSCs

We have confirmed that the rod-like TMV bionanoparticles play a critical role in directing MSC chondrogenesis in 3D scaffolds, and we hypothesized that the phenomenon was initially through the interaction of MSCs to spatial-controlled nanotopography offered by the surface of TMV, which mimic the native extracellular matrix proteins. However, it may be possible that the promotion is originated by the symmetry of rod-like structures that help to support the differentiation of MSCs. In this way, we sought to create the similar rod-like structure to TMV, but lacked the spatial controlled surface nanotopography. GNRs were selected as the mimicked rod-like TMV, and incorporated into the *in situ* HA-based hydrogels to study the MSC chondrogenesis performance.

2.2.3.1 Formation of the In Situ GNR-Based HA Hydrogels

GNRs were first synthesized to obtain the mimicking dimension of TMV. Based on the characterization by transmission electron microscopy (TEM), GNRs showed the length of 300-400 nm and the width of 18-20 nm which are similar to the previous protocol report[47] and the TMV structure as expected (as shown in Figure 2.4). The cetyltrimethylammonium bromide (CTAB), a surface stabilizer of GNRs,[47,48] required to

المنارة للاستشارات
www.manaraa.com

be removed before using due to interruption of hydrogel formation. After removing the CTAB by centrifugation at 6000 rpm and replacing with fresh PBS for several times, the surface of synthesized GNRs was then treated with DTT, thiol molecules, to inhibit the aggregation of GNR particles. The excess of DTT must be removed and washed for several times to avoid unwanted DTT react to MeHA during hydrogel formation step. The *in situ* GNR-based HA hydrogels (here after denoted as GNR-HA) were then formulated in the same manner to previous mentioned. It should be noted that there was no expected thiol-ene "click" reaction occurring between GNRs and MeHA. Hence, the *in situ* wide-type TMV-based HA hydrogels (denoted as TMV-HA) were formulated and used as comparison purpose. HA hydrogels were also generated and used as the controls (Table 2.2).

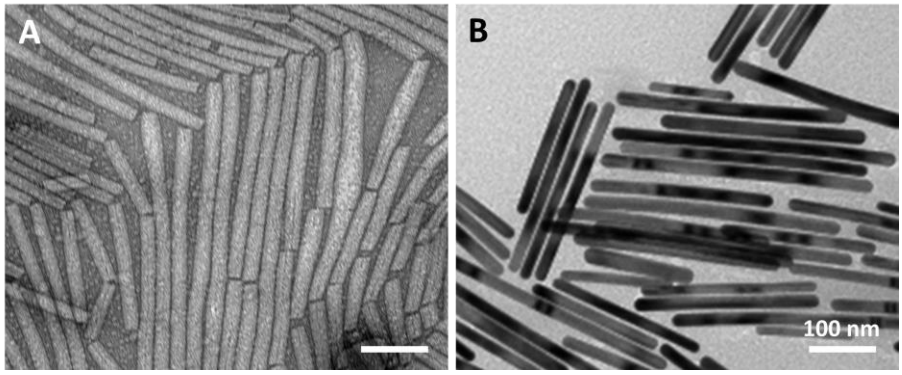

Figure 2.4. Transmission electron micrograph of wide-type TMVs (A) and GNRs (B).

Table 2.2. Formulation of HA, wide-type TMV-based HA, and GNR-based HA hydrogels.

Formulation	40-50% DM MeHA	TMV-wt	GNR	0.5 M DTT (molar ratio)	Solvent, pH system
HA	5%	-	-	2Ene:1SH	PBS, pH 7.4
TMV-HA	5%	0.1%	-	2Ene:1SH	PBS, pH 7.4
GNR-HA	5%	-	0.1%*	2Ene:1SH	PBS, pH 7.4

* The amount of GNRs was calculated based on ICP-MS results.

المنارة للاستشارات
www.manaraa.com

2.2.3.2 Physical Properties of the In Situ GNR-Based HA Hydrogels

Before moving forward to *in vitro* study, it is important to determine how GNRs impact on the physical properties of HA hydrogels which are crucial for MSC survival and responses. The microstructure of GNR-HA was determined by SEM images and compared to TMV-HA and HA systems (Figure 2.5A). The similarities in porosity, and interconnectivity were observed in all hydrogels. That is, they showed high density of macropores which were well-interconnected with thin layers of compacted outer edge. However, they were some differences in ranges of pore size. TMV-HA and GNR-HA showed a similar range of pore sizes from 100-150 µm, while the HA hydrogels showed a wider range of pore size from 50-150 µm. The exterior surfaces of all hydrogels were rough, folded, and dense. The mechanical properties of these hydrogels were also investigated using DHR-3 Rheometer (Figure 2.5B). Incorporation of GNR in HA hydrogels showed no impact to complex modulus of the HA hydrogels, which were approximately 3000 Pa. However, incorporation of TMV-wt into HA scaffolds lead to the lower complex modulus (1800 Pa), which was similar to the mechanical property results observed in TMV-Cys-HA (data was not shown). Bovine serum albumin (BSA) protein was selected as a protein model to assess the diffusibility of the hydrogels. We found that the BSA diffusibility of in GNR-HA was not significantly different compared to HA hydrogels, while the BSA diffusibility in TMV-HA was significantly higher than it in HA hydrogels (Figure 2.5C). Moreover, we observed that all hydrogels had water content more than 90%, and showed high swelling ratio. The statistically lower swelling ratio was observed for GNR-HA compared to TMV-HA hydrogels (Figure 2.5D, E). Taken together, we can see that the incorporation of GNRs into HA hydrogels provided no significant

المنارة للاستشارات
www.manaraa.com

impact to the overall physical properties contrast to the incorporation of TMV-wt and its mutants (the results are shown in previous chapter).

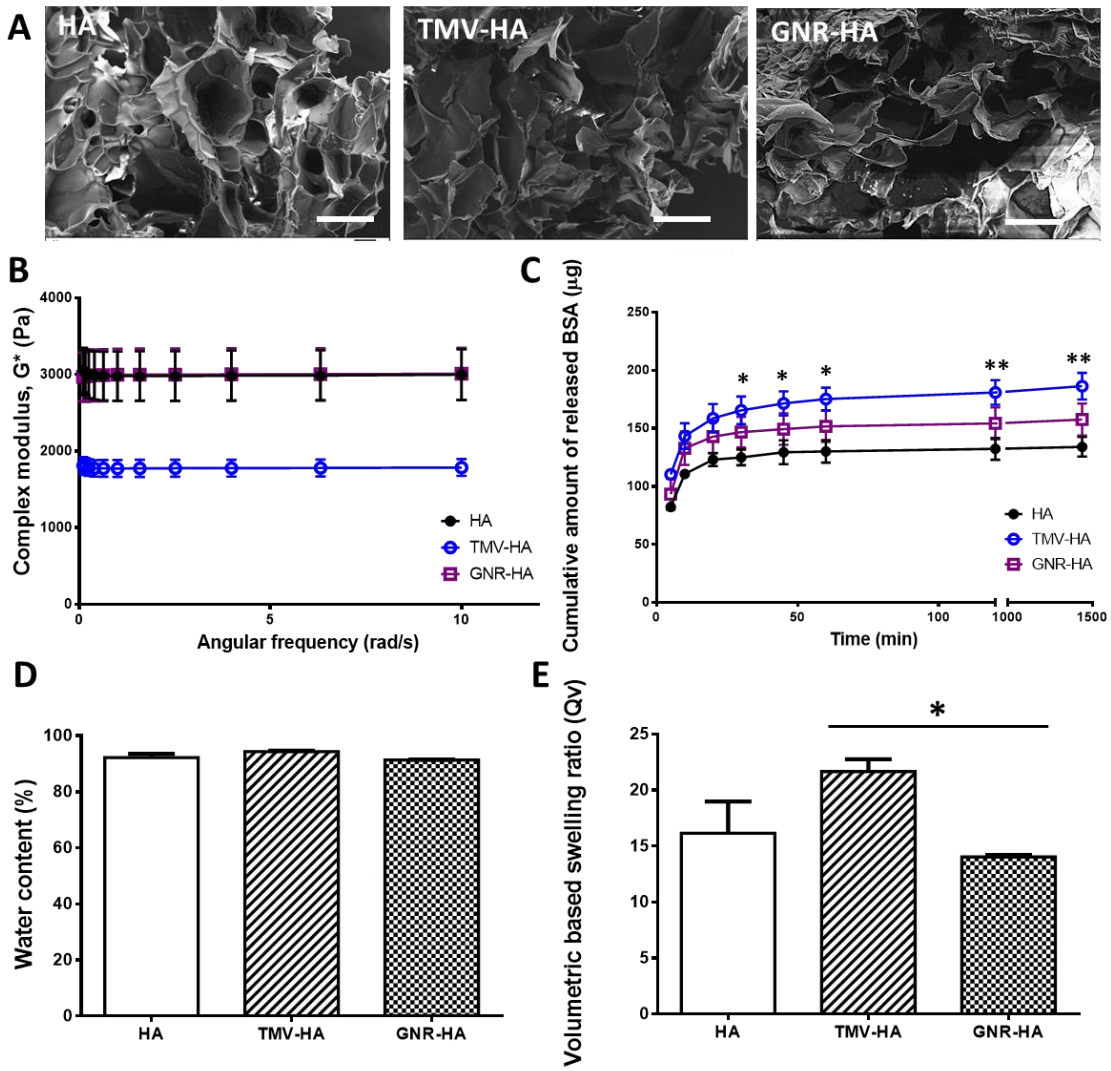

Figure 2.5. Physical properties of the *in situ* GNR-based HA hydrogels compared to HA and TMV-based HA hydrogels. (A) Exterior and cross-section SEM micrographs of the *in situ* HA, TMV-based HA, and GNR-based HA hydrogels after freeze-drying. Scale bars for all images: 100 µm. (B) Average complex modulus of the hydrogels after gelation for 2 days (n = 3). (C) BSA release profile of the hydrogels showing the cumulative amount of BSA released from the hydrogels to supernatant for 24 h (n = 3). Statistics: ANOVA with Tukey's multiple comparisons tests, *$p < 0.05$, **$p < 0.01$, ***$p < 0.001$, ****$p < 0.0001$. (D) Water content of the hydrogels after being immersed in PBS for 2 days. (E) Volumetric-based swelling ratio of the hydrogels (n = 4). Statistics: ANOVA with Tukey's multiple comparisons tests, *$p < 0.05$, **$p < 0.01$, ***$p < 0.001$, ****$p < 0.0001$.

المنارة للاستشارات
www.manaraa.com

2.2.3.3 In Vitro MSC chondrogenesis in the In Situ GNR-Based HA Hydrogels

For application in MSC chondrogenesis, the biocompatibility of GNR-HA was validated using CellTiter-Blue (CTB) cell viability assay, fluorometric method measuring the metabolic capacity of cells (Figure 2.6). After culturing in primary media for 7 days, it demonstrated that more than 70 % of MSCs were viable in GNR-HA similar to in HA, TMV-HA. Nevertheless, the compromised viability of the encapsulated cells was occurred during first few days in 3D scaffolds due to less of oxygen and nutrients compared to that in 2D culture.[49]

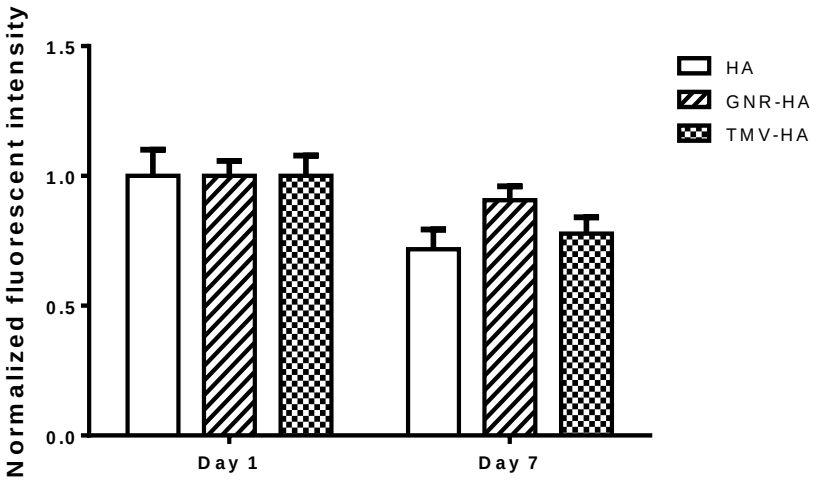

Figure 2.6. Celltiter-Blue assay of viable MSCs encapsulated in the hydrogels after 7 days of culturing in primary media (n = 3). Statistics: ANOVA with Tukey's multiple comparisons tests, *$p < 0.05$, **$p < 0.01$, ***$p < 0.001$, ****$p < 0.0001$.

The chondrogenesis performance of differentiated MSCs in the GNR-HA was evaluated by measuring collagen accumulation (total collagen and type II collagen) and mechanical property of the cell-encapsulated hydrogels. We found that it was very difficult to quantify collagen accumulation using immunohistological staining of the GNR-HA hydrogel-embedded paraffin sections. That is, unlike other hydrogels, the cell-encapsulated GNR-HA hydrogels became pink and very brittle after paraffin embedding, resulting in a

المنارة للاستشارات
www.manaraa.com

failure to section the hydrogels. The cryo-sectioning technique can be an alternative for the *in vitro* GNR-HA, however, it was not accessed in this study. The mechanical property of the cell-encapsulated GNR-HA was further measured after 28 days of chondrogenic cultures. No significantly promoted complex modulus was observed in the cell-encapsulated GNR-HA compared to that in the cell-encapsulated HA hydrogels. In contrast, the average complex modulus of the *in vitro* TMV-HA hydrogels showed significantly higher than that in GNR-HA (Figure 2.7A).

The impact of incorporated GNRs in HA-based scaffolds on chondrogenic differentiation progression was also investigated. As described earlier that the chondrogenic-differentiated MSCs are possible to develop to unwanted hypertrophy stage, the alkaline phosphatase (ALP) activity and calcium deposition, common hypertrophy markers, were quantified in the hydrogels after 28 days. The results of ALP activities demonstrated that the differentiated MSCs in GNR-HA and HA hydrogels secreted ALP significantly higher than that in TMV-HA (Figure 2.7B). Although calcium deposition was hardly quantified in all the hydrogels due to the background color, it slightly showed the calcium deposited spots spread out throughout in the matrix of GNR-HA and HA samples, but not in TMV-HA (Figure 2.7C).

Based on these results, it seems to us that GNRs incorporated HA hydrogels did not promote the MSC chondrogenesis, contrast to the results observed in TMV-incorporated or TMV-crosslinked HA hydrogels. It is possible that the surface of GNRs is covered with DTT providing no any special surface nanotopography. Conversely, the TMV surface displays 2,130 identical coat proteins in the spatial organization which could offer the cell surface interaction and protein absorption. However, in this study, to firmly conclude the

المنارة للاستشارات
www.manaraa.com

impact of nanoscale surface topography by TMV compared to similar rod-like nanostructure, *i.e.* GNRs, in 3D scaffolds on MSC chondrogenesis, several experiments should be further evaluated, such as type II, I, X collagen and chondroitin sulfate accumulation.

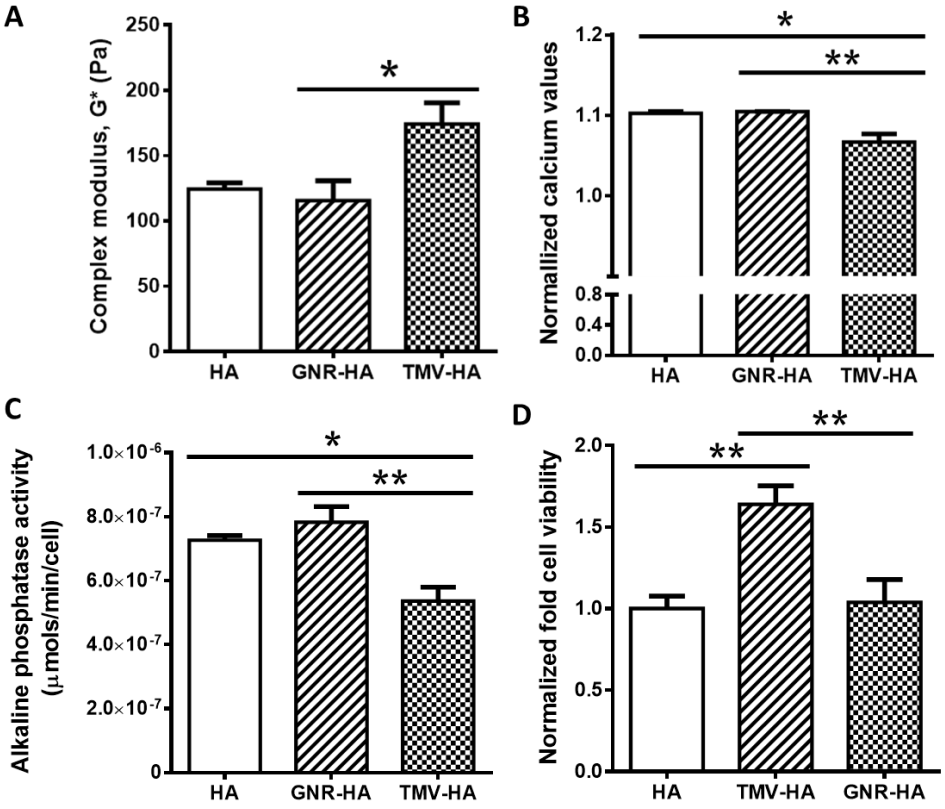

Figure 2.7. The results of *in vitro* chondrogenesis of MSCs in the *in situ* GNR-based HA hydrogels compared to the *in situ* HA and TMV-based HA hydrogels. (A) Biomechanical properties of the differentiated MSCs hydrogels after 28 days in chondrogenic conditions. Each plot expressed mean ± SEM, $n = 3$. (B) Quantification of the signal intensities of calcium deposition of differentiated MSCs in the hydrogels under chondrogenic conditions after 28 days. The intensity of calcium in each sample was normalized to the intensity of calcium signal in negative control (HA hydrogel without cells). Each plot expressed mean ± SEM, $n = 3$ with one repeated experiments. (C) ALP activities of differentiated MSCs in the hydrogels under chondrogenic conditions after 28 days. ALP activities were performed by pnitrophenyl phosphate assay. Each plot expressed mean ± SEM, $n = 6$. (D) Celltiter-Blue assay of viable differentiated MSCs encapsulated in the hydrogels after 28 days in chondrogenic conditions. The viability of each sample was normalized to the viability of cells in HA. Each plot expressed mean ± SEM, $n = 6$. Statistics: ANOVA with Tukey's multiple comparisons tests, *$p < 0.05$, **$p < 0.01$, ***$p < 0.001$, ****$p < 0.0001$.

المنارة للاستشارات
www.manaraa.com

2.3 CONCLUSIONS

In situ TMV-based HA hydrogels supported significantly greater chondrogenesis in terms of compositions and biomechanical properties compared to the HA hydrogels. The introduction of other rod-like nanoparticles into HA hydrogels was also studied which aims for understanding the role of topographical features of nanoparticles in chondrogenesis process. The incorporation of TMV-RGD1 in HA hydrogels further promoted *in vitro* chondrogenesis of BMSCs. Meanwhile, the incorporation of gold nanorods, which provide similar size and shape to TMV, in HA hydrogels seemed likely to no promotion of the *in vitro* chondrogenesis. This implied that the influences of nanoscale topography and biochemistry provided by TMV and TMV-RGD1 play critical roles in directing encapsulated MSC chondrogenesis. Currently, the *in vivo* studies have been conducted to test the biocompatibility and *in vivo* cartilage formation using TMV-incorporated injectable hydrogels.

2.4 MATERIALS AND METHODS

2.4.1 Synthesis of Rod-Like Nanoparticles and Rod-Like Nanoparticle-HA Hydrogels

TMV-wt, TMV1cys and TMV-RGD1 were isolated from infected tobacco leaves following previously established protocols.[50,51] Gold nanorods (GNRs) were synthesized following previously established protocol.[47] After removing the CTAB by centrifugation at 6000 rpm for several times, The CTAB surfactant-directing agents on surface of synthesized GNRs were removed by centrifugation at 6000 rpm and replacing with PBS for several times. The surface of synthesized GNRs was then treated with DTT, thiol

المنارة للاستشارات
www.manaraa.com

molecules, for 30 min with stirring. The excess of DTT was removed and washed by centrifugation at 6000 rpm for several times. The structure integrity of TMV particles and GNRs were verified by TEM electron micrograph.

To form the rod-like nanoparticles based HA hydrogels (TMV-Cys-HA, 2X TMV-Cys-HA, TMV-Cys-RGD-HA, TMV-HA and GNR-HA), MeHA polymers with 40–50% degree of modification were dissolved in a PBS at 5 wt% concentration, and TMV1cys, TMV-RGD1, TMV-wt, or GNRs in potassium phosphate buffer was added to make a final concentration of 0.1 or 0.2 wt% (the detailed formulations are in Table 2.1 and 2.2). A cross-linking agent, dithiotreitol (DTT), was then added at a molar ratio of thiol/ene = 1:4 or 1:2 (Table 2.1 and 2.2). For comparison purposes, the HA hydrogels were also synthesized by the same procedure, except adding the rod-like nanoparticle solution.

2.4.2 Characterization of GNR-Based HA Hydrogels

2.4.2.1 Microstructure Analysis

Microstructure of the hydrogels was characterized using Scanning Electron Microscope (SEM). The hydrogel samples were lyophilized, then cross-sectioned and mounted on metal stubs with carbon tape. The samples were sputtered coated with gold/palladium for 30 sec on a Denton Desk II sputter coater with global rotation and tilt. The surfaces of the gold/palladium-coated hydrogels samples were observed at 5-8 random locations per sample (n = 3) on a Zeiss Ultraplus Thermal Field Emission SEM at 10 kV.

المنارة للاستشارات
www.manaraa.com

2.4.2.2 Mechanical Properties

Complex modulus (G*) of the hydrogels was determined using a DHR-3 rheometer (TA Instruments) with 12 mm diameter parallel-plate geometry at 25 °C. The hydrogels were prepared previously described by using PBS as the medium. After gelation for 2 days, the samples were prepared and tested following our previous protocol.[52]

2.4.2.3 Swelling Properties

The hydrogels (50 μL) were prepared previously described by using PBS as the medium. After gelation, the hydrogels were swollen in PBS for 2 days and were then blotted to remove excess water and weighed to obtain the swollen hydrogel mass (M_s). The dry mass of these hydrogels (M_d) was then determined after drying by the lyophilization method. Water content, the mass-based swelling ratio (Q_m), and the volumetric-based swelling ratios (Q_v) were calculated based on the equations reported in the previous literature.[53]

2.4.2.4 Protein Release Profile

To study the protein release profile and protein accumulation within the hydrogels, bovine serum albumin (BSA) was chosen as the model solute for diffusion. The experimental procedure was adapted from the literature.[54] Briefly, the hydrogels (2 mm thickness, 4 mm diameter) were immersed in BSA solution (1 mg/mL) at room temperature for 30 h to achieve uniform protein loading.[54,55] After that, all of BSA solution was removed, and the BSA-loaded hydrogels were immersed in PBS. All supernatant was collected and replaced by fresh PBS at 5, 10, 15, 30, 45, 60, 90, 120 min, and 24 h. A

المنارة للاستشارات
www.manaraa.com

Coomassie (Bradford) protein assay (Thermo Scientific) was used to quantify the amount of released BSA in the supernatant following the manufacturer's protocol.

2.4.3 Bone Marrow Stem Cells (BMSCs) Isolation and Maintenance

Primary BMSCs were isolated from the bone marrow of young adult 160–180 g male Sprague–Dawley rats (Charles River Laboratories). The procedures were performed in accordance with the guidelines for animal experimentation by the Institutional Animal Care and Use Committee, School of Medicine, University of South Carolina. Cells were maintained in complete primary media (Dulbecco's Modified Eagle's Medium (DMEM) supplemented with 10% fetal bovine serum (FBS)), kept at 37 °C in a CO_2 incubator with 5% CO_2/95% air, and passaged no more than seven times after isolation.

2.4.4 In Situ Cell Encapsulation and Culture

The hydrogels were prepared previously described except that the preparation occurred under sterile condition and prewarmed complete DMEM media was used to dissolve the polymer. TMV1cys, TMV-RGD1, TMV-wt and GNRs were filtered to remove any pathogens before mixing. All other components including 5 M NaOH and 0.5 M DTT in PBS were also filtered with 0.2 μm PES membranes. BMSCs passage 3 or 4 were harvested from the tissue culture plate after reaching 80% confluency. The cells were then mixed with the mixture of prewarmed hydrogel in DMEM media at concentration of 10^6cells/mL right after addition of DTT. The cells–hydrogel mixture (150 μL) was then pipetted into each Transwell (Corning) that was inserted and anchored in a 24-well tissue culture plate and incubated at 37 °C in a CO_2 incubator with 5% CO_2/95% air. After 6 h of

المنارة للاستشارات
www.manaraa.com

initial incubation, chondrogenic media (800 μL) was added into each well. The media was exchanged every 2 days for the entire experimental period.

Chondrogenic supplemented media comprised of DMEM (Hyclone, Thermo scientific), 1% fetal bovine serum (Atlanta biologicals), 1× penicillin-streptomycin-amphotericin B (from MP Biomedicals, 100 U/mL penicillin and 1000 U/mL streptomycin solution, 0.25 μg/mL amphotericin B), 100 nM dexamethasone (Enzo Life Sciences), 10 ng/mL TGF β1 (R&D System), 50 μg/mL ascorbic acid (Sigma-Aldrich), 1 mM sodium pyruvate (Hyclone, Thermo scientific), 1 × ITS^{+3}(from Sigma-Aldrich, contains 1.0 mg/mL insulin from bovine pancreas, 0.55 mg/mL human transferrin (substantially iron-free), 0.5 μg/mL sodium selenite, 470 μg/mL linoleic acid, 470 μg/mL oleic acid, and 50 mg/mL bovine serum albumin), 2 mM l-glutamine (Hyclone, Thermo scientific), and 40 μg/mL l-proline (Sigma-Aldrich).

2.4.5 BMP-2 Gene Expression Analysis

The hydrogels were harvested and analyzed for BMP-2 gene expression after 8 h, 2 and 7 days in chondrogenic culture. The sample was rinsed twice with PBS buffer and stabilized in RNAlater solution (protecting RNA from degradation) overnight at 4 °C. The sample was then lysed by high-speed homogenizer at 20000 rpm in RNAzol (Sigma-Aldrich) at room temperature for 5 min. The total RNA was extracted according to the manufacturer's protocol. Briefly, the quality and quantity of the extracted total RNA were analyzed using Experion RNA StdSens Analysis Kit (Bio-Rad) and was reverse transcribed to cDNA using qScript cDNA Synthesis kit (Quanta Biosciences). RT-qPCR (iQ5 real-time PCR detection system Bio-Rad Laboratories) was then performed by the method

المنارة للاستشارات
www.manaraa.com

described as 45 cycles of PCR (95 °C for 20 s, 58 °C for 15 s, and 72 °C for 15 s), after initial denaturation step of 5 min at 95 °C, by using 12.5 μL of iQ5 SYBR Green I Supermix 2 pmol/mL of each forward and reverse primers and 0.5 μL cDNA templates in a final reaction volume of 25 μL. Glyceraldehyde 3-phosphate dehydrogenase (GAPDH) was used as the housekeeping gene. Data collection was enabled at 72 °C in each cycle and CT (threshold cycle) values were calculated using the iQ5 optical system software version 2.1. The expression levels of differentiated genes and undifferentiated genes were calculated using Pfaffl's method for group-wise comparison and statistical analysis of relative expression results in real-time PCR, using GAPDH as the reference gene. Quantification of gene expression was based on the CT value of each sample which was calculated as the average of three replicate measurements for each sample analyzed. The fold change of each gene expression level is normalized to BMSCs before encapsulation in the hydrogels. The primers were synthesized commercially (Integrated DNA Technologies, Inc.), and evaluated at an annealing temperature of 58 °C.

2.4.6 Histological and Immunohistochemical Analysis

The culture samples were fixed in 4% paraformaldehyde for at least 24 h at 4 °C, dehydrated with a graded ethanol series, and then embedded in paraffin. The sections, 10 μm in thickness, were stained with Sirius Red and Fast Green stain by using Sirius Red/Fast Green Collagen staining kit (Chondrex, Inc.) for collagen quantification. The samples were stained according to the manufacturer's protocol. The stained sections were imaged by a light microscope (Olympus IX81) under 20× lens.

المنارة للاستشارات
www.manaraa.com

For the immunohistochemical staining of type II collagen, separate sections were permeabilized with 0.05% Tween20 in Tris-buffered saline solution (TBS) for 15 min and blocked in 2% BSA in TBS for 20 min. The sections were then incubated with rabbit anticollagen type II monoclonal antibody (Sigma-Aldrich) at 1:100 dilution in blocking buffer at room temperature for 2 h. After the samples were washed thrice with TBS, they were incubated with secondary antibody detection Alexafluor 546 at 1:200 dilution in blocking buffer at room temperature for 1 h. They were then washed thrice with TBS and counterstained with DAPI (4,6-diamidino-2-phenylindole, 100 ng/mL) for 15 min. Finally, the sections were mounted for microscopic observation. Images of the stained sections were collected using Olympus IX81 epi-flour mode under 20× lens, exposure times 50 ms for DAPI and 1000 ms for collagen II.

2.4.7 Biomechanical Property Analysis

The hydrogels were collected at days 0, 14, and 28 of chondrogenic culturing and subjected to test storage (G') and loss (G'') moduli using DHR-3 rheometer (TA Instruments) with 12 mm diameter parallel-plate geometry and temperature controlled Peltier plate. The samples were cut into uniform cylinders and placed on a metal plate, where the tests were performed. Amplitude sweeps at constant frequency (1 rad/s) were performed to determine the linear viscoelastic range of deformation for each sample, after which frequency sweeps (0.1–10 rad/s) were performed at a strain amplitude within the linear range (2%). In amplitude and frequency sweeps measurement, the geometry gaps were conditioned by axial force at 0.5 N for every run. The linear equilibrium modulus plateau (G_e) of hydrogels was calculated from the average of storage modulus (G') over the frequency range.

المنارة للاستشارات
www.manaraa.com

2.4.8 Alkaline Phosphatase (ALP) Activity Test

Alkaline phosphatase (ALP) activity was determined using pNPP (pnitrophenyl phosphate) assay (Thermo Scientific). After 3, 7 and 28 days of induction in the osteogenic media, the hydrogels with cells were prewashed with PBS then incubated with pNPP solution at room temperature for 1 h. Absorbance was read using a M2 SpectraMax plate reader at 405 nm, indicating ALP activity levels. The enzyme activity was calculated from Beer−Lambert law as follows,

$$\text{Enzyme activity } (\mu\text{mol}/\text{min}/\text{construct}) = \frac{V(\mu L) \times OD_{405\ nm}\ (cm^{-1})}{\varepsilon \times \text{incubation time (min)} \times \text{cell}}$$

where ε is the molar extinction coefficient ($M^{-1} \times cm^{-1}$). For pNPP, $\varepsilon = 1.78 \times 10^4\ M^{-1} \times cm^{-1}$, $OD_{405\ nm}$ (cm^{-1}) is the absorbance at 405 nm divided by the light-path length (cm), and V is the final assay volume.

2.4.9 Histological Staining for Calcium Deposition

Alizarin Red S (ARS) staining for Ca^{2+} was performed after 28 days of chondrogenic cultures. The hydrogels with cells were washed three times with PBS, and were stained with 0.1% solution of ARS (Sigma-Aldrich) pH 4.2 for 30 min, washed with PBS to remove excess stain. The stained hydrogels were imaged by a light microscope (Olympus I×81) under 4× lens. Negative control experiments (before induction in the chondrogenic media) were conducted for all types of the hydrogels.

المنارة للاستشارات
www.manaraa.com

2.5 REFERENCES

(1) Tenney, R. M.; Discher, D. E. Stem Cells, Microenvironment Mechanics, and Growth Factor Activation. *Curr. Opin. Cell Biol.* **2009,** *21*, 630-635.

(2) Harada, T.; Swift, J.; Irianto, J.; Shin, J.-W.; Spinler, K. R.; Athirasala, A.; Diegmiller, R.; Dingal, P. D. P.; Ivanovska, I. L.; Discher, D. E. Nuclear Lamin Stiffness Is a Barrier to 3d Migration, but Softness Can Limit Survival. *J. Cell Biol.* **2014**, jcb. 201308029.

(3) Takagi, J.; Petre, B. M.; Walz, T.; Springer, T. A. Global Conformational Rearrangements in Integrin Extracellular Domains in Outside-in and inside-out Signaling. *Cell* **2002,** *110*, 599-611.

(4) Park, J.; Bauer, S.; von der Mark, K.; Schmuki, P. Nanosize and Vitality: Tio2 Nanotube Diameter Directs Cell Fate. *Nano Lett.* **2007,** *7*, 1686-1691.

(5) Crisan, M.; Yap, S.; Casteilla, L.; Chen, C.-W.; Corselli, M.; Park, T. S.; Andriolo, G.; Sun, B.; Zheng, B.; Zhang, L. A Perivascular Origin for Mesenchymal Stem Cells in Multiple Human Organs. *Cell stem cell* **2008,** *3*, 301-313.

(6) Chen, W.; Shao, Y.; Li, X.; Zhao, G.; Fu, J. Nanotopographical Surfaces for Stem Cell Fate Control: Engineering Mechanobiology from the Bottom. *Nano Today* **2014,** *9*, 759-784.

(7) Kim, H. N.; Jiao, A.; Hwang, N. S.; Kim, M. S.; Kang do, H.; Kim, D. H.; Suh, K. Y. Nanotopography-Guided Tissue Engineering and Regenerative Medicine. *Adv Drug Deliv Rev* **2013,** *65*, 536-558.

(8) Das, R. K.; Zouani, O. F.; Labrugère, C.; Oda, R.; Durrieu, M.-C. Influence of Nanohelical Shape and Periodicity on Stem Cell Fate. *ACS Nano* **2013,** *7*, 3351-3361.

المنارة للاستشارات
www.manaraa.com

(9) Lemischka, I. R.; Moore, K. A. Stem Cells: Interactive Niches. *Nature* **2003,** *425*, 778-779.

(10) Sun, Y.; Chen, C. S.; Fu, J. Forcing Stem Cells to Behave: A Biophysical Perspective of the Cellular Microenvironment. *Annual review of biophysics* **2012,** *41*, 519-542.

(11) Kim, D.-H.; Provenzano, P. P.; Smith, C. L.; Levchenko, A. Matrix Nanotopography as a Regulator of Cell Function. *The Journal of Cell Biology* **2012,** *197*, 351-360.

(12) Li, W.-J.; Mauck, R. L.; Cooper, J. A.; Yuan, X.; Tuan, R. S. Engineering Controllable Anisotropy in Electrospun Biodegradable Nanofibrous Scaffolds for Musculoskeletal Tissue Engineering. *J. Biomech.* **2007,** *40*, 1686-1693.

(13) Baker, B. M.; Nathan, A. S.; Gee, A. O.; Mauck, R. L. The Influence of an Aligned Nanofibrous Topography on Human Mesenchymal Stem Cell Fibrochondrogenesis. *Biomaterials* **2010,** *31*, 6190-6200.

(14) Wu, Y.-N.; Law, J. B. K.; He, A. Y.; Low, H. Y.; Hui, J. H. P.; Lim, C. T.; Yang, Z.; Lee, E. H. Substrate Topography Determines the Fate of Chondrogenesis from Human Mesenchymal Stem Cells Resulting in Specific Cartilage Phenotype Formation. *Nanomed. Nanotechnol. Biol. Med.* **2014,** *10*, 1507-1516.

(15) Pacifici, M.; Golden, E. B.; Oshima, O.; Shapiro, I. M.; Leboy, P. S.; Adams, S. L. Hypertrophic Chondrocytes. The Terminal Stage of Differentiation in the Chondrogenic Cell Lineage? *Ann. N.Y. Acad. Sci.* **1990,** *599*, 45-57.

(16) Pelttari, K.; Winter, A.; Steck, E.; Goetzke, K.; Hennig, T.; Ochs, B. G.; Aigner, T.; Richter, W. Premature Induction of Hypertrophy During in Vitro Chondrogenesis of Human Mesenchymal Stem Cells Correlates with Calcification and Vascular Invasion after Ectopic Transplantation in Scid Mice. *Arthritis Rheum.* **2006,** *54*, 3254-3266.

المنارة للاستشارات
www.manaraa.com

(17) Yoo, J. U.; Johnstone, B. The Role of Osteochondral Progenitor Cells in Fracture Repair. *Clin Orthop Relat Res* **1998**, S73-81.

(18) van der Kraan, P. M.; van den Berg, W. B. Osteophytes: Relevance and Biology. *Osteoarthritis Cartilage* **2007,** *15*, 237-244.

(19) Steinert, A. F.; Ghivizzani, S. C.; Rethwilm, A.; Tuan, R. S.; Evans, C. H.; Nöth, U. Major Biological Obstacles for Persistent Cell-Based Regeneration of Articular Cartilage. *Arthrit. Res. Ther.* **2007,** *9*, 213.

(20) Goldring, M. B.; Otero, M.; Plumb, D. A.; Dragomir, C.; Favero, M.; El Hachem, K.; Hashimoto, K.; Roach, H. I.; Olivotto, E.; Borzì, R. M.; Marcu, K. B. Roles of Inflammatory and Anabolic Cytokines in Cartilage Metabolism: Signals and Multiple Effectors Converge Upon Mmp-13 Regulation in Osteoarthritis. *European cells & materials* **2011,** *21*, 202-220.

(21) Marcu, K. B.; Otero, M.; Olivotto, E.; Borzi, R. M.; Goldring, M. B. Nf-Kb Signaling: Multiple Angles to Target Oa. *Curr. Drug Targets* **2010,** *11*, 599-613.

(22) Loeser, R. F. Age-Related Changes in the Musculoskeletal System and the Development of Osteoarthritis. *Clin. Geriatr. Med.* **2010,** *26*, 371-386.

(23) Nurminskaya, M.; Linsenmayer, T. F. Identification and Characterization of up-Regulated Genes During Chondrocyte Hypertrophy. *Dev. Dyn.* **1996,** *206*, 260-271.

(24) Kirsch, T.; von der Mark, K. Remodelling of Collagen Types I, Ii and X and Calcification of Human Fetal Cartilage. *Bone Miner.* **1992,** *18*, 107-117.

(25) Alvarez, J.; Balbin, M.; Santos, F.; Fernandez, M.; Ferrando, S.; Lopez, J. M. Different Bone Growth Rates Are Associated with Changes in the Expression Pattern of Types Ii

المنارة للاستشارات
www.manaraa.com

and X Collagens and Collagenase 3 in Proximal Growth Plates of the Rat Tibia. *J. Bone Miner. Res.* **2000,** *15*, 82-94.

(26) Binette, F.; McQuaid, D. P.; Haudenschild, D. R.; Yaeger, P. C.; McPherson, J. M.; Tubo, R. Expression of a Stable Articular Cartilage Phenotype without Evidence of Hypertrophy by Adult Human Articular Chondrocytes in Vitro. *J. Orthop. Res.* **1998,** *16*, 207-216.

(27) Johnson, K. A.; Van Etten, D.; Nanda, N.; Graham, R. M.; Terkeltaub, R. A. Distinct Transglutaminase 2-Independent and Transglutaminase 2-Dependent Pathways Mediate Articular Chondrocyte Hypertrophy. *J. Biol. Chem.* **2003,** *278*, 18824-18832.

(28) Mueller, M. B.; Tuan, R. S. Functional Characterization of Hypertrophy in Chondrogenesis of Human Mesenchymal Stem Cells. *Arthritis & Rheumatology* **2008,** *58*, 1377-1388.

(29) Solomon, L. A.; Bérubé, N. G.; Beier, F. Transcriptional Regulators of Chondrocyte Hypertrophy. *Birth Defects Res. C. Embryo Today Rev.* **2008,** *84*, 123-130.

(30) Horner, A.; Bishop, N.; Bord, S.; Beeton, C.; Kelsall, A.; Coleman, N.; Compston, J. Immunolocalisation of Vascular Endothelial Growth Factor (Vegf) in Human Neonatal Growth Plate Cartilage. *The Journal of Anatomy* **1999,** *194*, 519-524.

(31) Fuerst, M.; Bertrand, J.; Lammers, L.; Dreier, R.; Echtermeyer, F.; Nitschke, Y.; Rutsch, F.; Schafer, F. K.; Niggemeyer, O.; Steinhagen, J.; Lohmann, C. H.; Pap, T.; Ruther, W. Calcification of Articular Cartilage in Human Osteoarthritis. *Arthritis Rheum.* **2009,** *60*, 2694-2703.

المنارة للاستشارات
www.manaraa.com

(32) Sitasuwan, P.; Lee, L. A.; Bo, P.; Davis, E. N.; Lin, Y.; Wang, Q. A Plant Virus Substrate Induces Early Upregulation of Bmp2 for Rapid Bone Formation. *Integrative biology : quantitative biosciences from nano to macro* **2012,** *4*, 651-660.

(33) Luckanagul, J.; Lee, L. A.; Nguyen, Q. L.; Sitasuwan, P.; Yang, X.; Shazly, T.; Wang, Q. Porous Alginate Hydrogel Functionalized with Virus as Three-Dimensional Scaffolds for Bone Differentiation. *Biomacromolecules* **2012,** *13*, 3949-3958.

(34) Chubinskaya, S.; Segalite, D.; Pikovsky, D.; Hakimiyan, A. A.; Rueger, D. C. Effects Induced by Bmps in Cultures of Human Articular Chondrocytes: Comparative Studies. *Growth Factors* **2008,** *26*, 275-283.

(35) Schmitt, B.; Ringe, J.; Haupl, T.; Notter, M.; Manz, R.; Burmester, G. R.; Sittinger, M.; Kaps, C. Bmp2 Initiates Chondrogenic Lineage Development of Adult Human Mesenchymal Stem Cells in High-Density Culture. *Differentiation* **2003,** *71*, 567-577.

(36) Fischer, L.; Boland, G.; Tuan, R. S. Wnt Signaling During Bmp-2 Stimulation of Mesenchymal Chondrogenesis. *J. Cell. Biochem.* **2002,** *84*, 816-831.

(37) Duprez, D. M.; Coltey, M.; Amthor, H.; Brickell, P. M.; Tickle, C. Bone Morphogenetic Protein-2 (Bmp-2) Inhibits Muscle Development and Promotes Cartilage Formation in Chick Limb Bud Cultures. *Dev. Biol.* **1996,** *174*, 448-452.

(38) Luyten, F. P.; Yu, Y. M.; Yanagishita, M.; Vukicevic, S.; Hammonds, R. G.; Reddi, A. H. Natural Bovine Osteogenin and Recombinant Human Bone Morphogenetic Protein-2b Are Equipotent in the Maintenance of Proteoglycans in Bovine Articular Cartilage Explant Cultures. *J. Biol. Chem.* **1992,** *267*, 3691-3695.

المنارة للاستشارات
www.manaraa.com

(39) Sailor, L. Z.; Hewick, R. M.; Morris, E. A. Recombinant Human Bone Morphogenetic Protein-2 Maintains the Articular Chondrocyte Phenotype in Long-Term Culture. *J. Orthop. Res.* **1996,** *14*, 937-945.

(40) Lee, L. A.; Nguyen, Q. L.; Wu, L.; Horvath, G.; Nelson, R. S.; Wang, Q. Mutant Plant Viruses with Cell Binding Motifs Provide Differential Adhesion Strengths and Morphologies. *Biomacromolecules* **2012,** *13*, 422-431.

(41) Sitasuwan, P.; Lee, L. A.; Li, K.; Nguyen, H. G.; Wang, Q. Rgd-Conjugated Rod-Like Viral Nanoparticles on 2d Scaffold Improve Bone Differentiation of Mesenchymal Stem Cells. *Frontiers in chemistry* **2014,** *2*, 31.

(42) Maturavongsadit, P.; Bi, X.; Gado, T. A.; Nie, Y.-Z.; Wang, Q. Adhesive Peptides Conjugated Pamam Dendrimer as a Coating Polymeric Material Enhancing Cell Responses. *Chin. Chem. Lett.* **2016,** *27*, 1473-1478.

(43) Villanueva, I.; Weigel, C. A.; Bryant, S. J. Cell-Matrix Interactions and Dynamic Mechanical Loading Influence Chondrocyte Gene Expression and Bioactivity in Peg-Rgd Hydrogels. *Acta Biomater.* **2009,** *5*, 2832-2846.

(44) Deponti, D.; Giancamillo, A. D.; Gervaso, F.; Domenicucci, M.; Domeneghini, C.; Sannino, A.; Peretti, G. M. Collagen Scaffold for Cartilage Tissue Engineering: The Benefit of Fibrin Glue and the Proper Culture Time in an Infant Cartilage Model. *Tissue Engineering Part A* **2013,** *20*, 1113-1126.

(45) Kawamura, S.; Wakitani, S.; Kimura, T.; Maeda, A.; Caplan, A. I.; Shino, K.; Ochi, T. Articular Cartilage Repair: Rabbit Experiments with a Collagen Gel-Biomatrix and Chondrocytes Cultured in It. *Acta Orthop. Scand.* **1998,** *69*, 56-62.

المنارة للاستشارات
www.manaraa.com

(46) Nguyen, L. H.; Kudva, A. K.; Guckert, N. L.; Linse, K. D.; Roy, K. Unique Biomaterial Compositions Direct Bone Marrow Stem Cells into Specific Chondrocytic Phenotypes Corresponding to the Various Zones of Articular Cartilage. *Biomaterials* **2011,** *32*, 1327-1338.

(47) Gole, A.; Murphy, C. J. Seed-Mediated Synthesis of Gold Nanorods: Role of the Size and Nature of the Seed. *Chem. Mater.* **2004,** *16*, 3633-3640.

(48) Nikoobakht, B.; El-Sayed, M. A. Evidence for Bilayer Assembly of Cationic Surfactants on the Surface of Gold Nanorods. *Langmuir* **2001,** *17*, 6368-6374.

(49) Luca, A. C.; Mersch, S.; Deenen, R.; Schmidt, S.; Messner, I.; Schäfer, K.-L.; Baldus, S. E.; Huckenbeck, W.; Piekorz, R. P.; Knoefel, W. T.; Krieg, A.; Stoecklein, N. H. Impact of the 3d Microenvironment on Phenotype, Gene Expression, and Egfr Inhibition of Colorectal Cancer Cell Lines. *PLoS One* **2013,** *8*, e59689.

(50) Niu, Z.; Bruckman, M. A.; Li, S.; Lee, L. A.; Lee, B.; Pingali, S. V.; Thiyagarajan, P.; Wang, Q. Assembly of Tobacco Mosaic Virus into Fibrous and Macroscopic Bundled Arrays Mediated by Surface Aniline Polymerization. *Langmuir* **2007,** *23*, 6719-6724.

(51) Bruckman, M. A.; Kaur, G.; Lee, L. A.; Xie, F.; Sepulveda, J.; Breitenkamp, R.; Zhang, X.; Joralemon, M.; Russell, T. P.; Emrick, T.; Wang, Q. Surface Modification of Tobacco Mosaic Virus with "Click" Chemistry. *ChemBioChem* **2008,** *9*, 519-523.

(52) Maturavongsadit, P.; Luckanagul, J. A.; Metavarayuth, K.; Zhao, X.; Chen, L.; Lin, Y.; Wang, Q. Promotion of in Vitro Chondrogenesis of Mesenchymal Stem Cells Using in Situ Hyaluronic Hydrogel Functionalized with Rod-Like Viral Nanoparticles. *Biomacromolecules* **2016,** *17*, 1930-1938.

المنارة للاستشارات
www.manaraa.com

(53) Wieland, J. A.; Houchin-Ray, T. L.; Shea, L. D. Non-Viral Vector Delivery from Peg-Hyaluronic Acid Hydrogels. *J. Controlled Release* **2007,** *120*, 233-241.

(54) Lee, S.; Tong, X.; Yang, F. The Effects of Varying Poly(Ethylene Glycol) Hydrogel Crosslinking Density and the Crosslinking Mechanism on Protein Accumulation in Three-Dimensional Hydrogels. *Acta Biomater.* **2014,** *10*, 4167-4174.

(55) Weber, L. M.; Lopez, C. G.; Anseth, K. S. Effects of Peg Hydrogel Crosslinking Density on Protein Diffusion and Encapsulated Islet Survival and Function. *Journal of Biomedical Materials Research Part A* **2009,** *90A*, 720-729.

المنارة للاستشارات
www.manaraa.com

CHAPTER 3

THE OPTIMIZATION OF PHYSICAL AND MECHANICAL PROPERTIES OF THE THIOL–ENE "CLICK" HA HYDROGELS THROUGH CHEMISTRIES OF CROSS-LINKERS FOR OSTEOCHONDRAL REGENERATION APPLICATIONS[1]

3.1 INTRODUCTION

In this chapter, the physical properties of scaffolds, i.e., mechanical stiffness,[1] network porosity,[2] permeability,[3,4] and degradation rates,[5,6] are particularly focused to develop in order to better support the differentiation of encapsulated MSCs. Especially, the mechanical properties of the scaffold have attracted greater attention as the role of the extracellular matrix (ECM) in directing stem cell fate.[7-9] The scaffolds for cartilage and subchondral bone tissue engineering must provide adequate mechanical strength to support cells and withstand *in vivo* forces during joint movement. Many studies showed that chondrogenesis and osteogenesis of MSCs could be promoted in stiff scaffolds, approximately 1-3 kPa,[10,11] and 11-250 kPa,[12,13] respectively. With recent advances, researchers have attempted to enhance the mechanical properties of traditional hydrogels by many strategies, such as increasing crosslinking density, and addition of multiple polymers, often including two or more independent networks (Figure 3.1).[14] These systems not only typically achieve stronger mechanical properties than the conventional hydrogels,

[1] Portions of this chapter were adapted with permission from Maturavongsadit, P.; Bi, X.; Metavarayuth, K.; Amie Luckanagul, J.; Wang, Q. *ACS Applied Materials and Interfaces* **2017**, *9* (4), 3318–3329. Copyright (2017) American Chemical Society (Appendix D).

المنارة للاستشارات
www.manaraa.com

but may exhibit superior promotion of tissue formation[15,16] and integration with surrounding tissue *in vivo*.[17-19] Therefore, we sought to develop our *in situ* forming hydrogel systems using these strategies, in particular the dual networks, to better recapitulate cartilage tissue structure on the macroscale.

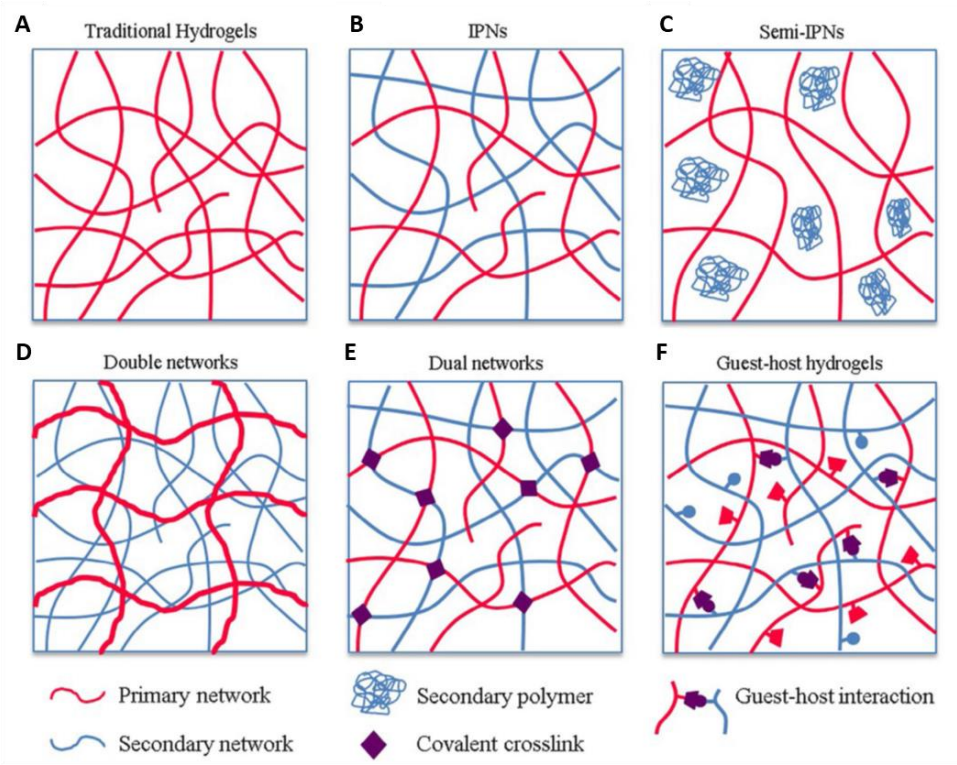

Figure 3.1. Schematic representation of different strategies utilized to improve the mechanical properties of hydrogels. (A) Traditional single polymer networks. (B) Interpenetrating networks (IPNs) comprised of two or more separate crosslinked networks not covalently bound to each other, but rather partially intertwined. (C) Semi-IPNs comprised of a crosslinked network with either linear or branched polymers embedded within the network. (D) Double networks consisted of two networks with significantly different mechanical properties may crosslinked together. (E) Dual networks consisted of two materials crosslinked together into the same network with similar crosslinking mechanisms. (F) Guest-host networks defined as two types of materials interacted rapidly to form hydrogels via guest-host interactions. Reprinted from Vega, S. L.; Kwon, M. Y.; Burdick, J. A. *Recent advances in hydrogels for cartilage tissue engineering* **2017**, 33, 59-75. Copyright (2016) Burdick, J.A., Open Access. Published by AO Research Institute Davos.

المنارة للاستشارات
www.manaraa.com

We have used the dithiothreitol (DTT)-cross-linked HA hydrogel as a scaffolding material to study the influence of rod-like nanoparticles on chondrogenesis of MSCs.[20] However, the physical properties, particularly mechanical stiffness, of this hydrogel system were far inferior to native cartilage. It is difficult to further improve the mechanical stiffness of hydrogels using DTT as the linker because the increased crosslink density with DTT may compromise the viability of encapsulated cells due to the concentration-dependent toxicity of DTT.[21] We therefore explore the usage of other type of cross-linking agents or combination of DTT with other cross-linking agents as the alternative. With the aim of increasing the mechanical properties of hydrogels to approach the native cartilage, this study aimed to examine the effect of cross-linker types on the physical properties of the thiol–ene "click" HA hydrogels in terms of mechanical stiffness, gelation time, morphology, solute diffusivity, and degradability. A 4-arm PEG was selected as one of the cross-linkers due to its biocompatible and highly hydrophilic properties. Importantly, 4-arm PEG could provide higher mechanical strength, quicker gelation time and more sensitive degradation compared to linear PEG, and better support chondrocytes compared to 8-arm PEG.[22,23] Although PEG is inherently cell repellent and nondegradable, these properties can be readily modified by the chemical modification with native ECM components[24,25] and degradable linkages.[26-28] PAMAM dendrimers were another chosen cross-linkers in this study due to their controllable size, shape, branching length, density, and surface functionality.[29-31] Compared to linear polymers, the multiple-armed dendrimers may allow more controllable mechanical properties and degradation times by means of variations in generation and end-group chemistry. Previous studies have shown that biochemical-modified PAMAM dendrimers and PAMAM-based hydrogels could

المنارة للاستشارات
www.manaraa.com

support the adhesion, proliferation and differentiation of MSCs and pheochromocytoma (PC12) cells without any cytotoxic effects (Figure 3.2).[32-34]

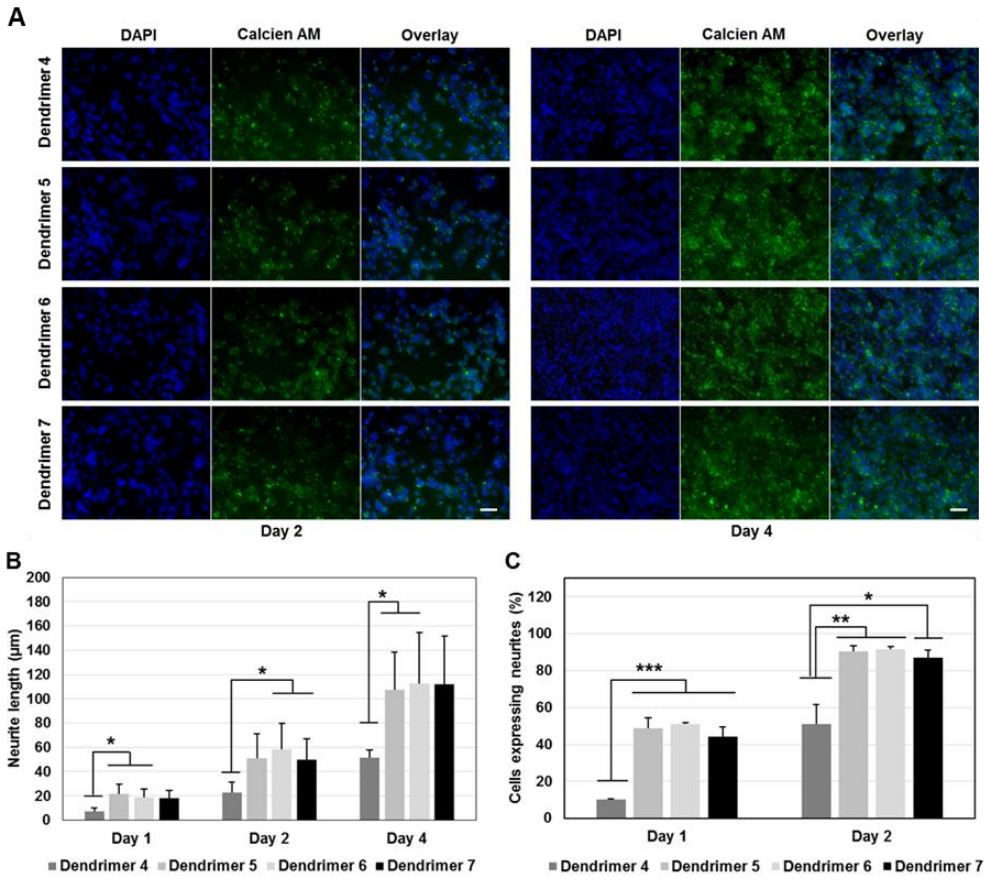

Figure 3.2. *In vitro* cell proliferation and differentiation on the biochemical-modified PAMAM dendrimers. (A) Confocal Microscopic images for viability of differentiated PC12 cells cultured on substrates coated with native PAMAM carrying DVS (dendrimer **4**), RGD modified PAMAM (dendrimer **5**), YIGSR modified PAMAM (dendrimer **6**), or IKVAV modified PAMAM (dendrimer **7**) in NGF supplemented culture medium for 2 and 4 days. The blue nuclei of cells were stained with DAPI. The green live cells were stained with Calcein AM. All images share the same scale bar: 50 μm. (B, C) Neurite outgrowth analysis of PC12 cells cultured on substrates coated with native PAMAM carrying DVS (dendrimer **4**), RGD modified PAMAM (dendrimer **5**), YIGSR modified PAMAM (dendrimer **6**), and IKVAV modified PAMAM (dendrimer **7**) in NGF supplemented culture medium for 1 day, 2 and 4 days. (B) Average neurite length of PC12 cells on different PAMAM dendrimer matrices at different time points. (C) Percentage of cells displaying neurite outgrowths on different PAMAM dendrimer matrices at different time points. The values expressed are means (n = 4) ± SD. Samples were compared using two-tailed equal variance Student t tests, * $P < 0.05$, ** $P < 0.005$, *** $P < 0.0005$. Reprinted from Chinese Chemical Letters, 27(9), Maturavongsadit, P.; Bi, X.; Gado, T. A.; Nie, Y.-Z.; Wang, Q. Adhesive Peptides Conjugated PAMAM Dendrimer as a Coating Polymeric Material Enhancing Cell Responses, 1473-1478, Copyright (2016), with permission from Elsevier (Appendix E).

المنارة للاستشارات
www.manaraa.com

We hypothesized that changing structures of the cross-linkers had a considerable impact on the physical properties of the resulting hydrogels, including gelation time, mechanical stiffness, morphology, solute diffusivity, and degradability. The ultimate goal of this study is to improve the *in situ*-forming HA-based hydrogels in terms of physical properties for cartilage and bone tissue engineering applications.

3.2 RESULTS AND DISCUSSION

3.2.1 Preparation of Thiol–Ene "Click" HA Hydrogels

Before synthesis of the thiol–ene "click" hydrogels, MeHA with approximate 40% degree of methacrylate modification was consistently generated by the reaction of HA monomer and methacrylic anhydride at 1:6 molar ratio as determined by ^{1}H NMR (see Figure 1.3 in Chapter 1). In addition, PAMAM-G2-16SH and PAMAM-G3-32SH were synthesized by the reaction of G2- and G3-PAMAM and iminothiolane hydrochloride. The ^{1}H NMR was used to confirm the existence of the conjugated thiol groups, and the typical spectra of native PAMAM-G2, native PAMAM-G3, PAMAM-G2-16SH, and PAMAM-G3-32SH are shown in Figures 3.4 and 3.5. Seven different hydrogel formulations were successfully formed via thiol–ene "click" reaction at room temperature and pH ~ 8 (Figure 3.3 and Table 3.1).

المنارة للاستشارات
www.manaraa.com

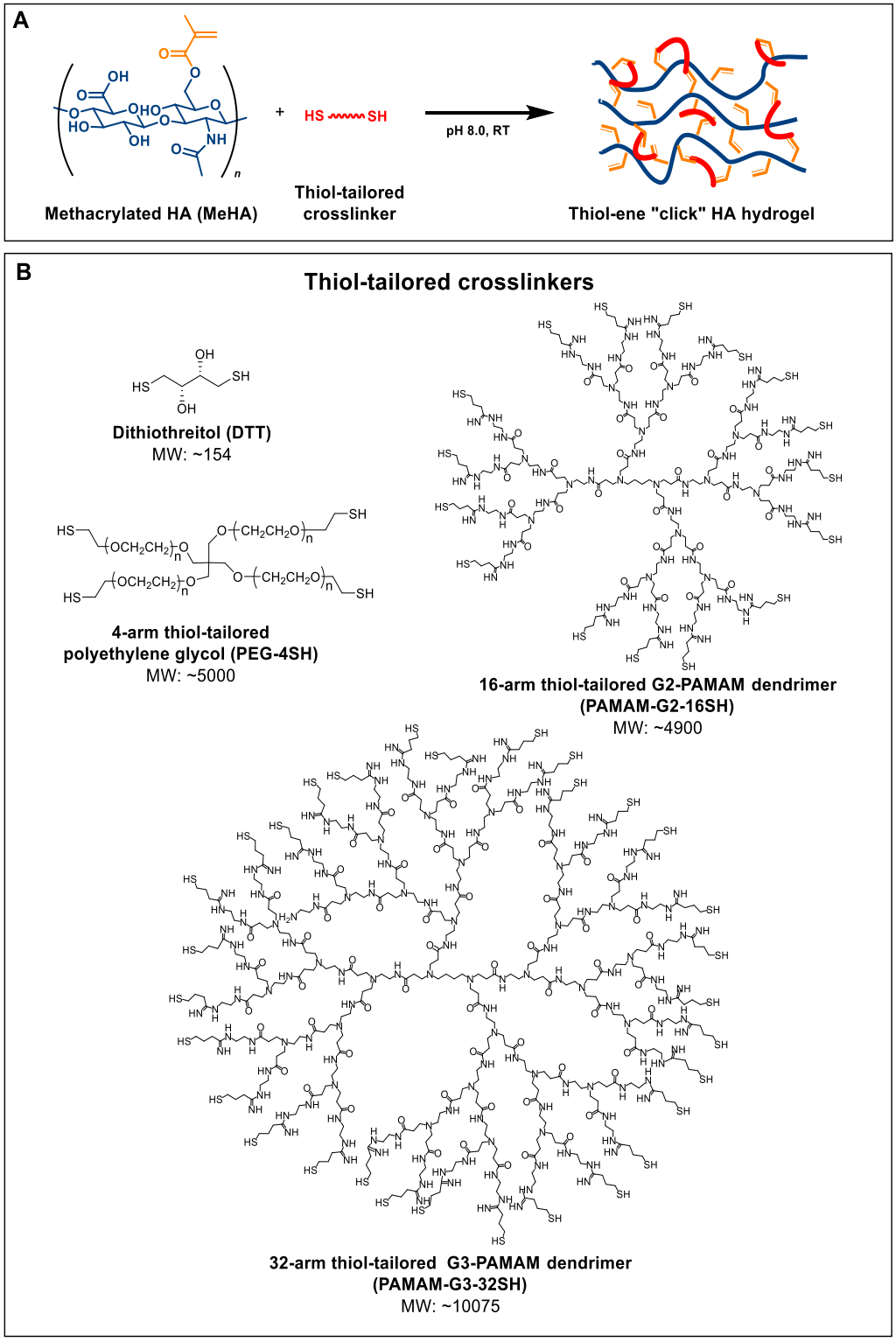

Figure 3.3. Schematic illustrating the formation of the thiol–ene "click" HA hydrogels. (A) Synthesis of the thiol–ene "click" HA hydrogel by the reaction between methacrylate groups on HA and thiol groups on the crosslinkers. (B) The structures of thiol-tailored crosslinkers used for synthesis of the thiol–ene "click" HA hydrogel.

المنارة للاستشارات
www.manaraa.com

Table 3.1. Summary of the thiol–ene "click" HA hydrogel formulations.

Hydrogel name	Crosslinker type	Crosslinker (%w/v)	40DM MeHA (%w/v)	Crosslinking molar ratio (SH:Ene)
DTT	Dithiothreitol	0.00154	3	2:1
G2	PAMAM-G2-16SH	2	3	6.5:1
G2DTT	PAMAM-G2-16SH and dithiothreitol	2.00154	3	8.5:1
G3	PAMAM-G3-32SH	2	3	6.3:1
G3DTT	PAMAM-G3-32SH and dithiothreitol	2.00154	3	8.3:1
PEG	PEG-4SH	2	3	1.6:1
PEGDTT	PEG-4SH and dithiothreitol	2.00154	3	3.6:1

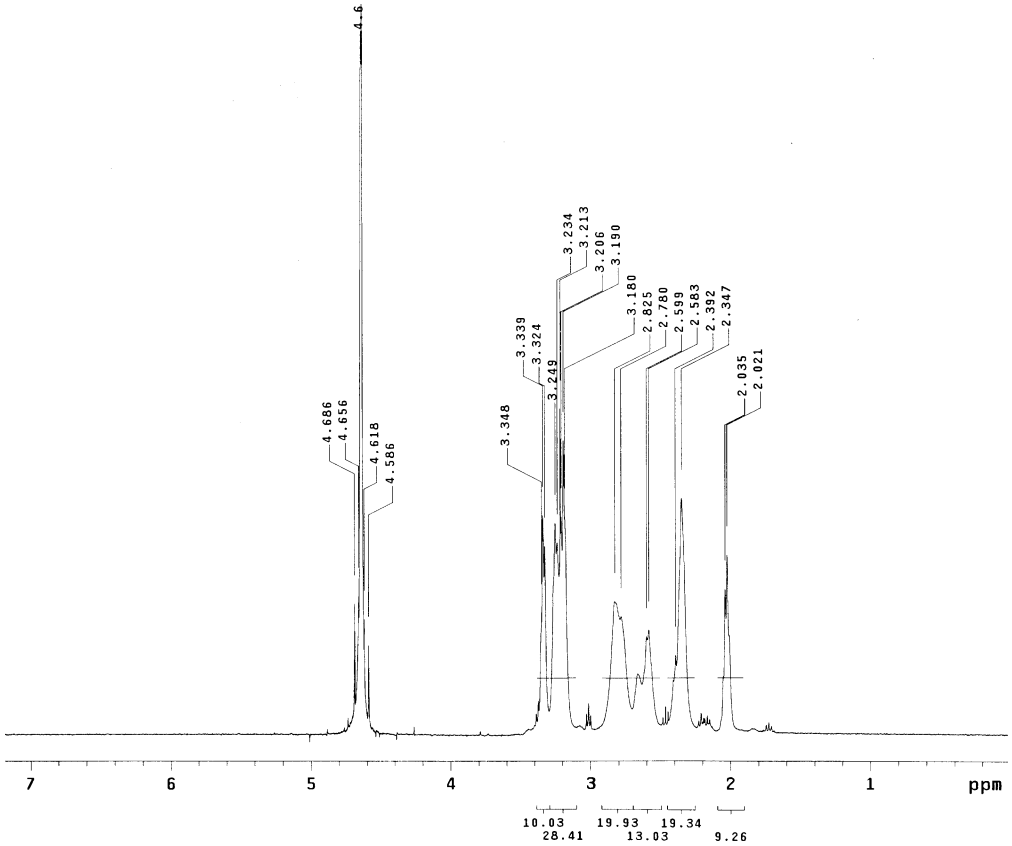

Figure 3.4. ^{1}H NMR spectra of the thiol-tailored G2-PAMAM with approximate 100% degree of modification (16 thiol groups on the structure).

المنارة للاستشارات
www.manaraa.com

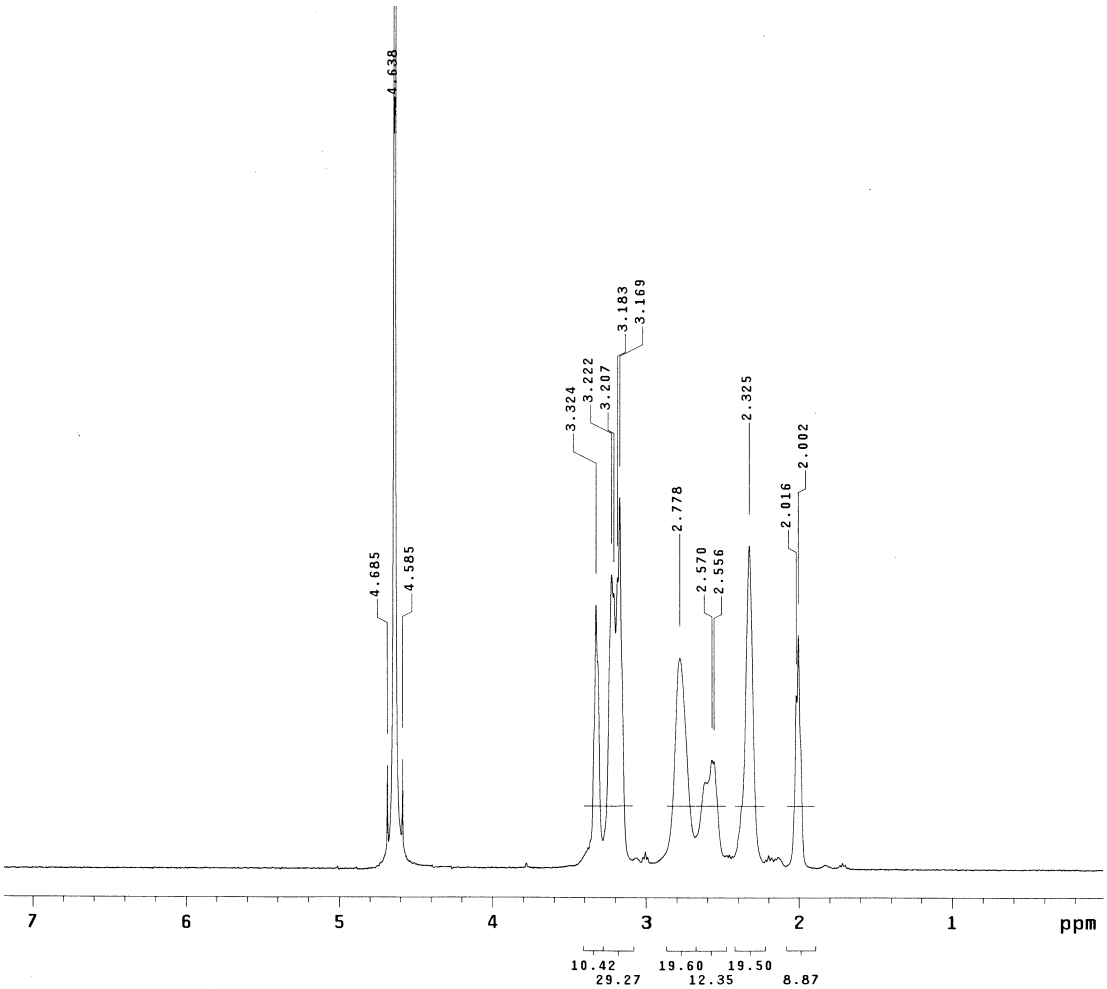

Figure 3.5. ^{1}H NMR spectra of the thiol-tailored G3-PAMAM with approximate 100% degree of modification (32 thiol groups on the structure).

In the preliminary step, the formulation of the hydrogels was optimized by considering three variables: cross-linking molar ratio (thiol:ene), cross-linker concentration, and total polymer concentration. The different cross-linking molar ratios, in the range of 1SH:4Ene to 4SH:1Ene, were first studied in each hydrogel by fixing HA concentration at 5% w/v (based on our previous work in Chapter 1). We found that the comparison in the effect of cross-linkers by controlling the cross-linking molar ratio was not practical. Different hydrogel formulations would result in a large difference in total polymer concentration that would eventually have a high impact on cell survival.

المنارة للاستشارات
www.manaraa.com

Specifically, at the ratio 4SH:1Ene, G2 and G3 concentrations were approximately 1.5% w/v of the hydrogel solution while PEG concentration was 25%, resulting in no survival cells observed (data not shown). In addition, increasing concentration of DTT was limited by its concentration-dependent toxicity. We found that the 2SH:1Ene was the maximum ratio of DTT that could support cell survival (data not shown). Moreover, the studies by Erickson et al. and Bian *et al*. have used 3% w/v of HA contained in the hydrogels for promotion of chondrogenesis and matrix formation. Therefore, we minimized the HA concentration to 3% w/v and compared the effect of cross-linkers by controlling concentrations.[6,35] The cross-linker concentrations in the range of 1–5% w/v were studied in each hydrogel (except DTT). Increasing the concentration of cross-linkers leads to the increase in total polymer concentration, which afforded a higher modulus. However, there were less than 70% of survival cells in the hydrogels containing more than 2% w/v of cross-linkers. Taken all into account, the formulations composed of 3% w/v of HA and 2% w/v of cross-linkers were selected as the master recipes in this research in order to study the improvement of the mechanical properties of the hydrogels influenced by the cross-linkers.

3.2.2 Effect of Cross-Linkers on Physical Properties of Thiol–Ene "Click" HA Hydrogels

3.2.2.1 Microstructure of the Hydrogels

The morphology of the seven different hydrogels was determined by SEM micrographs (Figure 3.6). The differences in pore size, porosity, and interconnectivity were observed among the different hydrogels. Namely, pore size of DTT hydrogel was in a range of 100–150 μm. While G2 and G3 hydrogels showed large pore sizes, a range of 100–200 μm, G2DTT and G3DTT hydrogels provided smaller pore sizes, a range of 70–110 and

المنارة للاستشارات
www.manaraa.com

50–100 μm, respectively. PEG hydrogels displayed a range of 100–200 μm in pore size, whereas PEGDTT exhibited smaller sizes, 10–100 μm. Moreover, DTT, G2, G2DTT, G3, and G3DTT hydrogels presented a high density of macropores which were well-interconnected with thin layers of compacted outer edge. PEG hydrogels displayed lower degree of porosity and interconnectivity with thicker compacted outer edges. The porous structure of PEGDTT hydrogels was the most compact with the lowest degree of porosity and interconnectivity. The exterior surfaces of all hydrogels were rough, folded, and dense. Especially, PEG and PEGDTT hydrogels were denser compared to other hydrogels.

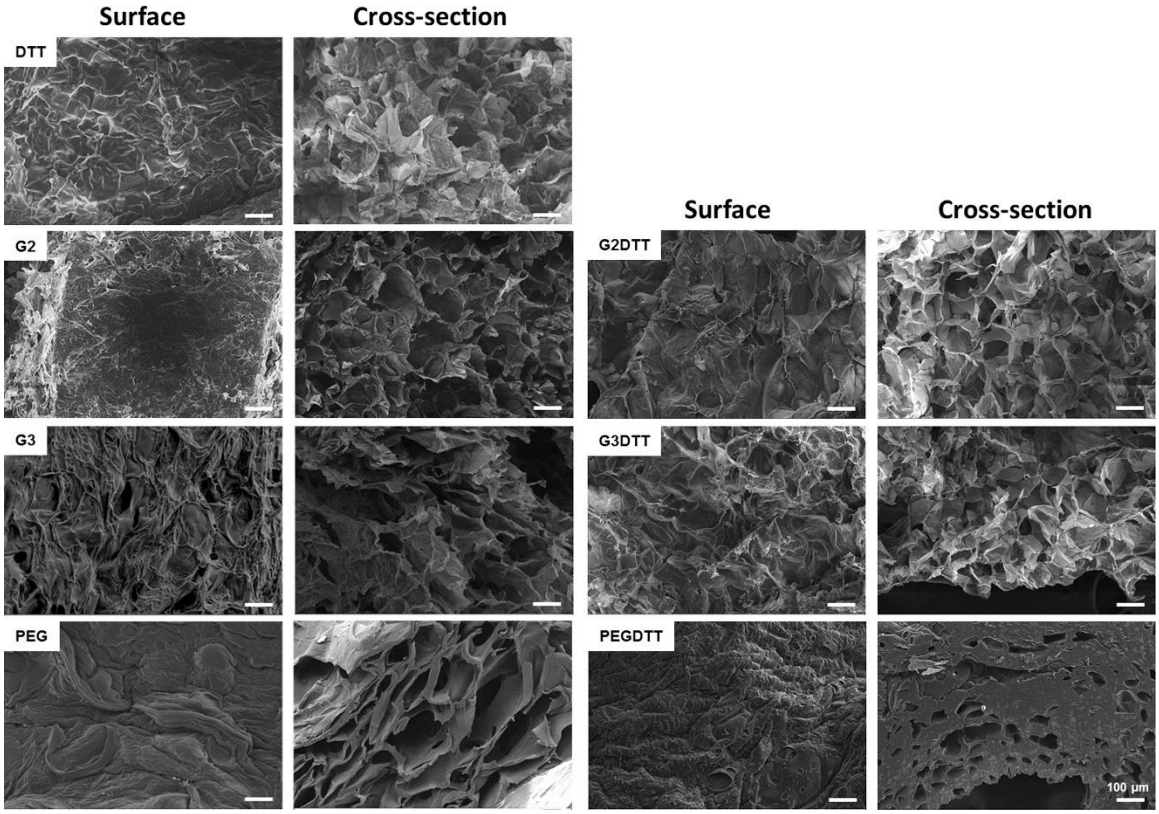

Figure 3.6. Exterior and cross-section SEM micrographs of the thiol–ene "click" HA hydrogels after freeze-drying. Scale bars for all images: 100 μm.

المنارة للاستشارات
www.manaraa.com

3.2.2.2 Mechanical Properties and Gelation Time of the Hydrogels

The mechanical properties of the hydrogels were determined by observing the complex modulus. It revealed that the average complex modulus of PEG and PEGDTT hydrogels were the highest (~1800 Pa) and was followed by G2DTT (~1240 Pa), G2 ~ G3DTT (~600 Pa), DTT (~400 Pa), and G3 hydrogels (~270 Pa), respectively (Figure 3.7A). As shown in Figure 3.7B, the gelation times of DTT, PEG, and PEGDTT hydrogels were similar and fastest, approximately 1 h, followed by G2DTT (~3 h), G2 ~ G3DTT (~5 h), and G3 (~18 h), respectively. The incorporation of DTT cross-linkers could further promote elasticity of the G2 and G3 hydrogels and shorten gelation time of the hydrogels (G2DTT and G3DTT compared to G2 and G3, respectively). We observed that the gelation time of the hydrogels, except for DTT hydrogel, was correlated nicely to the stiffness of the hydrogels such that the hydrogels with higher complex modulus showed faster gelation time.

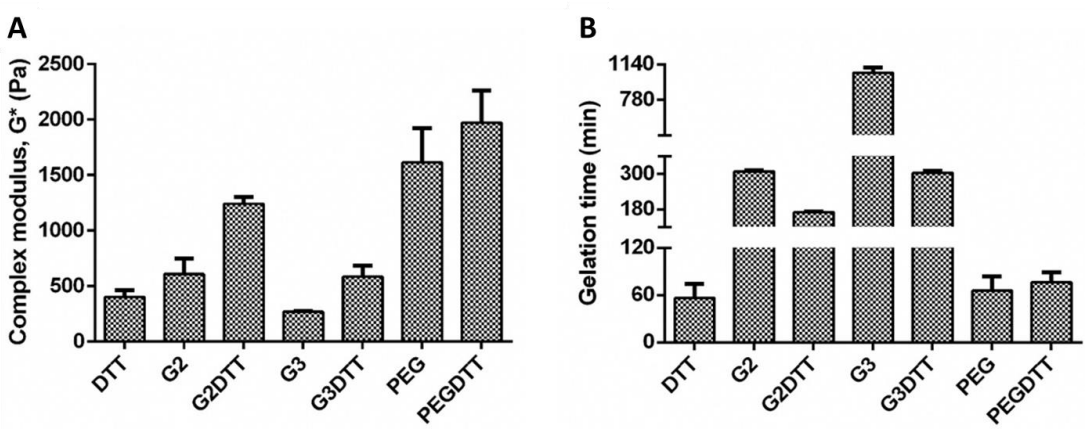

Figure 3.7. Mechanical properties and gelation time of the thiol–ene "click" HA hydrogels. (A) Average complex modulus of the hydrogels after gelation for 2 days (n = 4). (B) Average gelation time of the hydrogels (n = 6).

المنارة للاستشارات
www.manaraa.com

In hydrogel formation steps, the result obviously showed that the structure of cross-linker affected the gelation time of the thiol–ene "click" HA hydrogels. The overall rate and yield of Michael reactions are influenced by solvent polarity and pH, base catalyst strength, and steric bulk of the thiol group.[36] As shown in Figure 3.7, even providing higher thiol cross-linking sites, using large rigid and sterically bulky complex structure as PAMAM dendrimer led to longer gelation time compared to using small linear structure as DTT or branch polymer as 4-arm PEG. Furthermore, the hydrogel formed by larger (G3) PAMAM dendrimer showed significantly longer gelation time compared to using smaller (G2) PAMAM dendrimer. It showed that the flexibility and steric hindrance of the cross-linkers influenced the ability of MeHA to react with the tailored thiols. As expected, the combination of DTT could significantly fasten the gelation time of both PAMAM hydrogels. We believe that DTT helped to react to unoccupied methacrylate groups on HA of PAMAM hydrogels. Conversely, it could not help in PEG hydrogel because 4-arm PEG could effectively react to methacrylate groups on HA to form hydrogel. The mechanical property of the hydrogels is related to the properties of cross-linkers and the cross-linking density, dictated by the structure of cross-linkers. Specifically, PEG and PEGDTT hydrogels showed the similar highest stiffness because of a highly molecular weight polymer and effectively cross-linking of PEG. G3 hydrogels showed the lowest stiffness since the rigidity and steric hindrance of the bulky structures caused the low cross-linking density. The combination of DTT with G2- or G3-PAMAM dendrimers could significantly improve the stiffness of the G2 or G3 hydrogels by increasing cross-linking density. The microstructure of the hydrogels measured by SEM supports the result of mechanical properties. The hydrogels with a thicker layer of interior compacted outer edge and a denser

المنارة للاستشارات
www.manaraa.com

exterior surface (PEG and PEGDTT) exhibited higher mechanical stiffness. The G2DTT and G3DTT hydrogels with a smaller average pore size showed higher mechanical stiffness compared to G2 and G3 hydrogels because of increasing in cross-linking density. Although PEG and PEGDTT hydrogels provided the similar gelation time and mechanic stiffness, PEGDTT hydrogels exhibited a smaller average pore size and less porosity compare to PEG hydrogels. It could be explained by a formation of disulfide bond between the thiol groups of 4-arm PEG and DTT, leading to less available thiol groups to form thiol–ene linkages. Thus, the smaller average pore size and less porosity were observed in PEGDTT hydrogels.

3.2.2.3 Swelling Properties and Permeability of the Hydrogels

The swollen hydrogels reached the swelling equilibrium after being immersed in PBS for 2 days. We observed that swelling ratios of all hydrogels maintained the same after 14 days (data not shown). The water content and swelling ratios of the hydrogels are shown in Figure 3.8. All of the hydrogels had water content more than 90%. The swelling ratios of G3 hydrogel showed the highest ($Q_m \sim 70$, $Q_v \sim 86$) and were followed by G2 ($Q_m \sim 59$, $Q_v \sim 72$), DTT ~ G3DTT ~ G2DTT ($Q_m \sim 40$, $Q_v \sim 50$), and PEG ~ PEGDTT hydrogels ($Q_m \sim 16$, $Q_v \sim 20$), respectively. The statistically lower water content and swelling ratios were observed for G3DTT and G2DTT compared to G3 and G2 hydrogels, respectively.

المنارة للاستشارات
www.manaraa.com

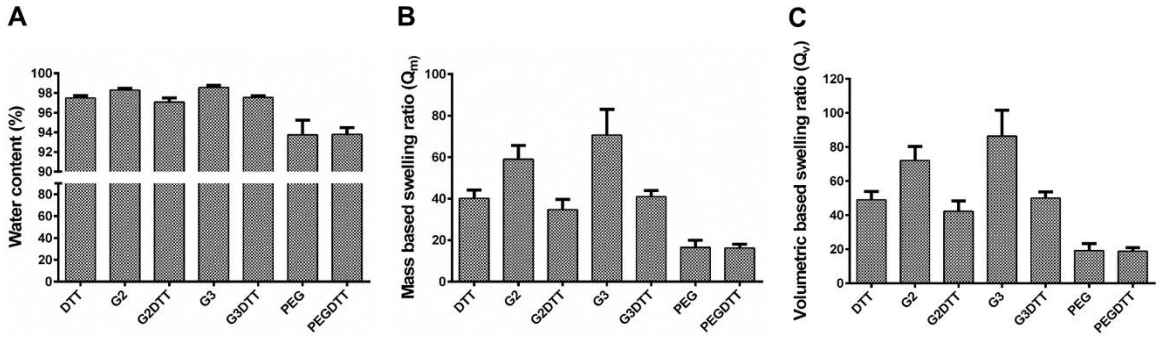

Figure 3.8. Swelling properties of the thiol–ene "click" HA hydrogels. (A) Water content of the hydrogels after being immersed in PBS for 2 days. (B) Mass-based swelling ratios of the hydrogels. (C) Volumetric-based swelling ratio of the hydrogels (n = 6).

The release of BSA proteins from the hydrogels was observed during 24 h. As shown in Figure 3.9A, the release of BSA from PEG and PEGDTT hydrogels was completed in 15 min, while the release of BSA from other hydrogels was not completed in 24 h. The release of BSA was rapid and became slower after 15 min in DTT and G2DTT hydrogels, 30 min in G3DTT hydrogels, and 60 min in G2 and G3 hydrogels. The total amount of BSA accumulated in the hydrogels was calculated by totaling BSA release during 24 h and any BSA entrapped within the hydrogels after 24 h (Figure 3.9B). In general, the total BSA accumulation in the hydrogels showed a similar trend to the swelling properties of the hydrogels. Namely, the total BSA accumulation in the G2 and G3 hydrogels showed the similar highest (~100 μg) and were followed by G3DTT (~72 μg), DTT ~ G2DTT (~45 μg), and PEGDTT ~ PEG hydrogels (~13 μg).

المنارة للاستشارات
www.manaraa.com

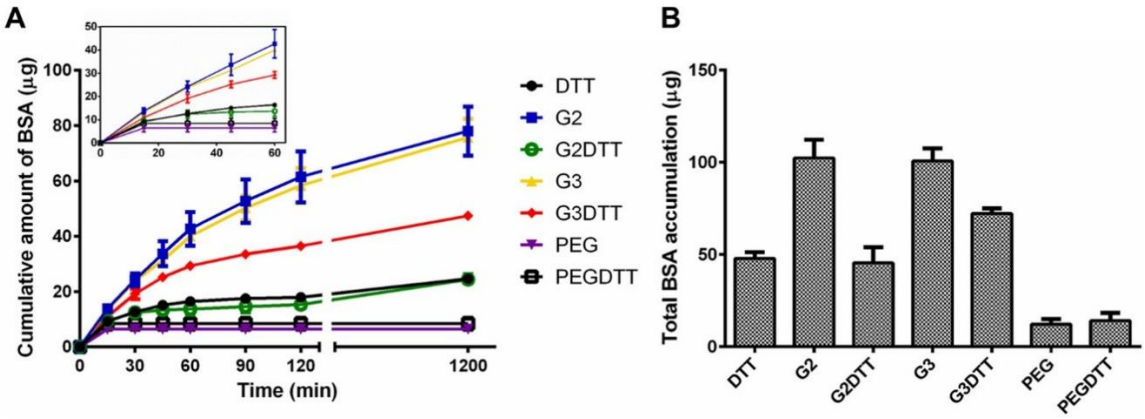

Figure 3.9. Permeability of the thiol–ene "click" HA hydrogels. (A) BSA release profile of the hydrogels showing the cumulative amount of BSA released from the hydrogels to supernatant for 24 h. The inset shows the BSA release profile of the hydrogels in first 60 min. (B) Total amount of BSA accumulated in the hydrogel scaffolds (n = 6).

The swelling properties, BSA release profile, and BSA accumulation were associated with the mechanical property and microstructure of the hydrogels. Overall, the hydrogels with a lower mechanic stiffness, larger pore size, and thinner layer of outer edge provided higher swelling properties, BSA release and BSA accumulation. The chemical properties of the cross-linkers should be also considered for BSA accumulation. As shown in Figure 3.8B, the BSA accumulation in both PEG and PEGDTT hydrogels was greatly lower than others. It could be the result of inherently protein-repellent properties of PEG, besides the hydrogel architectures. PEG rarely adsorb proteins since the surfaces of PEG can interact to a number of water molecules via hydrogen bonds and form repulsive forces to proteins.[37]

3.2.2.4 Degradation Time of the Hydrogels

The amount of uronic acid released in a solution of 100 U hyaluronidase/mL of PBS is shown in Figure 3.10A. For DTT as well as G2 and G3 hydrogels, more than 65% of uronic acid was found within 1 day of degradation, and the complete degradation was

المنارة للاستشارات
www.manaraa.com

observed within 2 or 3 days. For G3DTT hydrogels, ~90% of the uronic acid was detected within 3 days, and then the degradation extended to 6 days. PEG and PEGDTT hydrogels showed a similar degradation profile; more than 50% of the uronic acid was observed within 3 days, and the complete degradation extended to 10 days. The slow release of uronic acid was observed in G2DTT hydrogel; ~40% of uronic acid was found in the first 3 days, then the degradation rate was slower until 5 days, and the complete degradation was observed ~13 days. The complete degradation time of the hydrogels in the hyaluronidase solutions is shown in Figure 3.10B.

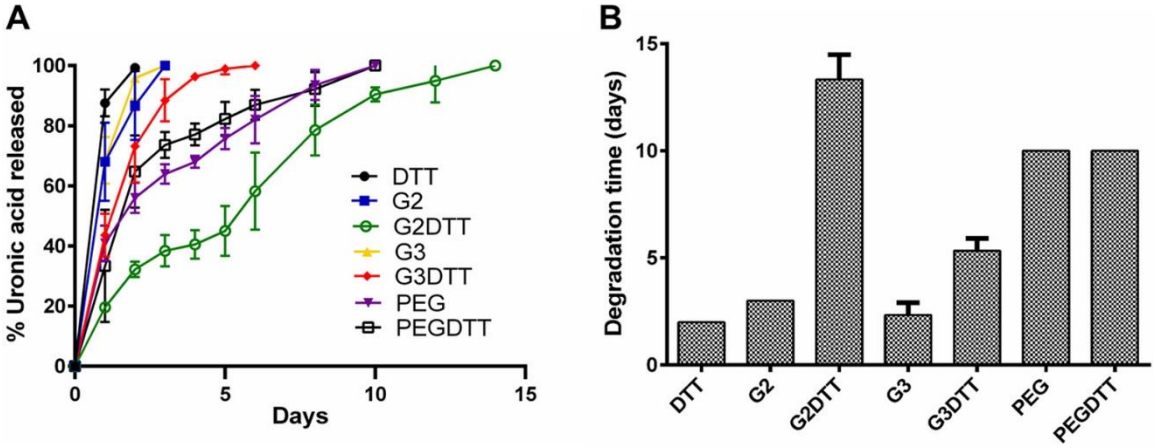

Figure 3.10. Degradation of the thiol–ene "click" HA hydrogels. (A) Degradation profile of the hydrogels plotted as the percentage of total uronic acid released with degradation time. (B) Degradation time of the hydrogels (n = 3).

The degradation of the hydrogels by hyaluronidase was from the cleavage of HA at the endo-β-*N*-acetyl-d-glucosaminidic linkages, resulting in oligomers with *N*-acetylglucosamine and glucuronic acid. Overall, the size of the hydrogels was decreased during exposure to the hyaluronidase, which was similarly observed in other cross-linked HA hydrogels.[38] Importantly, we observed a good correlation between the degradation time and microstructure and swelling properties of the hydrogels. Also, it should be noted that

المنارة للاستشارات
www.manaraa.com

the results are only relative degradation times. The actual *in vitro* degradation times depend on the concentration of hyaluronidase from cells.

3.3 CONCLUSIONS

The structure of thiol-tailored cross-linkers significantly influences the physical properties of the thiol–ene "click" HA hydrogels by change the morphology, mechanical stiffness, permeability, and degradation rate of the hydrogels. The 4-arm-PEG cross-linker generated the highest stiffed hydrogel, largest pore size, lowest permeability, and longest degradation time compared to the hydrogels created by DTT and PAMAM cross-linkers. The PAMAM cross-linkers, both G2 and G3, did not improve the mechanical properties of the hydrogels, but promoted a wider range of pore sizes, higher permeability, and longer degradation rate compared to the DTT-HA hydrogels. The combination of PAMAM and DTT cross-linkers could create higher mechanical properties, porosity, smaller pore sizes compared to their individual-crosslinked hydrogels. However, the combination of 4-arm PEG and DTT did not showed significantly improved mechanical properties of the hydrogels, instead, it generated a less porous hydrogels compared to their individual-crosslinked hydrogels.

3.4 MATERIALS AND METHODS

3.4.1 Modification of HA

Methacrylated HA (MeHA) was synthesized following the literature protocols.[20,39,40] Briefly, HA of molecular weight 47 kDa (Dali) was dissolved at 1 wt% in potassium phosphate buffer, pH 8, and methacrylic anhydride (Alfa Aesar) of 6-fold molar excess (relative to the HA disaccharide repeat unit) was added dropwise to the solution at

المنارة للاستشارات
www.manaraa.com

0 °C. The pH of the two-phase reaction mixture was adjusted to 8.0 with 5 M NaOH aq., and the reaction continued for 24 h at 4 °C with frequent re-adjustment of the solution pH. The product was dialyzed against Milli-Q water for at least 48 h, followed by centrifugation to remove the precipitate, which was then flash frozen in liquid nitrogen, and lyophilized, resulting in powder which was analyzed degree of modification by ^{1}H NMR.

3.4.2 Synthesis of Thiol-tailored G2 and G3 PAMAM Dendrimers

PAMAM dendrimer of generation 2 and generation 3 (G2- and G3-PAMAM) with amine terminal groups was ordered from Dendritech Inc. (Midland, MI, USA). 2-Iminothiolane hydrochloride was ordered from Chem-Impex International, Inc. (Wood Dale, IL). Compounds were used in the synthesis without further purification.

To synthesize thiol-tailored G2-PAMAM (PAMAM-G2-16SH), G2-PAMAM (281 mg, 0.0863 mmol) was dissolved in deionized water (15 mL) before 2-iminothiolane hydrochloride (190 mg, 1.38 mmol) was added to the dendrimer solution. Nitrogen gas was bubbled into the solution to replace oxygen in solution as well as in the reaction flask. The resulting mixture was stirred at room temperature for 24 h. The product G2-16SH (383 mg) was obtained in 91% yield after membrane filtration through a 1,000-molecular weight cut-off (MWCO) membrane followed by lyophilization. The degree of thiolation was confirmed by ^{1}H NMR and MALDI-TOF analyses.

To synthesize thiol-tailored G3-PAMAM (PAMAM-G3-32SH), G3-PAMAM (388 mg, 0.0561 mmol) was dissolved in deionized water (20 mL). 2-Iminothiolane hydrochloride (247 mg, 1.80 mmol) was added to the dendrimer solution. Nitrogen gas was bubbled into the solution to replace oxygen in solution as well as in the reaction flask. The

المنارة للاستشارات
www.manaraa.com

resulting mixture was stirred at room temperature for 24 h. The product G3-32SH (507 mg) was obtained in 89% yield after membrane filtration through a 1,000-MWCO membrane followed by lyophilization. The degree of thiolation was confirmed by ^{1}H NMR and MALDI-TOF.

3.4.3 Hydrogel Formation

Seven different HA hydrogels were formed via thiol–ene "click" reaction (see Table 3.1 and Figure 3.3). To form the thiol–ene "click" HA hydrogels, MeHA polymers with approximate 40% degree of modification were dissolved in a phosphate buffered saline solution (PBS) at 3 wt% concentration, and the PAMAM-G2-16SH, PAMAM-G3-32SH or 4-arm thiol-tailored PEG (Jenkem Technology, PEG-4SH) in PBS was added to make a final concentration of 2 wt% (the calculated molar ratio of thiol:ene in each formulation was shown in Table 3.1). The pH of the mixture was adjusted to 8.0 with 2 M NaOH aq. For enhancing matrix stiffness purposes, DTT crosslinkers was then additionally added at a molar ratio of thiol:ene = 2:1. For comparison purposes, the thiol–ene "click" HA hydrogels were also synthesized by the same procedure with only DTT as a crosslinker.

3.4.4 Microstructure Analysis

Microstructure of the hydrogels was characterized using Scanning Electron Microscope (SEM). The hydrogel samples were lyophilized, then cross-sectioned and mounted on metal stubs with carbon tape. The samples were sputtered coated with gold/palladium for 30 sec on a Denton Desk II sputter coater with global rotation and tilt. The surfaces of the gold/palladium-coated hydrogels samples were observed at 5-8 random locations per sample (n = 3) on a Zeiss Ultraplus Thermal Field Emission SEM at 10 kV.

المنارة للاستشارات
www.manaraa.com

3.4.5 Gelation Test

The hydrogels were prepared previously described by using PBS as the medium. The gelation time was measured by the vial tilting method.[41] When the sample showed no flow within 20 s, it was considered as being completely formed hydrogel.

3.4.6 Mechanical Properties

Oscillatory shear test was performed using a DHR-3 rheometer (TA instrument) with 12 mm diameter parallel-plate geometry and temperature controlled Peltier plate. The hydrogels were prepared previously described by using PBS as the medium. After gelation for 2 days, the samples were cut into uniform cylinders and placed on a metal plate, where the tests were performed. Amplitude sweeps at constant frequency (1 rad/s) were performed to determine the linear viscoelastic range of deformation for each sample, after which frequency sweeps (0.1-10 rad/s) were performed at a strain amplitude within the linear range (1%). In amplitude and frequency sweeps measurement, the geometry gaps were conditioned by axial force at 0.2 N for every run.

3.4.7 Swelling Properties

The hydrogels were prepared from 50 μL of polymer solutions. Hydrogels were allowed to swell for 2 days in PBS and were then blotted to remove excess water and weighed to obtain the swollen hydrogel mass, M_s. These hydrogels were then dried by lyophilizing to determine the final dry mass, M_d. After that, water content and swelling ratios were calculated from the swollen and dry hydrogel masses. The percent water content was determined by:

المنارة للاستشارات
www.manaraa.com

$$(M_s - M_d / M_s) \times 100 = \text{water content}$$

The mass based swelling ratio, Q_M, was calculated by dividing the hydrogel mass after swelling, M_s, by the mass after the hydrogel has dried, M_d. The volumetric based swelling ratio, Q_v, was then calculated from Q_M according to equation:

$$Q_v = 1 + \rho_p / \rho_s (Q_M - 1)$$

where ρ_p is the density of the dry polymer (1.229, 1.222, and 1.094 g/cm^3 for MeHA, PAMAM, and PEG-4SH, respectively) and ρ_s is the density of the solvent (1 g/cm^3 for water). Values for ρ_p of the G2, G2DTT, G3, G3DTT, PEG and PEGDTT hydrogels were calculated by estimating the molar volume for the PAMAM-G2-16SH/MeHA, PAMAM-G3-32SH/MeHA or PEG-4SH/MeHA polymer segment and divided by the molecular weight of the segment.

3.4.8 Protein Release Profile and Protein Accumulation

To study the protein release profile and protein accumulation within the hydrogels, bovine serum albumin (BSA) was chosen as the model solute for diffusion. To mimic exogenously supplemented growth factor accumulation in 3D tissue engineering scaffolds, the premade hydrogels (2 mm thickness, 4 mm diameter) were immersed in BSA solution (1 mg/ml) at room temperature for 30 h to achieve uniform protein loading. For protein diffusivity on the order of 10^{-7} cm^2/s, the diffusion time is 15 h for a diffusion length of 1.5 mm ($t \sim L^2/4D$). Therefore, a 30-h loading time should be sufficient to achieve equilibrium protein concentrations within the hydrogels. The loading time observed in similar studies of various model proteins through even denser polymer networks further support the rationale for a 30 h loading time.[42]

المنارة للاستشارات
www.manaraa.com

To study the protein release profile, the BSA-loaded hydrogels were immersed in PBS. All supernatant was collected and replaced by fresh PBS at different time points (t = 5, 10, 15, 30, 45, 60, 90, 120 min and 24 h). Any proteins that remained entrapped in the hydrogels after 24 h were released by mechanically breaking down the hydrogels in fresh PBS using a homogenizer. To quantify the protein in the supernatant, a Coomassie (Bradford) protein assay (Thermo scientific) was performed following the manufacturer's protocol. The standard calibration curve of BSA was also established in order to determine the amount of BSA (Figure 3.11).

Protein accumulation was calculated from the protein released into supernatant at different time points and the protein that remained trapped in the gel after the 24 h release.

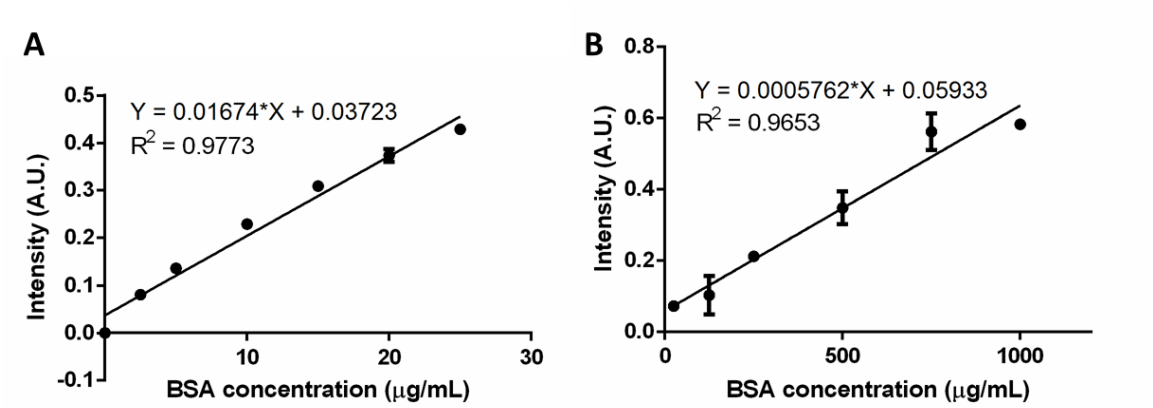

Figure 3.11. Fluorescence spectroscopy calibration with linear fitting curve and equation for quantification of BSA proteins at concentration of 0-25 µg/mL (A), and 50-1000 µg/mL (B).

3.4.9 Degradation Profile

Hydrogels (40 µL, 2 mm thickness, 4 mm diameter) were loaded into a 48-well plate. The samples were digested in 400 µL of 100 U hyaluronidase (Sigma) in PBS (replaced every 24 h throughout the study and stored frozen until analysis) at 37°C. The

المنارة للاستشارات
www.manaraa.com

amount of uronic acid (a degradation component of HA) released during degradation was measured using a carbazole assay in a 96-well plate.[43] Briefly, 50 µL of the degradation solution was added in a 96-well plate. 200 µL of a solution of 25 mM sodium tetraborate in sulfuric acid was added. The plate was heated for 10 min at 100 °C in an oven. After cooling at room temperature for 15 min, 50 µL of 0.125% carbazole in absolute ethanol were carefully added. After heating at 100 °C for 10 min in an oven and cooling at room temperature for 15 min, the plate was read in a SpectraMax M2 Multi-Mode microplate reader (Molecular Devices) at a wavelength of 550 nm. Any possible lid on the plate was avoided as a decrease in the reaction intensity.[43]

The amount of uronic acid was determined using a serial dilution of 1 mg/mL of the 47 kDa HA solution as a standard (Figure 3.12). The time for complete degradation of the hydrogels was reported as no amount of the uronic acid and scaffold remainder were observed. The percent degradation at each time point was calculated by dividing the amount of uronic acid released at a given time point by the final amount of uronic acid collected when the hydrogel was completely degraded.

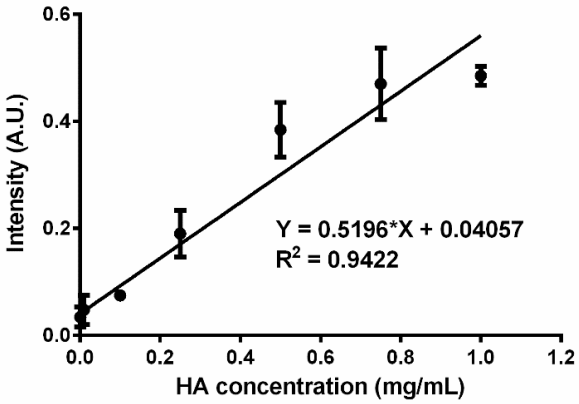

Figure 3.12. UV-Vis spectroscopy calibration with linear fitting curve and equation for quantification of HA at concentration of 0-1 mg/mL.

المنارة للاستشارات
www.manaraa.com

3.5 REFERENCES

(1) Engler, A. J.; Sen, S.; Sweeney, H. L.; Discher, D. E. Matrix Elasticity Directs Stem Cell Lineage Specification. *Cell* **2006,** *126*, 677-689.

(2) Vickers, S. M.; Gotterbarm, T.; Spector, M. Cross-Linking Affects Cellular Condensation and Chondrogenesis in Type Ii Collagen-Gag Scaffolds Seeded with Bone Marrow-Derived Mesenchymal Stem Cells. *J. Orthop. Res.* **2010,** *28*, 1184-1192.

(3) Serpooshan, V.; Julien, M.; Nguyen, O.; Wang, H.; Li, A.; Muja, N.; Henderson, J. E.; Nazhat, S. N. Reduced Hydraulic Permeability of Three-Dimensional Collagen Scaffolds Attenuates Gel Contraction and Promotes the Growth and Differentiation of Mesenchymal Stem Cells. *Acta Biomater* **2010,** *6*, 3978-3987.

(4) Kemppainen, J. M.; Hollister, S. J. Differential Effects of Designed Scaffold Permeability on Chondrogenesis by Chondrocytes and Bone Marrow Stromal Cells. *Biomaterials* **2010,** *31*, 279-287.

(5) Bryant, S.; Nuttelman, C.; Anseth, K. The Effects of Crosslinking Density on Cartilage Formation in Photocrosslinkable Hydrogels. *Biomed. Sci. Instrum.* **1998,** *35*, 309-314.

(6) Erickson, I. E.; Huang, A. H.; Sengupta, S.; Kestle, S.; Burdick, J. A.; Mauck, R. L. Macromer Density Influences Mesenchymal Stem Cell Chondrogenesis and Maturation in Photocrosslinked Hyaluronic Acid Hydrogels. *Osteoarthritis Cartilage* **2009,** *17*, 1639-1648.

(7) Gilbert, P. M.; Havenstrite, K. L.; Magnusson, K. E. G.; Sacco, A.; Leonardi, N. A.; Kraft, P.; Nguyen, N. K.; Thrun, S.; Lutolf, M. P.; Blau, H. M. Substrate Elasticity Regulates Skeletal Muscle Stem Cell Self-Renewal in Culture. *Science* **2010,** *329*, 1078-1081.

المنارة للاستشارات
www.manaraa.com

(8) Parekh, S. H.; Chatterjee, K.; Lin-Gibson, S.; Moore, N. M.; Cicerone, M. T.; Young, M. F.; Simon Jr, C. G. Modulus-Driven Differentiation of Marrow Stromal Cells in 3d Scaffolds That Is Independent of Myosin-Based Cytoskeletal Tension. *Biomaterials* **2011,** *32*, 2256-2264.

(9) Khetan, S.; Guvendiren, M.; Legant, W. R.; Cohen, D. M.; Chen, C. S.; Burdick, J. A. Degradation-Mediated Cellular Traction Directs Stem Cell Fate in Covalently Crosslinked Three-Dimensional Hydrogels. *Nature materials* **2013,** *12*, 458-465.

(10) Wang, T.; Lai, J. H.; Han, L.-H.; Tong, X.; Yang, F. Chondrogenic Differentiation of Adipose-Derived Stromal Cells in Combinatorial Hydrogels Containing Cartilage Matrix Proteins with Decoupled Mechanical Stiffness. *Tissue Engineering Part A* **2014,** *20*, 2131-2139.

(11) Park, J. S.; Chu, J. S.; Tsou, A. D.; Diop, R.; Tang, Z.; Wang, A.; Li, S. The Effect of Matrix Stiffness on the Differentiation of Mesenchymal Stem Cells in Response to Tgf-B. *Biomaterials* **2011,** *32*, 3921-3930.

(12) Wu, C.; Zhang, Y.; Zhu, Y.; Friis, T.; Xiao, Y. Structure–Property Relationships of Silk-Modified Mesoporous Bioglass Scaffolds. *Biomaterials* **2010,** *31*, 3429-3438.

(13) Huebsch, N.; Arany, P. R.; Mao, A. S.; Shvartsman, D.; Ali, O. A.; Bencherif, S. A.; Rivera-Feliciano, J.; Mooney, D. J. Harnessing Traction-Mediated Manipulation of the Cell/Matrix Interface to Control Stem-Cell Fate. *Nat Mater* **2010,** *9*, 518-526.

(14) Vega, S. L.; Kwon, M. Y.; Burdick, J. A. Recent Advances in Hydrogels for Cartilage Tissue Engineering. *European cells & materials* **2017,** *33*, 59-75.

المنارة للاستشارات
www.manaraa.com

(15) Levett, P. A.; Hutmacher, D. W.; Malda, J.; Klein, T. J. Hyaluronic Acid Enhances the Mechanical Properties of Tissue-Engineered Cartilage Constructs. *PLoS One* **2014,** *9*, e113216.

(16) Little, C. J.; Kulyk, W. M.; Chen, X. The Effect of Chondroitin Sulphate and Hyaluronic Acid on Chondrocytes Cultured within a Fibrin-Alginate Hydrogel. *Journal of Functional Biomaterials* **2014,** *5*, 197-210.

(17) Palumbo, F. S.; Fiorica, C.; Di Stefano, M.; Pitarresi, G.; Gulino, A.; Agnello, S.; Giammona, G. In Situ Forming Hydrogels of Hyaluronic Acid and Inulin Derivatives for Cartilage Regeneration. *Carbohydr Polym* **2015,** *122*, 408-416.

(18) Ogawa, M.; Kitamura, N.; Kurokawa, T.; Arakaki, K.; Tanaka, Y.; Gong, J. P.; Yasuda, K. Poly(2-Acrylamido-2-Methylpropanesulfonic Acid) Gel Induces Articular Cartilage Regeneration in Vivo: Comparisons of the Induction Ability between Single- and Double-Network Gels. *Journal of Biomedical Materials Research Part A* **2012,** *100A*, 2244-2251.

(19) Kitamura, N.; Yokota, M.; Kurokawa, T.; Gong, J. P.; Yasuda, K. In Vivo Cartilage Regeneration Induced by a Double-Network Hydrogel: Evaluation of a Novel Therapeutic Strategy for Femoral Articular Cartilage Defects in a Sheep Model. *J Biomed Mater Res A* **2016,** *104*, 2159-2165.

(20) Maturavongsadit, P.; Luckanagul, J. A.; Metavarayuth, K.; Zhao, X.; Chen, L.; Lin, Y.; Wang, Q. Promotion of in Vitro Chondrogenesis of Mesenchymal Stem Cells Using in Situ Hyaluronic Hydrogel Functionalized with Rod-Like Viral Nanoparticles. *Biomacromolecules* **2016,** *17*, 1930-1938.

المنارة للاستشارات
www.manaraa.com

(21) Held, K. D.; Sylvester, F. C.; Hopcia, K. L.; Biaglow, J. E. Role of Fenton Chemistry in Thiol-Induced Toxicity and Apoptosis. *Radiat. Res.* **1996,** *145*, 542-553.

(22) Park, Y.; Lutolf, M. P.; Hubbell, J. A.; Hunziker, E. B.; Wong, M. Bovine Primary Chondrocyte Culture in Synthetic Matrix Metalloproteinase-Sensitive Poly (Ethylene Glycol)-Based Hydrogels as a Scaffold for Cartilage Repair. *Tissue Eng.* **2004,** *10*, 515-522.

(23) Tan, H.; DeFail, A.; Rubin, J. P.; Chu, C. R.; Marra, K. G. Novel Multi-Arm Peg-Based Hydrogels for Tissue Engineering. *J Biomed Mater Res A* **2010,** *92*, 979-987.

(24) Salinas, C. N.; Anseth, K. S. Decorin Moieties Tethered into Peg Networks Induce Chondrogenesis of Human Mesenchymal Stem Cells. *Journal of Biomedical Materials Research Part A* **2009,** *90A*, 456-464.

(25) Steinmetz, N. J.; Aisenbrey, E. A.; Westbrook, K. K.; Qi, H. J.; Bryant, S. J. Mechanical Loading Regulates Human Msc Differentiation in a Multi-Layer Hydrogel for Osteochondral Tissue Engineering. *Acta Biomater* **2015,** *21*, 142-153.

(26) Stevens, K. R.; Miller, J. S.; Blakely, B. L.; Chen, C. S.; Bhatia, S. N. Degradable Hydrogels Derived from Peg-Diacrylamide for Hepatic Tissue Engineering. *Journal of Biomedical Materials Research Part A* **2015,** *103*, 3331-3338.

(27) Mann, B. K.; Gobin, A. S.; Tsai, A. T.; Schmedlen, R. H.; West, J. L. Smooth Muscle Cell Growth in Photopolymerized Hydrogels with Cell Adhesive and Proteolytically Degradable Domains: Synthetic Ecm Analogs for Tissue Engineering. *Biomaterials* **2001,** *22*, 3045-3051.

المنارة للاستشارات
www.manaraa.com

(28) Aimetti, A. A.; Machen, A. J.; Anseth, K. S. Poly(Ethylene Glycol) Hydrogels Formed by Thiol-Ene Photopolymerization for Enzyme-Responsive Protein Delivery. *Biomaterials* **2009,** *30*, 6048-6054.

(29) Yang, H.; Kao, W. J. Dendrimers for Pharmaceutical and Biomedical Applications. *J. Biomater. Sci. Polym. Ed.* **2006,** *17*, 3-19.

(30) Desai, P. N.; Yuan, Q.; Yang, H. Synthesis and Characterization of Photocurable Polyamidoamine Dendrimer Hydrogels as a Versatile Platform for Tissue Engineering and Drug Delivery. *Biomacromolecules* **2010,** *11*, 666-673.

(31) Jiang, L.-Y.; Lv, B.; Luo, Y. The Effects of an Rgd-Pamam Dendrimer Conjugate in 3d Spheroid Culture on Cell Proliferation, Expression and Aggregation. *Biomaterials* **2013,** *34*, 2665-2673.

(32) Bi, X.; Liang, A.; Tan, Y.; Maturavongsadit, P.; Higginbothem, A.; Gado, T.; Gramling, A.; Bahn, H.; Wang, Q. Thiol-Ene Crosslinking Polyamidoamine Dendrimer-Hyaluronic Acid Hydrogel System for Biomedical Applications. *J. Biomater. Sci. Polym. Ed.* **2016**, 1-27.

(33) Wang, Y.; Zhao, Q.; Zhang, H.; Yang, S.; Jia, X. A Novel Poly(Amido Amine)-Dendrimer-Based Hydrogel as a Mimic for the Extracellular Matrix. *Adv. Mater.* **2014,** *26*, 4163-4167.

(34) Bi, X.; Amie Luckanagul, J.; Allen, A.; Ramaboli, M.; Campbell, E.; West, D.; Maturavongsadit, P.; Brummett, K.; Wang, Q. Synthesis of Pamam Dendrimer-Based Fast Cross-Linking Hydrogel for Biofabrication. *J. Biomater. Sci. Polym. Ed.* **2015,** *26*, 669-682.

المنارة للاستشارات
www.manaraa.com

(35) Bian, L.; Hou, C.; Tous, E.; Rai, R.; Mauck, R. L.; Burdick, J. A. The Influence of Hyaluronic Acid Hydrogel Crosslinking Density and Macromolecular Diffusivity on Human Msc Chondrogenesis and Hypertrophy. *Biomaterials* **2013,** *34*, 413-421.

(36) Hoyle, C. E.; Lowe, A. B.; Bowman, C. N. Thiol-Click Chemistry: A Multifaceted Toolbox for Small Molecule and Polymer Synthesis. *Chem Soc Rev* **2010,** *39*, 1355-1387.

(37) Zheng, J.; Li, L.; Tsao, H.-K.; Sheng, Y.-J.; Chen, S.; Jiang, S. Strong Repulsive Forces between Protein and Oligo (Ethylene Glycol) Self-Assembled Monolayers: A Molecular Simulation Study. *Biophys. J.* **2005,** *89*, 158-166.

(38) Prestwich, G. D.; Marecak, D. M.; Marecek, J. F.; Vercruysse, K. P.; Ziebell, M. R. Controlled Chemical Modification of Hyaluronic Acid: Synthesis, Applications, and Biodegradation of Hydrazide Derivatives. *J. Controlled Release* **1998,** *53*, 93-103.

(39) Smeds, K. A.; Pfister-Serres, A.; Miki, D.; Dastgheib, K.; Inoue, M.; Hatchell, D. L.; Grinstaff, M. W. Photocrosslinkable Polysaccharides for in Situ Hydrogel Formation. *J. Biomed. Mater. Res.* **2001,** *54*, 115-121.

(40) Marklein, R. A.; Burdick, J. A. Controlling Stem Cell Fate with Material Design. *Adv Mater* **2010,** *22*, 175-189.

(41) Hiemstra, C.; Zhou, W.; Zhong, Z.; Wouters, M.; Feijen, J. Rapidly in Situ Forming Biodegradable Robust Hydrogels by Combining Stereocomplexation and Photopolymerization. *J. Am. Chem. Soc.* **2007,** *129*, 9918-9926.

(42) Weber, L. M.; Lopez, C. G.; Anseth, K. S. Effects of Peg Hydrogel Crosslinking Density on Protein Diffusion and Encapsulated Islet Survival and Function. *Journal of Biomedical Materials Research Part A* **2009,** *90A*, 720-729.

المنارة للاستشارات
www.manaraa.com

(43) Cesaretti, M.; Luppi, E.; Maccari, F.; Volpi, N. A 96-Well Assay for Uronic Acid Carbazole Reaction. *Carbohydr Polym* **2003,** *54*, 59-61.

المنارة للاستشارات
www.manaraa.com

CHAPTER 4

THE *IN VITRO* MESENCHYMAL STEM CELL CHONDROGENESIS AND OSTEOGENESIS IN DIFFERENT THIOL–ENE "CLICK" HA HYDROGELS[1]

4.1 INTRODUCTION

Osteochondral defects are the results of traumatic injuries or natural degradation of cartilaginous tissue by aging and involve serious damages to articular cartilage and underlying calcified subchondral bone.[1] The techniques for osteochondral repairs are limited because of low self-healing capacity of damaged cartilage,[2-4] donor-site morbidity, potential infection, and low integration with surrounding tissues.[5-8] Hence, the research in osteochondral tissue engineering has been extensively investigated and developed.[9,10] Yet, many challenges remain to be addressed in fabricating tissue-engineered scaffolds to optimally achieve osteochondral regeneration. One of the major challenges of developing scaffolds for cartilage and bone tissue engineering is the design of scaffolds that have perfect biocompatibility, biodegradability, and favorable physical and mechanical properties for 3D cell differentiation.[11] We have tried to address this challenge by developing novel *in situ* thiol–ene "click" HA hydrogels which were presented in previous chapter. Herein, we aimed to use the developed thiol–ene "click" hydrogels for promotion

[1] Portions of this chapter were adapted with permission from Maturavongsadit, P.; Bi, X.; Metavarayuth, K.; Amie Luckanagul, J.; Wang, Q. *ACS Applied Materials and Interfaces* **2017**, *9* (4), 3318–3329. Copyright (2017) American Chemical Society (Appendix D).

المنارة للاستشارات
www.manaraa.com

of cartilage and bone differentiation of bone marrow mesenchymal stem cells (BMSCs), which is ultimately for osteochondral regeneration. The effect of the physical and mechanical properties of the developed thiol–ene "click" hydrogels on BMSCs chondrogenesis and osteogenesis were particularly studied (Figure 4.1). We hypothesized that these properties had a highly impact on the performance of chondrogenic and osteogenic differentiation of BMSCs.

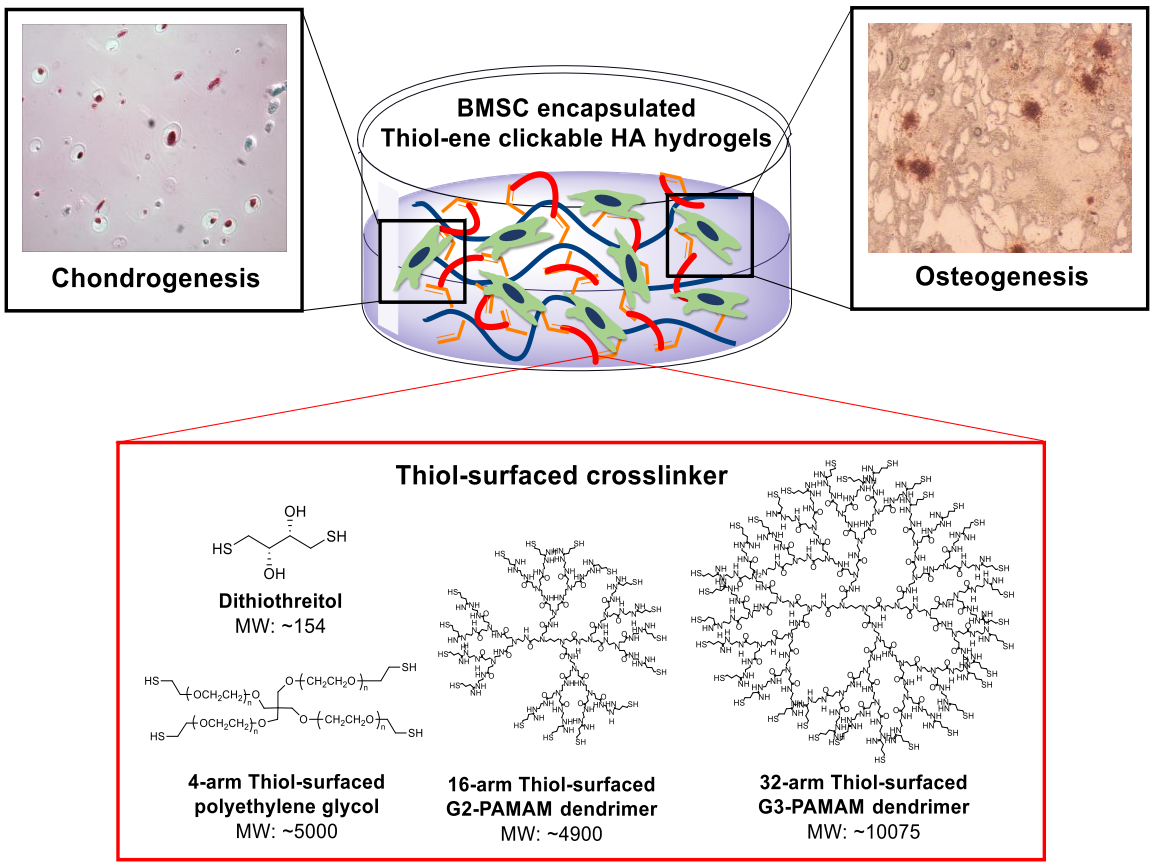

Figure 4.1. Schematic illustration of the research design for the study of the effect of cross-linker types on the chondrogenic and osteogenic differentiation by encapsulated BMSCs in the thiol–ene "click" HA hydrogels.

المنارة للاستشارات
www.manaraa.com

4.2 RESULTS AND DISCUSSION

4.2.1 Effect of Thiol–Ene "Click" HA Hydrogels on Viability of BMSCs

Before evaluation of the chondrogenic differentiation of BMSCs, the biocompatibility of the hydrogels was confirmed by CTB metabolic assay. BMSCs were encapsulated in the preformed hydrogel solutions at a concentration of 1×10^6 cells/mL. However, we observed that the gelation times of the encapsulated BMSC-G2 and -G3 hydrogels were longer than 12 h, which were unsuitable for *in vitro* study. The metabolic activities of the encapsulated BMSCs in other five hydrogels (DTT, G2DTT, G3DTT, PEG, and PEGDTT) indicated that more than 70% of the viable cells was observed in all groups after 7 days of culture (Figure 4.2C). However, the decrease in viability was seen in all hydrogels, especially in G3DTT hydrogels. The highest sustained viability was observed in DTT hydrogels. It is likely because the high cross-linking density and matrix stiffness can affect the transportation of nutrients and wastes between the culture media and encapsulated cells, which lead to compromised cell viability.[12] Nevertheless, the viability in the G3DTT hydrogels decrease significantly compared to the viability in other groups. It is conceivably due to incomplete modification of thiol group on G3-PAMAM dendrimers. Studies have showed that the toxicity of PAMAM dendrimers is dependent on their structures,[13,14] dose/concentration,[15-17] exposure duration, and generation.[15,16] The modification of the terminal groups of PAMAM dendrimer with negatively charged or neutral groups can reduce the toxicity.[16-18]

المنارة للاستشارات
www.manaraa.com

4.2.2 The Effect of Thiol–Ene "Click" HA Hydrogels on the In Vitro Chondrogenesis of MSCs

The stain for GAG of the encapsulated BMSC hydrogels under chondrogenic condition is shown in Figure 4.2A, and the quantitative analysis of the corresponded GAG signal intensities in Figure 4.2B. While light background staining was observed for the control hydrogels due to the HA composition (see Figure 4.3A), a more intense staining was observed in all hydrogels after 14 and 28 days of culture. Overall, the staining for GAG in all groups was consistently distributed. PEG hydrogels showed the significantly highest accumulation after 28 days. No significant difference of GAG values was observed among DTT, G2DTT, G3DTT, and PEGDTT hydrogels after 28 days.

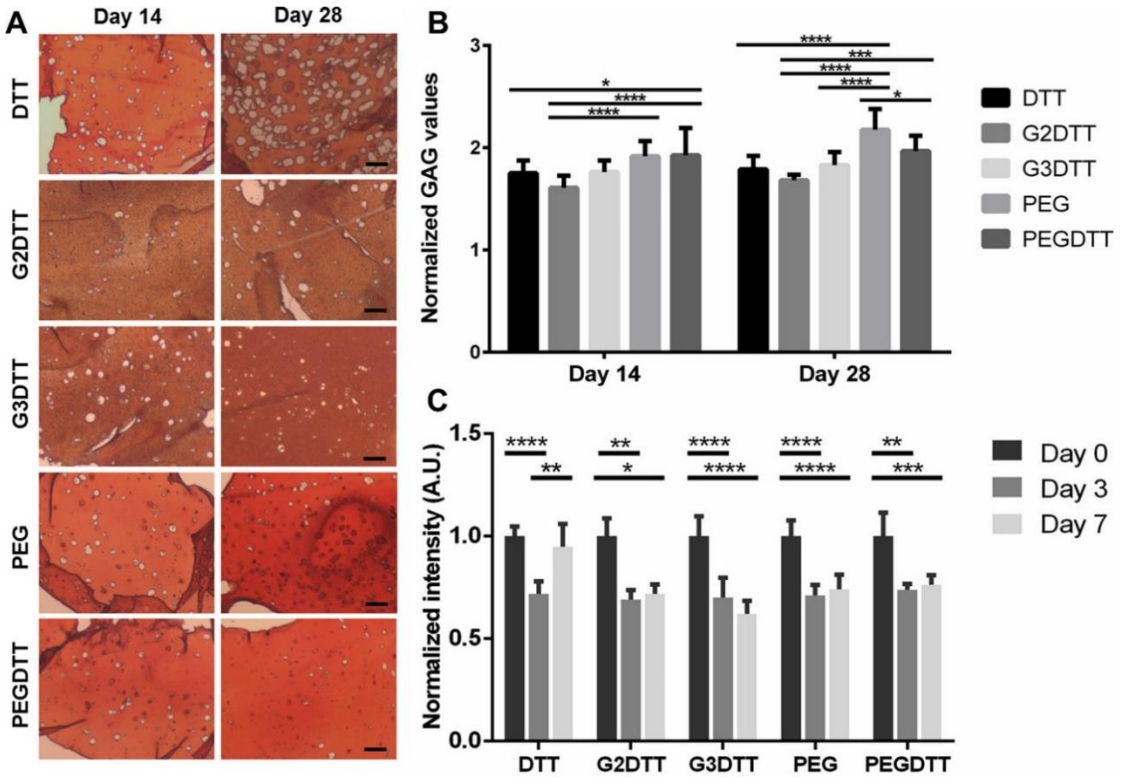

Figure 4.2. BMSC viability after culturing in complete growth media, and GAG accumulation of differentiated BMSCs in the hydrogels after culturing in chondrogenic media. (A) Histochemical staining for GAG (red) of differentiated BMSCs in the hydrogels

المنارة للاستشارات
www.manaraa.com

after 14 and 28 days of chondrogenic culture. The scale bar for all images: 100 µm. (B) The quantified signal intensities of GAG, shown in (A), normalized to the intensity of cytoplasm signal (green). (C) Cell metabolic activity of viable BMSCs in the hydrogels detected by Cell Titer-Blue assay. The intensity was normalized to the intensity values of day 0 for each hydrogel. Statistics: ANOVA with Tukey's multiple comparisons tests, n = 4, *p < 0.05, **p < 0.01, ***p < 0.005, ****p < 0.001.

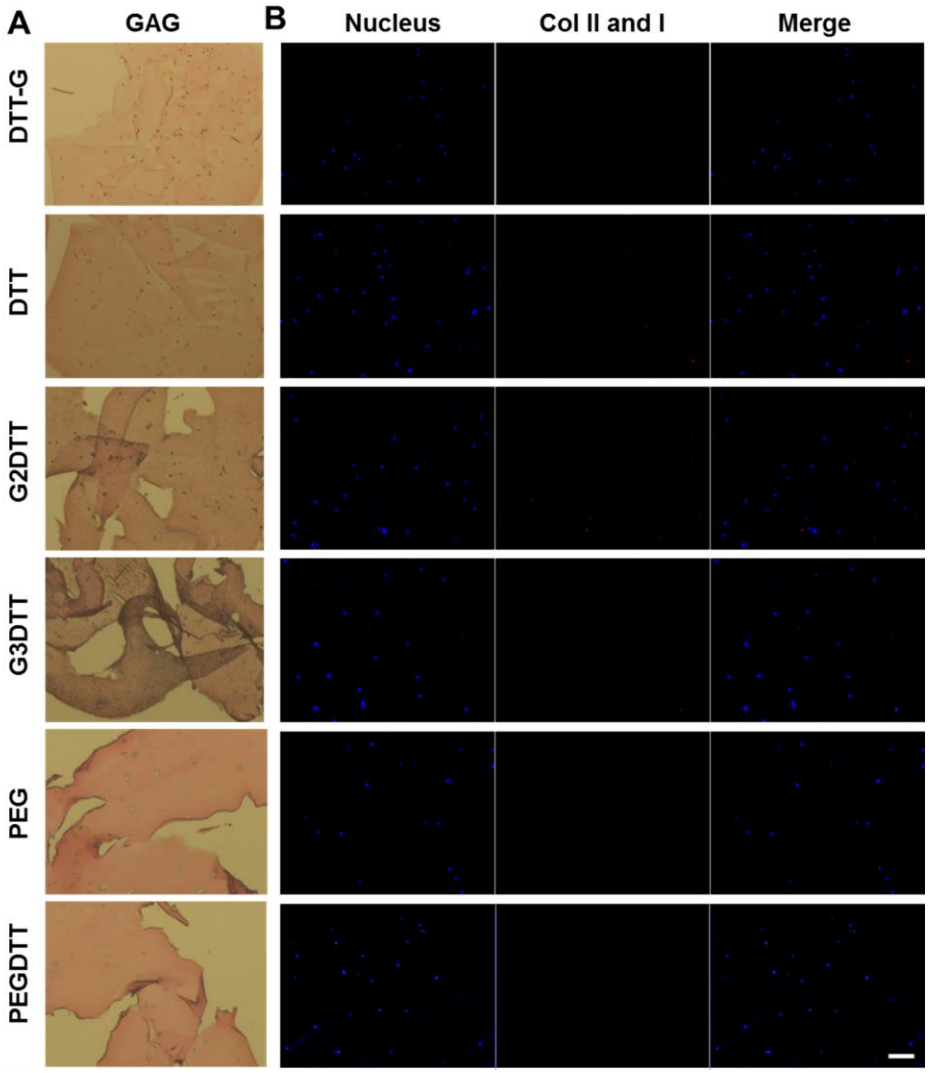

Figure 4.3. Negative controls of histochemical staining for GAG and immunohistostaining for type II and I collagen. (A) Histochemical staining for GAG (red) of non-differentiated BMSCs in the hydrogels after 3 days culturing in primary media (DTT-G) and after cell encapsulation (day 0) under chondrogenic condition. (B) Confocal images of non-differentiated BMSCs in the hydrogels under chondrogenic condition stained for nucleus (blue) type II collagen (red) and type I collagen (green) after cell encapsulation (day 0). All images share the same scale bar: 100 µm.

المنارة للاستشارات
www.manaraa.com

The immunohistochemical staining for type II collagen (chondrogenic marker) and type I collagen (hypertrophic marker) were further performed to evaluate the chondrogenesis of differentiated BMSC in the hydrogels. No color background was observed for the control hydrogels (see Figure 4.3B). Along culture period time, the staining of type II collagen in DTT, PEG, and PEGDTT groups was increasingly intense and mostly localized to the cellular region (Figure 4.4A, C). On the other hand, the staining of type II collagen in G2DTT and G3DTT groups was distributed lightly throughout the networks. PEG groups showed the highest of type II collagen accumulation, whereas G2DTT and G3DTT had the similar lowest of type II collagen accumulation. Unlike type II collagen results, on day 28, G2DTT and G3DTT groups displayed significantly more intense of type I collagen in the networks compared to DTT, PEG, and PEGDTT groups.

It is widely accepted that the quality of chondrogenesis of BMSCs is associated with subsequent hypertrophic differentiation, producing type I and X collagen, Runt-related transcription factor 2 (Runx2), alkaline phosphatase (ALP), and calcifications. The differentiated cells should produce substantial amounts of GAG and collagen type II instead of type I, in order to successfully form cartilage tissues.[19] In our results, the cells in PEG hydrogels showed the significantly highest GAG and type II collagen accumulation, while exhibiting the significantly lowest type I collagen accumulation compare to other hydrogels. In contrast, the cells in G2DTT and G3DTT hydrogels displayed the significantly lowest GAG and type II collagen accumulation, while exhibiting the significantly highest type I collagen accumulation. One plausible explanation for this observation relates to the mechanical stiffness, permeability, pore size, porosity, and chemistry of cross-linkers. In 2D systems, it has been shown that stiff substrates supported

المنارة للاستشارات
www.manaraa.com

chondrogenesis and suppressed chondrocyte hypertrophy by upregulation of a mechanotransduction mechanism through RhoA/ROCK signaling.[20] However, in 3D systems, the medium stiff matrix (~1–3 kPa) could support *in vitro* and *in vivo* chondrogenesis better than lower or higher stiffness.[21-23] Although the matrix stiffness of the ECM was shown to have crucial impacts in directing stem cell differentiation, it is not the only contributing factor to explain the phenomenon. Previous studies suggested that reducing the permeability of the scaffold was beneficial for chondrogenesis and would further reduce the amount of fibrous tissue formation, such as type I collagen, within the defect.[24,25] However, if the permeability of the scaffold is too low, it also leads to increased cell death. Whereas PEG and PEGDTT hydrogels provided the similar high stiffness and low permeability, the chondrogenesis in PEG hydrogels were significantly higher. It could be a result of the difference in pore size (100–200 μm for PEG hydrogels and 10–100 μm for PEGDTT hydrogels). Studies have suggested that larger pore sizes facilitated more newly secreted matrix. Chondrocytes in the scaffolds with pore size between 250 and 500 μm showed better ECM production and cell phenotype maintenance compared to the smaller ones (100 μm).[26-28] The cells in the smaller pores and high porosity often appeared as a dedifferentiated form, which also support our result showing the high production of type I collagen in G2DTT and G3DTT hydrogels.

المنارة للاستشارات
www.manaraa.com

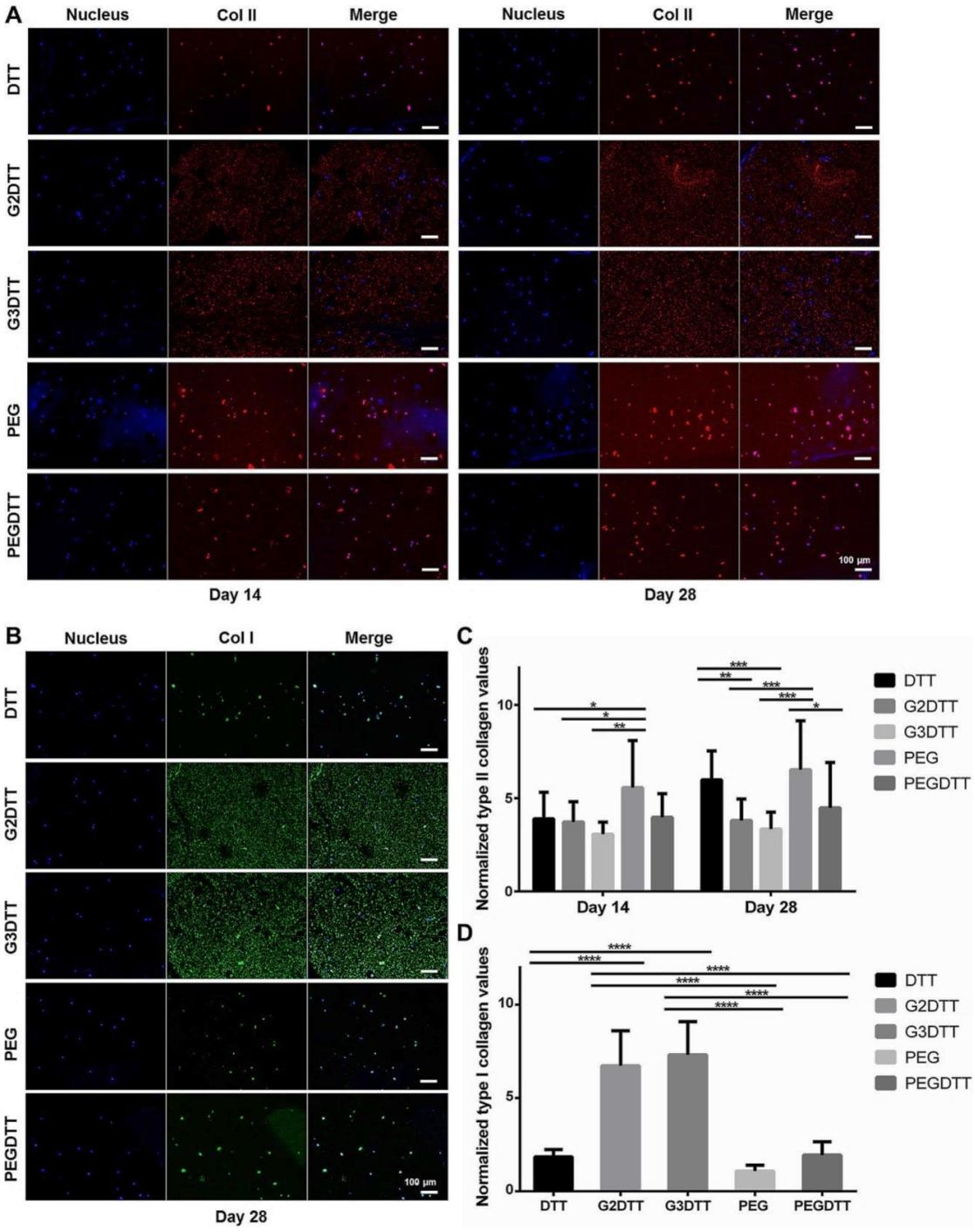

Figure 4.4. Type II and I collagen accumulation of differentiated BMSCs in the hydrogels after culturing in chondrogenic media. (A, B) Immunohistochemical staining for nucleus (blue), type II collagen (red), and type I collagen (green) of differentiated BMSCs in the hydrogels after 14 and 28 days of chondrogenic culture. The scale bars for all images: 100 µm. (C, D) The quantified signal intensities of type II and type I collagen shown in (A) and (B), respectively, normalized to the intensity of nucleus signal. Statistics: ANOVA with Tukey's multiple comparisons tests, $n = 4$, $*p < 0.05$, $**p < 0.01$, $***p < 0.005$, $****p < 0.001$.

المنارة للاستشارات
www.manaraa.com

Furthermore, the difference in chemistry of cross-linkers inside the hydrogels could also play a role. Evidence for this lies in the distribution of ECM components, such as type I and type II collagen, in the different hydrogel types. In DTT and PEG hydrogels, the cells produced ECM matrix and formed pericellular compact islands (Figure 4.4). In contrast, within PAMAM hydrogels, the secreted ECM products spread out in ECM network, likely due to the interaction between the PAMAM dendrimer linkers and the collagen I matrices.[29] While PEG has an intrinsic bioinert property, resulting in localization of Col I within the cells.[30]

4.2.3 The Effect of Thiol–Ene "Click" HA Hydrogels on the In Vitro Osteogenesis of MSCs

We further studied the *in situ* hybrid-HA hydrogels for facilitating the *in vitro* bone differentiation of MSCs in which the ultimate goal is to use as a hydrogel for osteochondral tissue regeneration. Early stage of osteogenesis of BMSCs encapsulated in the hydrogels was evaluated by *in situ* ALP activity assay on day 3 and 7 under osteogenic condition. As shown in Figure 4.5B, on day 3, ALP activity of BMSCs in PEG groups was highest compared to other groups. However, on day 7, the increase of ALP activity in G2DTT and PEG hydrogels were similar and significantly highest compared to other groups. Moreover, late stage of osteogenesis of BMSCs was evaluated by calcium staining on day 14 and 28 under osteogenic condition (Figure 4.5A). The background staining was observed for the control G2DTT and G3DTT hydrogels, yet the calcium stain was observed in the networks on day 28. Specifically, it primarily deposited on the outer of the G2DTT and G3DTT constructs, and somewhat in the middle of G3DTT constructs. For DTT, PEG and PEGDTT hydrogels, the control hydrogels displayed no background staining. The stain of

المنارة للاستشارات
www.manaraa.com

calcium in PEG constructs distributed in both inner and outer of the constructs and was highest compared to other constructs along the culture period time. Conversely, there was a small stain of calcium exhibited in PEGDTT networks.

Using these observed ALP activity and calcium mineralization, we estimate that the promotion of encapsulated-MSC osteogenesis is principally offered by matrix stiffness and pore architecture of the scaffolds, which were optimum approximately 1.6 kPa, 100-200 μm and moderate porosity, respectively. Numerous studies proved that the matrix stiffness of the scaffold is a key parameter governing the capacity of osteogenesis.[31] The study by Chen, *et al.* has elicited a according relationship of matrix stiffness and the accumulation of bone matrix proteins in 3D hydrogels.[32] Although PEG hydrogels in our study highly supported MSC osteogenesis, Huebsch, *et al*. found that the MSC osteogenesis occurred principally at 11–30 kPa in 3D hydrogels.[33] Although the underlying mechanism remains unclear, environmental stiffness may be perceived by the cell via the adhesion molecules to regulate the intracellular stress and subsequently the RhoA/ROCK signaling pathway for the ultimate control of cellular functions.[34,35] Additionally, based on our findings, it could be concluded that not only matrix stiffness but pore size and porosity of the hydrogels also greatly impacted osteogenesis of MSCs, in similar way to MSC chondrogenesis.[26-28] Based on the study of Hulbert *et al*., the minimum pore size for mineralized bone regeneration is considered to be approximately 100 μm. Namely, the scaffold with large pores between 100–200 μm showed substantial bone ingrowth. In contrast, smaller pores between 75–100 μm demonstrated solely the ingrowth of osteoid tissue (unmineralized bone matrix), and smallest pores between 10–75 μm were penetrated only by fibrous tissue.[36] It was believed that larger pores could allow vascularization and

المنارة للاستشارات
www.manaraa.com

high oxygenation which flavor to enhance osteogenesis.[37] Nevertheless, the appropriate pore size distribution for promotion of MSC osteogenesis remains open. Some studies have reported that MSC osteogenesis was not affected by pore size, rather was assisted by porosity.[38,39] Higher porosity better support osteogenesis due to facilitating ion exchange and nutrients,[40,41] which agrees to our results compared between PEG and PEGDTT hydrogels.

Taken together, the physical properties of HA hydrogels varied by the structure of cross-linker, shown in Table 4.1, significantly impact on the potential of BMSC differentiation. The needs of appropriate physical properties, such as mechanical properties, morphology (pore size and porosity), permeability, and degradation rate, set challenges for fabricating biomaterial scaffolds for the specific site of application.

Table 4.1. Summary of the impact physical properties of the thiol–ene "click" HA hydrogels on BMSC differentiation.

Hydrogel name	Total polymer concentration in scaffold (%w/v)	Pore size (μm)	Porosity	Complex modulus (Pa)	Swelling ratio (Qv)	Total protein accumulation in scaffold (μg)	Degradation time (days)
DTT	3	100 – 150	+++	400 ± 630	49 ± 5	48 ± 3	2.0 ± 0.0
G2DTT	5	70 – 100	++++	1240 ± 640	42 ± 6	45 ± 9	13.3 ± 1.2
G3DTT	5	50 – 100	++++	583 ± 101	50 ± 4	72 ± 3	5.3 ± 0.6
PEG	5	100 – 200	++	1613 ± 308	19 ± 4	12 ± 3	10.0 ± 0.0
PEGDTT	5	10 – 100	+	1973 ± 289	19 ± 2	14 ± 4	10.0 ± 0.0

المنارة للاستشارات
www.manaraa.com

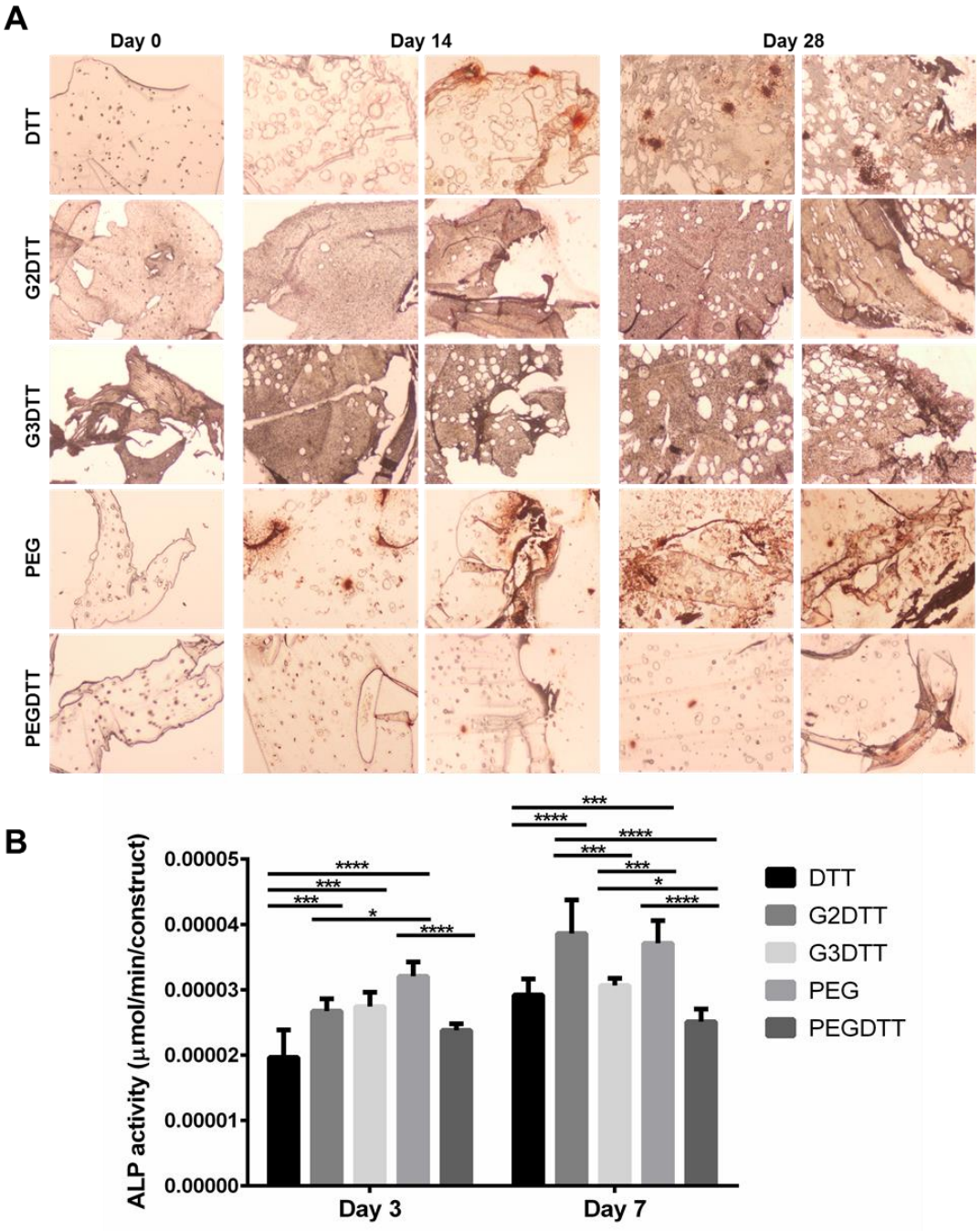

Figure 4.5. Osteogenesis performance of differentiated BMSCs in the hydrogels after culturing in osteogenic media. (A) Histochemical staining for calcium accumulation (red) of differentiated BMSCs in the hydrogels under osteogenic conditions after 14 and 28 days. (n = 4, *$p < 0.05$, **$p < 0.01$, ***$p < 0.005$, ****$p < 0.001$). (B) ALP activities of differentiated MSCs in the hydrogels under osteogenic conditions after 3, and 7 days. ALP activities were performed by *p*-nitrophenyl phosphate assay

المنارة للاستشارات
www.manaraa.com

4.3 CONCLUSIONS

The results of *in vitro* tests indicated all thiol–ene "click" HA hydrogels showed a good cell response in terms of viability but provided different chondrogenic and osteogenic performances. The evaluation of both chondrogenic and osteogenic differentiation markers through the measurement of glycosaminoglycan (GAG) and collagen accumulation, alkaline phosphatase (ALP) activity and calcium accumulation, the MSC differentiation was mostly supported in the PEG-cross-linked HA hydrogel, which is likely due to the optimum in the mechanical stiffness, permeability, pore size, and porosity of the hydrogels, compared to the other types of thiol–ene "click" HA hydrogels. The further *in vivo* study of the biocompatibility and cartilage regeneration using the PEG cross-linked HA scaffolds is the straightforward step for development of the injectable hydrogel for cartilage tissue regeneration.

4.4 MATERIALS AND METHODS

4.4.1 In Situ Cell Encapsulation, Chondrogenic and Osteogenic Culture

The hydrogels were prepared previously described in chapter 3 except that the preparation occurred under sterile condition and pre-warmed complete DMEM media was used to dissolve the polymer. BMSCs passage 3 or 4 were harvested from the 75 cm^2 tissue culture plate (Corning) after reaching 80% confluency. The cells were then trypsinized, counted, centrifuged, and gently mixed with the mixture of pre-warmed hydrogel in DMEM media at concentration of 10^6 cells/mL in the final suspension right after addition of the crosslinkers. The cells-hydrogel mixture (50 µL containing 5×10^4 cells) was then pipetted into each sterile 1 mL syringe mold (Norm-Ject®). After gelling, the hydrogels in

المنارة للاستشارات
www.manaraa.com

syringe molds were transferred to ultra-low attachment 24 well tissue culture plate and incubated at 37 °C in a CO_2 incubator with 5% CO_2/95% air. Chondrogenic or osteogenic media (1 mL) was added into each well to induce chondrogenesis or osteogenesis. The media was exchanged every 2 days for the entire experimental period.

Chondrogenic media is comprised of DMEM supplemented with 1% FBS, 1× Penicillin-Streptomycin-Amphotericin B (from MP Biomedicals, 100 U/mL penicillin and 1000 U/mL streptomycin solution, 0.25 μg/mL amphotericin B), 100 nM dexamethasone (Enzo Life Sciences), 10 ng/mL TGF β1 (R&D System), 50 μg/mL ascorbic acid (Sigma-Aldrich), 1 mM sodium pyruvate (Hyclone, Thermo scientific), 1×ITS^{+3} (from Sigma-Aldrich, contains 1.0 mg/mL insulin from bovine pancreas, 0.55 mg/mL human transferrin (substantially iron-free), 0.5 μg/mL sodium selenite, 470 μg/mL linoleic acid, 470 μg/mL oleic acid and 50 mg/mL bovine serum albumin), 2 mM L-glutamine (Hyclone, Thermo scientific) and 40 μg/mL L-proline (Sigma-Aldrich).[42,43]

Osteogenic media comprised of DMEM supplemented with 10% FBS, 1× Penicillin-Streptomycin-Amphotericin B, 10 mM sodium β-glycerolphosphate, 50 μg/mL ascorbic acid, and 10 nM dexamethasone.

4.4.2 Cell Viability Assay

CellTiter-Blue® (CTB) cell viability assay (Promega) was performed after day 0 (immediately after encapsulation), 3 and 7 of culturing BMSCs in the hydrogels. The primary media in each well was replaced by 300 μL of pre-warmed media containing 15% CTB and incubated for 20 h at 37 °C and 5% CO_2. The media containing CTB without cells was used as negative controls. The media containing metabolite of CTB was measured

المنارة للاستشارات
www.manaraa.com

for fluorescence intensity at 560/590 nm (Ex/Em) using SpectraMax M2 Multi-Mode microplate reader (Molecular Devices).

4.4.3 Chondrogenesis Study

After 14 and 28 days of chondrogenic cultures, the samples were fixed in 4% paraformaldehyde (PFA) for 24 h at 4 °C, dehydrated with a graded ethanol series, and then embedded in paraffin. For Glycosaminoglycan (GAG) histochemical staining, the sections, 8 mm in thickness, were stained with Safranin O and Light Green stain following the literature protocol.[44] The stained sections were imaged by a light microscope (Olympus I×81) under 10× lens at 15 random locations from three stained sections per sample (n = 4). Quantification of the signal intensities of GAG was analyzed with ImageJ. The intensity of GAG was normalized to the intensity of cytoplasm signal (green).

For the immunohistochemical staining of type II and type I collagen, separate sections were permeabilized with 0.05% Tween20 in Tris-buffered saline solution (TBS) for 15 min and blocked in 2% BSA in TBS for 20 min. The separate sections were then incubated with anti-rabbit collagen type II monoclonal antibody (Sigma-Aldrich) at 1:100 dilution in blocking buffer, or anti-mouse collagen type I monoclonal antibody (Sigma-Aldrich) at 1:2000 dilution in blocking buffer at room temperature for 2 h. After the samples were washed thrice with TBS, they were incubated with secondary antibody detection Alexa Fluor® 546 (for type II collagen) and secondary antibody detection Alexa Fluor® 488 (for type I collagen) at 1:200 dilution in blocking buffer at room temperature for 1 h. They were then washed thrice with TBS, and counterstained with DAPI (4, 6-diamidino-2-phenylindole, 100 ng/mL) for 15 min. Finally, the sections were mounted for

المنارة للاستشارات
www.manaraa.com

microscopic observation. Images of the stained sections were collected using Olympus I×81 epi-flour mode under 10× lens, exposure times 50 ms for DAPI, 500 ms for collagen II and I, at 30 random locations from three stained sections per sample (n = 4). Quantification of the signal intensities of type II and type I collagen were analyzed with ImageJ. The intensity of type II and type I collagen was normalized to the intensity of nucleus signal (DAPI).

4.4.4 Osteogenesis Study

Alkaline phosphatase (ALP) activity was determined using pNPP (*p*-nitrophenyl phosphate) assay (Thermo Scientific). After 3 and 7 days of induction in the osteogenic media, the hydrogels with cells were prewashed with PBS then incubated with pNPP solution at room temperature for 1 h. Absorbance was read using a M2 SpectraMax plate reader at 405 nm, indicating ALP activity levels. The enzyme activity was calculated from Beer−Lambert law as follows,

$$\text{Enzyme activity } (\mu\text{mol}/\text{min}/\text{construct}) = \frac{V(\mu L) \times OD_{405\ nm}\ (cm^{-1})}{\varepsilon \times \text{incubation time (min)} \times \text{construct}}$$

where ε is the molar extinction coefficient ($M^{-1} \times cm^{-1}$). For pNPP, $\varepsilon = 1.78 \times 10^4\ M^{-1} \times cm^{-1}$, $OD_{405\ nm}$ (cm^{-1}) is the absorbance at 405 nm divided by the light-path length (cm), and V is the final assay volume.[45]

Alizarin Red S (ARS) staining for Ca^{2+} was performed after 14 and 28 days of osteogenic cultures. The hydrogels with cells were washed three times with PBS and fixed in 4% PFA for 24 h at 4 °C, dehydrated with a graded ethanol series, and then embedded in paraffin. The sections, 8 mm in thickness, were stained with 0.1% solution of ARS (Sigma-Aldrich) pH 4.2 for 30 min, washed with PBS to remove excess stain and air dried.

المنارة للاستشارات
www.manaraa.com

The stained sections were imaged by a light microscope (Olympus I×81) under 4× lens. Negative control experiments (before induction in the osteogenic media) were conducted for all types of the hydrogels.

4.4.5 Statistical Analysis

All quantitative data are expressed as the mean ± standard deviation (SD). Statistical analysis was performed using ANOVA with Tukey's multiple comparisons tests. A value of $p < 0.05$ was considered to be statistically.

المنارة للاستشارات
www.manaraa.com

4.5 REFERENCES

(1) Martin, I.; Miot, S.; Barbero, A.; Jakob, M.; Wendt, D. Osteochondral Tissue Engineering. *J. Biomech.* **2007,** *40*, 750-765.

(2) Vilela, C.; Correia, C.; Oliveira, J. M.; Sousa, R. A.; Espregueira-Mendes, J.; Reis, R. L. Cartilage Repair Using Hydrogels: A Critical Review of in Vivo Experimental Designs. *ACS Biomaterials Science & Engineering* **2015,** *1*, 726-739.

(3) Liao, J.; Shi, K.; Ding, Q.; Qu, Y.; Luo, F.; Qian, Z. Recent Developments in Scaffold-Guided Cartilage Tissue Regeneration. *Journal of biomedical nanotechnology* **2014,** *10*, 3085-3104.

(4) Buckwalter, J. A. Articular Cartilage: Injuries and Potential for Healing. *J. Orthop. Sports Phys. Ther.* **1998,** *28*, 192-202.

(5) Tomlinson, R. E.; Silva, M. J. Skeletal Blood Flow in Bone Repair and Maintenance. *Bone research* **2013,** *1*, 311.

(6) Flierl, M. A.; Smith, W. R.; Mauffrey, C.; Irgit, K.; Williams, A. E.; Ross, E.; Peacher, G.; Hak, D. J.; Stahel, P. F. Outcomes and Complication Rates of Different Bone Grafting Modalities in Long Bone Fracture Nonunions: A Retrospective Cohort Study in 182 Patients. *Journal of orthopaedic surgery and research* **2013,** *8*, 33.

(7) Giannoudis, P. V.; Dinopoulos, H.; Tsiridis, E. Bone Substitutes: An Update. *Injury* **2005,** *36*, S20-S27.

(8) Sen, M.; Miclau, T. Autologous Iliac Crest Bone Graft: Should It Still Be the Gold Standard for Treating Nonunions? *Injury* **2007,** *38*, S75-S80.

(9) Zreiqat, H.; Dunstan, C. R.; Rosen, V., *A Tissue Regeneration Approach to Bone and Cartilage Repair*. Springer: 2015.

المنارة للاستشارات
www.manaraa.com

(10) Trachtenberg, J. E.; Vo, T. N.; Mikos, A. G. Pre-Clinical Characterization of Tissue Engineering Constructs for Bone and Cartilage Regeneration. *Ann. Biomed. Eng.* **2015,** *43*, 681-696.

(11) Peretti, G. M.; Xu, J. W.; Bonassar, L. J.; Kirchhoff, C. H.; Yaremchuk, M. J.; Randolph, M. A. Review of Injectable Cartilage Engineering Using Fibrin Gel in Mice and Swine Models. *Tissue Eng.* **2006,** *12*.

(12) Burdick, J. A.; Chung, C.; Jia, X.; Randolph, M. A.; Langer, R. Controlled Degradation and Mechanical Behavior of Photopolymerized Hyaluronic Acid Networks. *Biomacromolecules* **2005,** *6*, 386-391.

(13) Morgan, M. T.; Carnahan, M. A.; Immoos, C. E.; Ribeiro, A. A.; Finkelstein, S.; Lee, S. J.; Grinstaff, M. W. Dendritic Molecular Capsules for Hydrophobic Compounds. *J. Am. Chem. Soc.* **2003,** *125*, 15485-15489.

(14) Gillies, E. R.; Dy, E.; Fréchet, J. M.; Szoka, F. C. Biological Evaluation of Polyester Dendrimer: Poly (Ethylene Oxide)"Bow-Tie" Hybrids with Tunable Molecular Weight and Architecture. *Mol Pharm* **2005,** *2*, 129-138.

(15) Roberts, J. C.; Bhalgat, M. K.; Zera, R. T. Preliminary Biological Evaluation of Polyamidoamine (Pamam) Starbursttm Dendrimers. *J. Biomed. Mater. Res.* **1996,** *30*, 53-65.

(16) Malik, N.; Wiwattanapatapee, R.; Klopsch, R.; Lorenz, K.; Frey, H.; Weener, J.; Meijer, E.; Paulus, W.; Duncan, R. Dendrimers:: Relationship between Structure and Biocompatibility in Vitro, and Preliminary Studies on the Biodistribution of 125i-Labelled Polyamidoamine Dendrimers in Vivo. *J. Controlled Release* **2000,** *65*, 133-148.

المنارة للاستشارات
www.manaraa.com

(17) Jevprasesphant, R.; Penny, J.; Jalal, R.; Attwood, D.; McKeown, N.; D'emanuele, A. The Influence of Surface Modification on the Cytotoxicity of Pamam Dendrimers. *Int. J. Pharm.* **2003,** *252*, 263-266.

(18) Chen, H.-T.; Neerman, M. F.; Parrish, A. R.; Simanek, E. E. Cytotoxicity, Hemolysis, and Acute in Vivo Toxicity of Dendrimers Based on Melamine, Candidate Vehicles for Drug Delivery. *J. Am. Chem. Soc.* **2004,** *126*, 10044-10048.

(19) Studer, D.; Millan, C.; Ozturk, E.; Maniura-Weber, K.; Zenobi-Wong, M. Molecular and Biophysical Mechanisms Regulating Hypertrophic Differentiation in Chondrocytes and Mesenchymal Stem Cells. *European cells & materials* **2012,** *24*, 118-135; discussion 135.

(20) Wang, G.; Woods, A.; Sabari, S.; Pagnotta, L.; Stanton, L. A.; Beier, F. Rhoa/Rock Signaling Suppresses Hypertrophic Chondrocyte Differentiation. *J. Biol. Chem.* **2004,** *279*, 13205-13214.

(21) Wang, T.; Lai, J. H.; Han, L.-H.; Tong, X.; Yang, F. Chondrogenic Differentiation of Adipose-Derived Stromal Cells in Combinatorial Hydrogels Containing Cartilage Matrix Proteins with Decoupled Mechanical Stiffness. *Tissue Engineering Part A* **2014,** *20*, 2131-2139.

(22) Park, J. S.; Chu, J. S.; Tsou, A. D.; Diop, R.; Tang, Z.; Wang, A.; Li, S. The Effect of Matrix Stiffness on the Differentiation of Mesenchymal Stem Cells in Response to Tgf-B. *Biomaterials* **2011,** *32*, 3921-3930.

(23) Wang, L.-S.; Du, C.; Toh, W. S.; Wan, A. C. A.; Gao, S. J.; Kurisawa, M. Modulation of Chondrocyte Functions and Stiffness-Dependent Cartilage Repair Using an Injectable

المنارة للاستشارات
www.manaraa.com

Enzymatically Crosslinked Hydrogel with Tunable Mechanical Properties. *Biomaterials* **2014,** *35*, 2207-2217.

(24) Kemppainen, J. M.; Hollister, S. J. Differential Effects of Designed Scaffold Permeability on Chondrogenesis by Chondrocytes and Bone Marrow Stromal Cells. *Biomaterials* **2010,** *31*, 279-287.

(25) Jeong, C. G.; Hollister, S. J. Mechanical and Biochemical Assessments of Three-Dimensional Poly(1,8-Octanediol-Co-Citrate) Scaffold Pore Shape and Permeability Effects on in Vitro Chondrogenesis Using Primary Chondrocytes. *Tissue engineering. Part A* **2010,** *16*, 3759-3768.

(26) Lien, S. M.; Ko, L. Y.; Huang, T. J. Effect of Pore Size on Ecm Secretion and Cell Growth in Gelatin Scaffold for Articular Cartilage Tissue Engineering. *Acta Biomater* **2009,** *5*, 670-679.

(27) Yamane, S.; Iwasaki, N.; Kasahara, Y.; Harada, K.; Majima, T.; Monde, K.; Nishimura, S.-i.; Minami, A. Effect of Pore Size on in Vitro Cartilage Formation Using Chitosan-Based Hyaluronic Acid Hybrid Polymer Fibers. *Journal of Biomedical Materials Research Part A* **2007,** *81A*, 586-593.

(28) Im, G. I.; Ko, J. Y.; Lee, J. H. Chondrogenesis of Adipose Stem Cells in a Porous Polymer Scaffold: Influence of the Pore Size. *Cell Transplant.* **2012,** *21*, 2397-2405.

(29) Li, J.; Yang, J.; Li, J.; Chen, L.; Liang, K.; Wu, W.; Chen, X.; Li, J. Bioinspired Intrafibrillar Mineralization of Human Dentine by Pamam Dendrimer. *Biomaterials* **2013,** *34*, 6738-6747.

(30) Hoyle, C. E.; Lowe, A. B.; Bowman, C. N. Thiol-Click Chemistry: A Multifaceted Toolbox for Small Molecule and Polymer Synthesis. *Chem Soc Rev* **2010,** *39*, 1355-1387.

المنارة للاستشارات
www.manaraa.com

(31) Perez, R. A.; Won, J. E.; Knowles, J. C.; Kim, H. W. Naturally and Synthetic Smart Composite Biomaterials for Tissue Regeneration. *Adv Drug Deliv Rev* **2013,** *65*, 471-496.

(32) Chen, G.; Dong, C.; Yang, L.; Lv, Y. 3d Scaffolds with Different Stiffness but the Same Microstructure for Bone Tissue Engineering. *ACS applied materials & interfaces* **2015,** *7*, 15790-15802.

(33) Huebsch, N.; Arany, P. R.; Mao, A. S.; Shvartsman, D.; Ali, O. A.; Bencherif, S. A.; Rivera-Feliciano, J.; Mooney, D. J. Harnessing Traction-Mediated Manipulation of the Cell/Matrix Interface to Control Stem-Cell Fate. *Nat Mater* **2010,** *9*, 518-526.

(34) Engler, A. J.; Sen, S.; Sweeney, H. L.; Discher, D. E. Matrix Elasticity Directs Stem Cell Lineage Specification. *Cell* **2006,** *126*, 677-689.

(35) Kong, H. J.; Liu, J.; Riddle, K.; Matsumoto, T.; Leach, K.; Mooney, D. J. Non-Viral Gene Delivery Regulated by Stiffness of Cell Adhesion Substrates. *Nat Mater* **2005,** *4*, 460-464.

(36) Hulbert, S. F.; Young, F. A.; Mathews, R. S.; Klawitter, J. J.; Talbert, C. D.; Stelling, F. H. Potential of Ceramic Materials as Permanently Implantable Skeletal Prostheses. *J. Biomed. Mater. Res.* **1970,** *4*, 433-456.

(37) Hannink, G.; Arts, J. J. C. Bioresorbability, Porosity and Mechanical Strength of Bone Substitutes: What Is Optimal for Bone Regeneration? *Injury* **2011,** *42, Supplement 2*, S22-S25.

(38) Karageorgiou, V.; Kaplan, D. Porosity of 3d Biomaterial Scaffolds and Osteogenesis. *Biomaterials* **2005,** *26*, 5474-5491.

المنارة للاستشارات
www.manaraa.com

(39) Takahashi, Y.; Tabata, Y. Effect of the Fiber Diameter and Porosity of Non-Woven Pet Fabrics on the Osteogenic Differentiation of Mesenchymal Stem Cells. *J. Biomater. Sci. Polym. Ed.* **2004,** *15*, 41-57.

(40) Hing, K. A. Bone Repair in the Twenty-First Century: Biology, Chemistry or Engineering? *Philosophical transactions. Series A, Mathematical, physical, and engineering sciences* **2004,** *362*, 2821-2850.

(41) Hing, K. A. Bioceramic Bone Graft Substitutes: Influence of Porosity and Chemistry. *International Journal of Applied Ceramic Technology* **2005,** *2*, 184-199.

(42) Bhardwaj, N.; Kundu, S. C. Chondrogenic Differentiation of Rat Mscs on Porous Scaffolds of Silk Fibroin/Chitosan Blends. *Biomaterials* **2012,** *33*, 2848-2857.

(43) Salinas, C. N.; Anseth, K. S. The Enhancement of Chondrogenic Differentiation of Human Mesenchymal Stem Cells by Enzymatically Regulated Rgd Functionalities. *Biomaterials* **2008,** *29*, 2370-2377.

(44) Kahveci, Z.; Minbay, F. Z.; Cavusoglu, I. Safranin O Staining Using a Microwave Oven. *Biotech. Histochem.* **2000,** *75*, 264-268.

(45) Springsteen, G.; Wang, B. A Detailed Examination of Boronic Acid–Diol Complexation. *Tetrahedron* **2002,** *58*, 5291-5300.

المنارة للاستشارات
www.manaraa.com

CHAPTER 5

THE DEVELOPMENT OF HYBRIDIZED-GRAPHENE HA HYDROGELS AS CONTROLLED PERIVASCULAR DRUG DELIVERIES FOR VESSEL GRAFT REGENERATION

5.1 INTRODUCTION

Aside from an ideal candidate for tissue engineering applications, hyaluronic acid (HA) has recently been studied for the use in localized and controlled drug delivery applications.[1-3] It can be used as a macroscopic polymeric system for drug deliveries due to the unique physical properties, biocompatibility and biodegradability.[4] The porosity, swelling property, permeability of HA hydrogels allows loading of drugs into the hydrogel matrix and consequent releasing the drugs at a certain rate depended on the diffusion coefficient of the small molecule through the polymeric network. The hydrogels show highly flexibility, which is advantageous in immobilizing them at the site of application or in applying them on surfaces. Nevertheless, HA hydrogels still have several limitations regarding applications in drug delivery. For example, the hydrogels have restricted capacity and homogeneity of drug loading, particularly in the case of hydrophobic drugs. The burst or rapid drug release is often observed in the HA hydrogels due to high water content and large pore sizes.[5] These issues significantly limit the practical use of HA hydrogel-based drug deliveries in the clinic.

المنارة للاستشارات
www.manaraa.com

To overcome the pharmacological limitations of HA hydrogel-based drug deliveries, modifying the microstructure of the hydrogel,[6] incorporation of membranes,[7] micelles,[8] and nanoparticles,[9-11] has been explored to control the diffusion of drugs from the networks. Particularly, introduction of nanoparticles for controlling drug release has gained a lot of attraction[9,11,12] Graphene oxide is considered as the finest and most durable nanomaterial. The structure and presence of delocalized surface π electrons in graphene oxide can be used for drug loading via π–π stacking and electrostatic or hydrophobic interactions.[13-18] In addition, many of the *in vivo* studies on graphene have demonstrated its potential to use as drug delivery vehicles,[19,20] tissue engineered scaffolds and grafts,[21,22] biosensors,[23,24] *etc*.

Currently, treatment of cardiovascular disease by vascular graft is an alternative to be used to replace or bypass a damaged or occluded vessel. The grafting of autologous vein vessels represents the gold standard for vascular replacement of diseased small-diameter (<6 mm) vessels.[25] Nevertheless, the vessel patency rates for autologous vein vessel transplantation remain limited, showing failure rates of approximately 50% at 10 years.[25,26] The failures are most commonly associated with thrombosis,[27,28] neointimal hyperplasia,[29-31] atherosclerosis,[32] or infection.[33,34] So far, no effective strategy exists in clinical practice to prevent neointimal hyperplasia (NH), which is an overgrowth of cells into the intimal layer of blood vessels, caused by proliferation and migration of adventitial fibroblasts and medial smooth muscle cells (SMCs) to the intima. Interestingly, the studies by Cui's research lab, our collaborator, have found that the delivery of selective inhibitors of cyclin-dependent kinase 8 (CDK8), Senexin A, could facilitate the grafted decellularized vessels into mature arteries after transplantation *in vivo*, by dramatic suppression of the NH, and

المنارة للاستشارات
www.manaraa.com

the formation of SMC layer with sufficient patency up to 3 months. To effectively deliver Senexin A in vessel regeneration, a localized perivascular delivery approach is logical due to better targeting and retaining the drug at the vascular site, and preventing off-target drug effects compared to systemic approach.

Taken together, in this present work, we aimed to establish the efficacy of optimized Senexin A perivascular delivery using GO-hybridized HA-based hydrogel for the transformation of decellularized vessel scaffolds into arteries. HA serves as a biodegradable macroscale polymeric scaffold, making the prepared GO nanocarriers localized and stable in different microenvironments. The nanocarrier was firstly synthesized by attaching SNX to GO via strong π–π and electrostatic interaction, followed by the *in situ* encapsulation of GO-SNX with HA-based hydrogel. The *in vitro* drug release test was determined. The biocompatibility and efficacy of the materials were also evaluated in vessel smooth muscle cells (VSMCs).

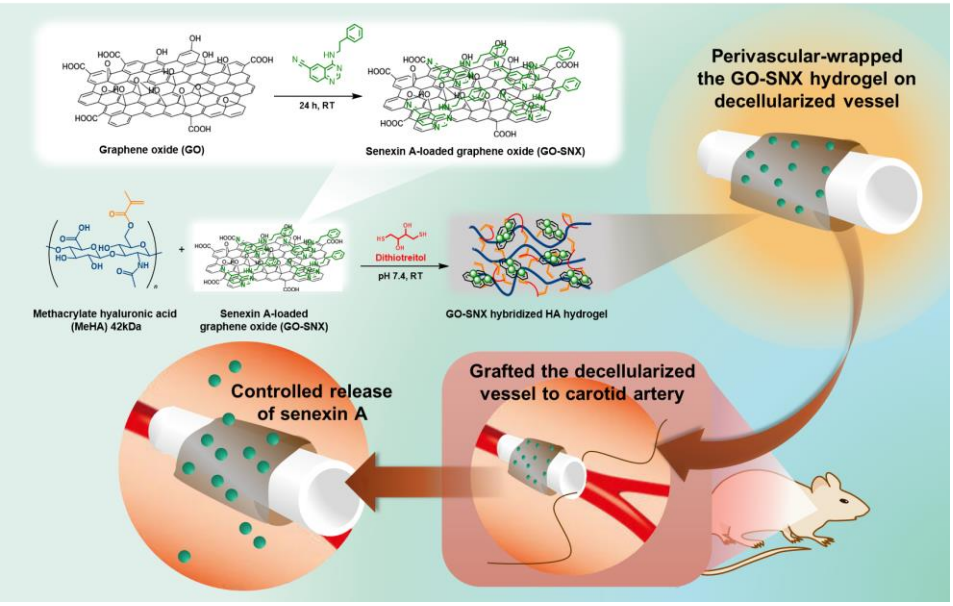

Figure 5.1. Schematic illustration of the experimental research of hybridized-graphene HA hydrogels as controlled perivascular drug deliveries for vessel graft regeneration.

المنارة للاستشارات
www.manaraa.com

5.2 RESULTS AND DISCUSSION

The goals of the development of hybridized-graphene HA hydrogels were: (1) to control the release of SNX *in vitro* in therapeutic concentration range of 3-30 μM for 3 weeks or longer, (2) can be biodegradable during vessel regeneration process, and (3) can effectively transform decellularized vessel scaffolds into mature arteries *in vivo* in similar manner to the delivery of SNX without toxicity.

6.2.1 Preparation of Drug-Loaded Graphene Oxide and Drug-Loaded Graphene HA Hydrogels

The water-soluble GO was firstly synthesized from graphene flake by modified Hummers' method.[35] The sub-microsized GO was created by further sonication treatment of the resulted GO, providing a size range of 200 nm–3.5 mm, as verified by SEM imaging (Figure 5.2A). Fourier transform infrared spectroscopy (FTIR) spectra and physical appearances of the GO were used to confirm the successful oxidation of graphene. Specifically, the resulted GO showed the broad characteristic peak of FTIR at 3600–3200 cm^{-1} which was from the stretching vibration of the OH group. The strong peaks at 1800–1600 cm^{-1} were attributed to the stretching vibration of the C=O carbonyl group, and the bands at 1170, 1090 and 1050 cm^{-1} were from C–O stretching vibrations. Additionally, the band at 1625 cm^{-1} was attributed to unoxidized C=C stretching vibration[36,37] (Figure 5.2D). The resulted GO showed highly water solubility and dark brown color, which were significantly different from the graphene flake prior to modification (Figure 5.2B, C).

المنارة للاستشارات
www.manaraa.com

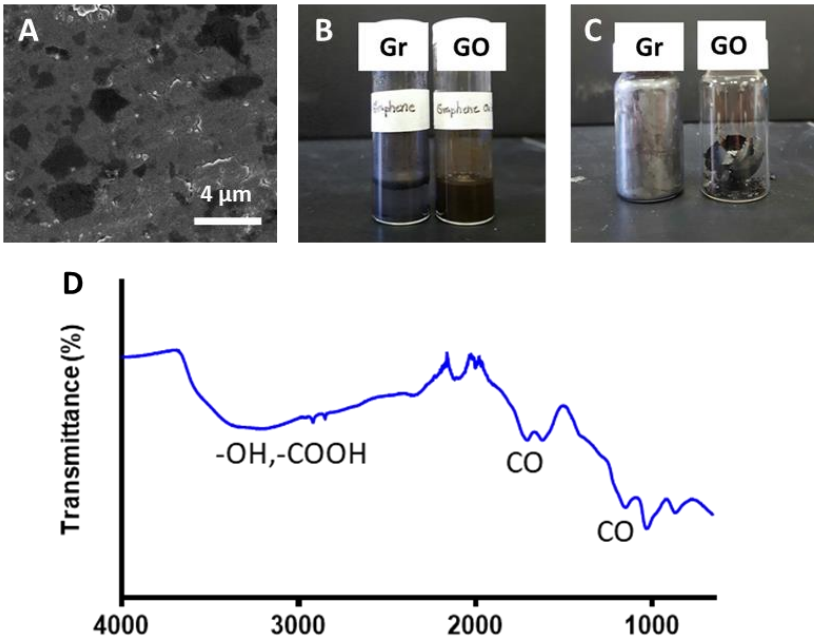

Figure 5.2. Characterization of the synthesized graphene oxide. (A) Scanning electron micrograph (SEM) of the synthesized graphene oxide after sonication for 1 h. (B) The physical appearances of graphene and the synthesized graphene oxide dispersed in PBS. (C) The physical appearances of graphene and the synthesized graphene oxide after drying. (D) Fourier transform infrared spectroscopy (FTIR) spectrum of the synthesized graphene oxide.

The GO was then reacted with SNX at different weight ratio (Figure 5.3A) in PBS for 24 h at room temperature to generate SNX-loaded GO (GO-SNX). As shown in Figure 5.3D, SNX could attach to GO at different amounts with almost 100% loading efficiency as determined by UV-Vis. The successful attachment of SNX to GO was further confirmed by FTIR and UV-Vis spectra (Figure 5.3B, C). Compared with SNX and GO shown in Figure 5.3B, the FTIR spectrum of GO-SNX at 1:3 loading ratio of GO:SNX showed the peaks at 3400, 3100–3010, 2260 cm^{-1} (corresponding to stretching bands of amine N–H, alkenyl C–H, and nitrile C≡N of SNX) and at 1600 and 900–600 cm^{-1} (corresponding to the bending band and wagging bands of amine N–H from SNX), in addition to the weak characteristic peaks belonging to GO. It should be noted that the observed characteristic

المنارة للاستشارات
www.manaraa.com

peaks from SNX were dominant in the FTIR of GO-SNX due to high SNX loading to GO. Additionally, the UV-Vis spectrum of GO-SNX showed the pronounced absorbance at both 230, and 323 nm, belonging to the absorbance of GO and SNX respectively (Figure 5.3C).

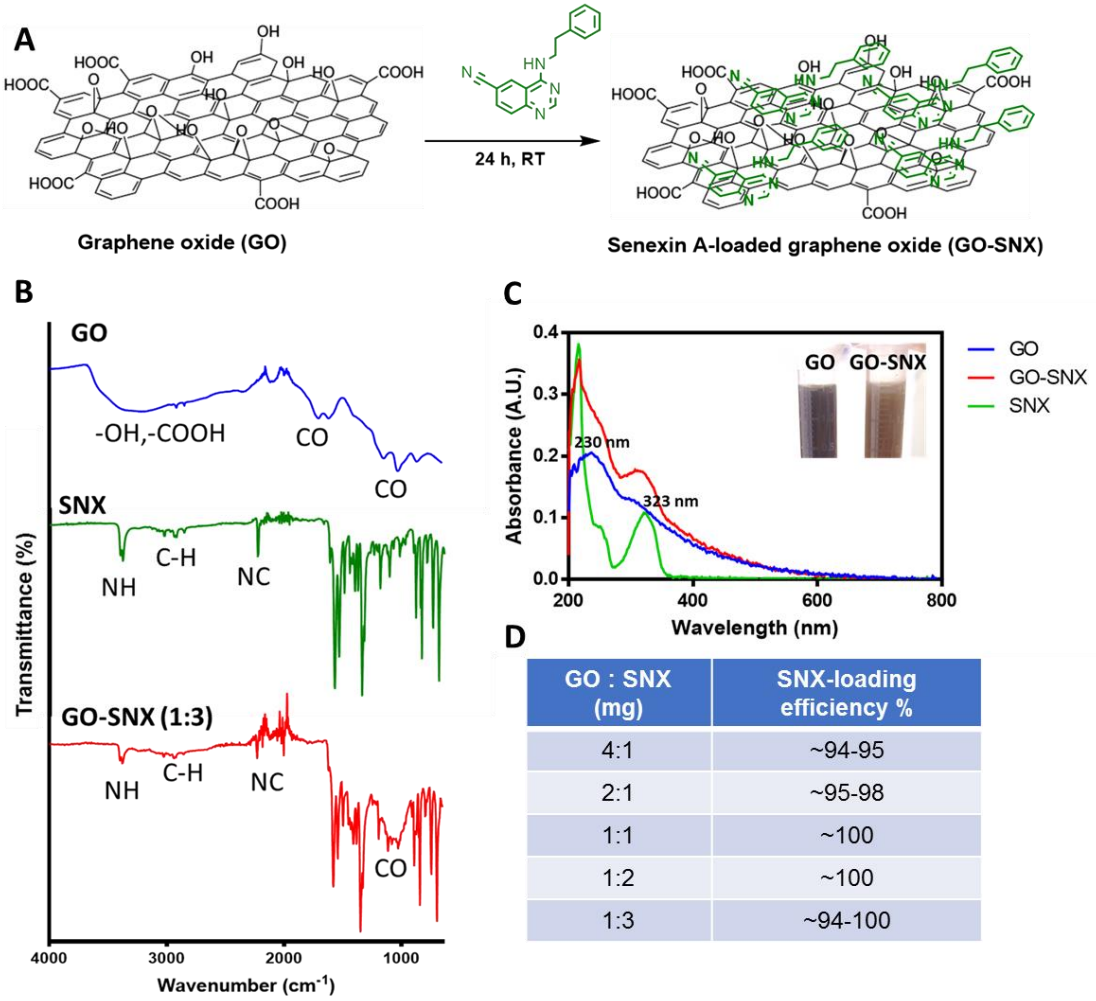

GO : SNX (mg)	SNX-loading efficiency %
4:1	~94-95
2:1	~95-98
1:1	~100
1:2	~100
1:3	~94-100

Figure 5.3. Preparation and characterization of Senexin A-loaded graphene oxide. (A) Schematic illustrating the preparation of Senexin A-loaded graphene oxide (GO-SNX). (B) FTIR spectra of GO, SNX, and GO-SNX. (C) Loading efficiency of SNX on to GO at different weight ratios (n = 3).

The GO-SNX HA hydrogel was formed by simply mixing 3% of MeHA polymer with 0.1% of GO-SNX in PBS and adding DTT (as shown in Figure 5.4). Without the

المنارة للاستشارات
www.manaraa.com

addition of DTT, the mixture of GO-SNX and HA was highly viscous due to the electrostatic interaction (H-bonding), yet the interaction was not strong enough to create the hydrogel. The thiol–ene "click" reaction between thiol of DTT and methacrylate group of HA occurred after adding DTT, resulting in the hydrogel formation.

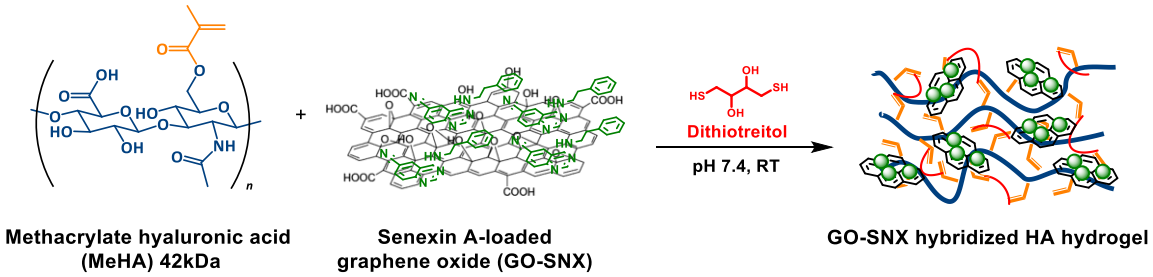

Figure 5.4. Schematic illustrating the synthesis of Senexin A-loaded graphene HA hydrogels via thiol–ene "click" reaction.

5.2.2 Gelation time and Mechanical Properties of Senexin A-Loaded Graphene HA Hydrogels

The gelation time and mechanical properties of the hydrogels are critical for the application of perivascular wrap for drug delivery system. Owing to the restricted time of decellularized vessel exposing to air environment, the wrapping process of the hydrogel onto decellularized vessel is required to complete within 20 min. Specifically, the hydrogel must be formed within 20 min during the process, and the hydrogel must be highly flexible and attachable onto the decellularized vessel. In this way, the gelation time and mechanical properties of GO-SNX HA hydrogels were studied and optimized. The amount of DTT and GO-SNX were varied in each hydrogel formulation, and the gelation time of each GO-SNX HA hydrogels was determined by tilting method. The results showed that increasing the amount of DTT caused faster gelation time, while increasing the amount of GO-SNX did not always fasten the gelation time. The impact of GO-SNX concentration to gelation

المنارة للاستشارات
www.manaraa.com

time was dependant on the amount of DTT. At lower concentration of DTT (2 and 4 μL/100 μL), high GO-SNX concentration retarded the gel formation time. In contrast, when the concentration of DTT was high enough, high GO-SNX concentration could shorten the gelation time to 8-10 min. However, these resulted hydrogels were very rigid, shrink in the middle of the container, and surrounded by HA solution (shown in Figure 5.5E). It is because DTT also serve as the reducing agent creating the reduce GO, and later crosslinking each other to the reduced GO hydrogels instead of GO HA hydrogels. Thus, the formulation containing low DTT and GO-SNX concentration was selected as the master recipe for the rest of experiments.

Table 5.1. The gelation time of different Senexin A-loaded graphene HA hydrogels, which were determined by tilting method. The values expressed are means (n = 4) ± SD.

Formulation	HA	0.5 M DTT-Crosslinker (μL/100 μL)	GO-SNX (μg/μL)	Gelation time (min)
Control	3%	2	0	25-40
1	3%	2	1	35-48
2	3%	2	3	50-96
3	3%	4	1	N/A
4	3%	4	3	40-50
5	3%	6	1	8-12
6	3%	6	3	6-10

We further observed the mechanical properties of the hydrogels using rheometer. The results showed the average complex modulus of the hydrogels was approximately 35 Pa, highly flexible and soft right after gelling. The hydrogels then became more rigid (approximate 100 Pa) and less flexible after gelling for 3 days (Figure 5.5A-D, F). Furthermore, the hydrogels were *in situ* applied on to the decellularized scaffolds by drop-coating technique, as shown in Figure 5.6. The hydrogels were firmly attached on the vessel

المنارة للاستشارات
www.manaraa.com

scaffolds, and stable after storage 1 day in PBS, providing a promising result for future *in vivo* applications.

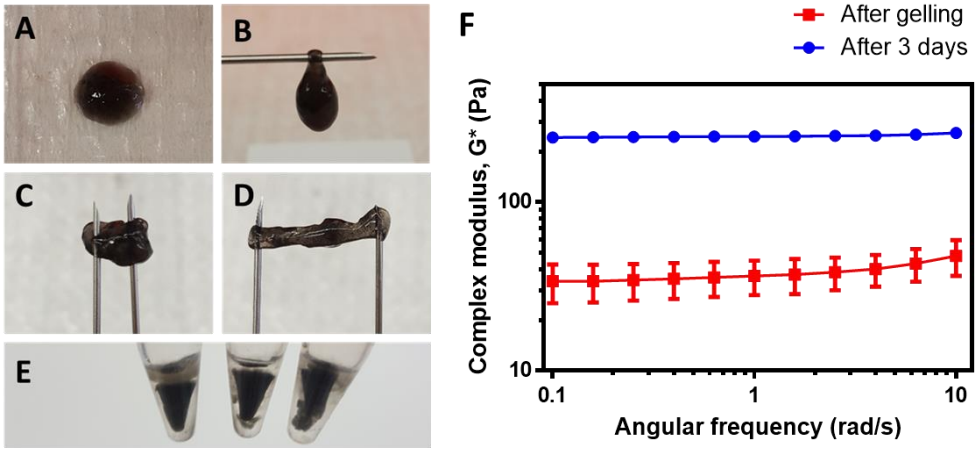

Figure 5.5. Physical and mechanical properties of Senexin A-loaded graphene HA hydrogels. (A, B) Physical appearances of Senexin A-loaded graphene HA hydrogels right after gelling (C, D) Physical appearances of Senexin A-loaded graphene HA hydrogels after gelling for 3 days. (E) The formation of reduced GO hydrogels when using high DTT, 6 µL/100 µL. (F) Mechanical properties of Senexin A-loaded graphene HA hydrogels right after gelling, and after gelling for 3 days. The values expressed are means (n = 3) ± SD.

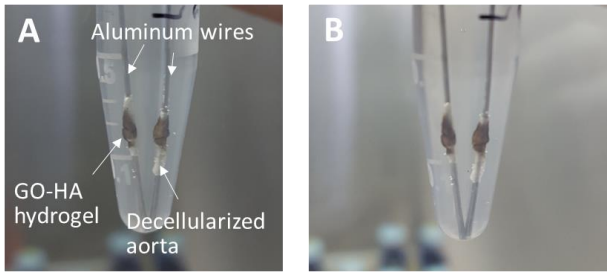

Figure 5.6. The attachment of Senexin A-loaded graphene HA hydrogels to the decellularized scaffolds in PBS after gelling (A) and 1 day (B).

5.2.3 In Vitro Drug Release of Senexin A-Loaded Graphene HA Hydrogels

We next evaluated whether SNX could be delivered and controllably released from the hybridized GO-HA hydrogels. Drug release from a GO nanocarrier depends on different factors, such as pH,[38] GO sizes, and interactions between drug and GO carriers.

المنارة للاستشارات
www.manaraa.com

In the study, *in vitro* release behavior of SNX from GO-SNX HA hydrogels was investigated at 37 °C in PBS and DMEM media with pH 7.4, representing normal physiological pH. The release of SNX from SNX loaded HA hydrogels was also studied for comparison. It showed that the SNX released from the GO-SNX HA and SNX-loaded HA hydrogels reached equilibrium within 2 h at a concentration of 100 μM and 200 μM in PBS, respectively (Figure 5.7A). The release of SNX from the GO-SNX HA systems maintained constantly, while the release from the SNX loaded HA hydrogels tended to slow down after 2 days of the study (Figure 5.7B). The cumulative release of SNX from SNX loaded HA-based hydrogels was 3 times higher than that in GO-SNX HA hydrogels after 5 days of the study (Figure 5.7C). These results can be ascribed to the strong hydrogen-bond and π-π stacking interactions between SNX and GO at pH 7.4 media which slowed down the release of SNX from the networks.[39-41]

The release concentration of SNX from GO-SNX HA systems was further optimized to reach the therapeutic window, ranging from 3 -30 μM. Several methods were used to optimize the release of SNX, such as increasing polymer density, modifying GO surface, and varying the loading ratios of GO to SNX. It was found that lower the SNX loaded onto GO could significantly slow down the drug release (shown in Figure 5.7D). The 4:1 loading ratio of GO to SNX was found to be optimal for a controlled release of SNX at ~ 30 μM, and it could facilitate the constant release of SNX for 17 days (Figure 5.8A). Before completion of the release profile, the SNX release became higher, suggesting that the degradation of HA polymer was involved. The completion of release was in 22 days (Figure 5.8B).

المنارة للاستشارات
www.manaraa.com

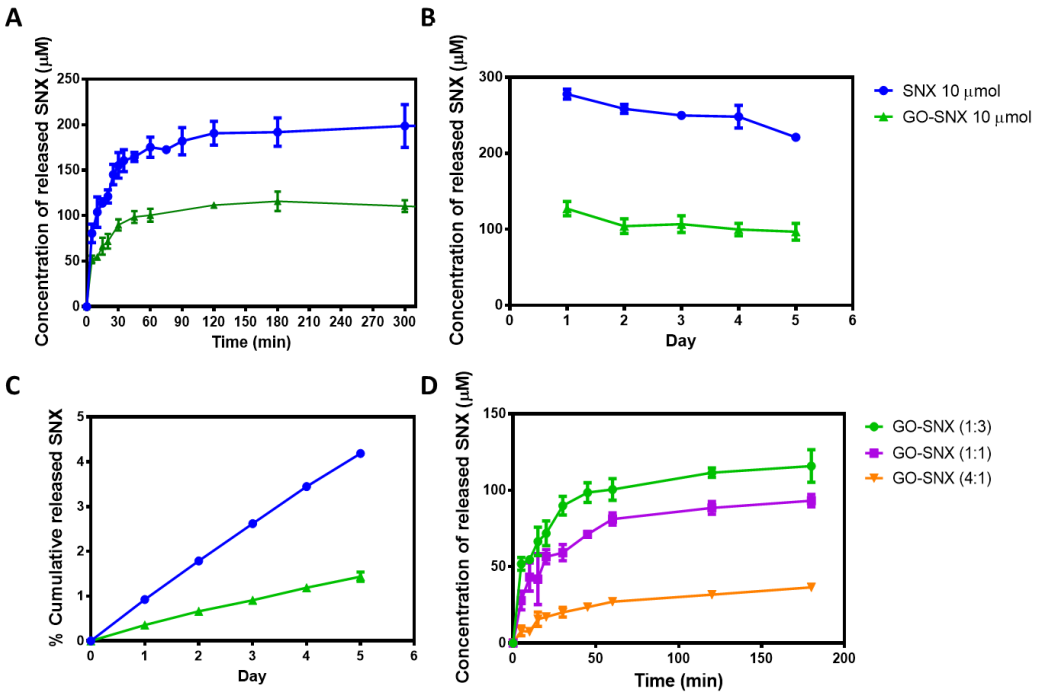

Figure 5.7. *In vitro* SNX release profiles of Senexin A-loaded graphene (GO-SNX) HA hydrogels. (A) *In vitro* SNX release profiles of GO-SNX HA hydrogels compared to SNX loaded HA hydrogels in first 5 hours of incubation in PBS at 25 ºC. The values expressed are means (n = 3) ± SD. (B) *In vitro* SNX release profiles of GO-SNX HA hydrogels and SNX loaded HA hydrogels for 5 days in PBS at 37 ºC. The values expressed are means (n = 3) ± SD. (C) *In vitro* cumulative release profile of SNX from GO-SNX HA hydrogels and SNX-loaded HA hydrogels calculated from Figure (B). The values expressed are means (n = 3) ± SD. (D) Influence of the loading ratio of GO:SNX (1:3, 1:1, and 4:1) on *in vitro* SNX release profiles of GO-SNX HA hydrogels in PBS at 25 ºC. The values expressed are means (n = 3) ± SD.

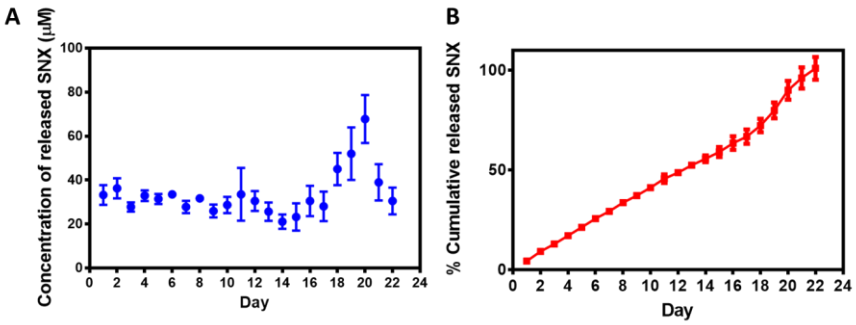

Figure 5.8. *In vitro* SNX release profiles of GO-SNX (4:1) HA hydrogels. (A) *In vitro* SNX release profiles of GO-SNX HA hydrogels using 4:1 loading ratio of GO:SNX in PBS at 37 ºC. The values expressed are means (n = 3) ± SD. (B) The cumulative release profile of SNX from GO-SNX HA hydrogels shown in (A). The values expressed are means (n = 3) ± SD.

المنارة للاستشارات
www.manaraa.com

To describe the possible controlled release mechanisms and estimate SNX release rate constant from the GO-SNX HA hydrogels, the release kinetics of SNX from the systems were analyzed using different kinetic models for controlled drug delivery systems, including zero order, first order, and Higuchi model equations.[42] As shown in Figure 5.9, 5.10 and Table 5.2, it obviously confirmed that the release of SNX form HA and GO-HA hydrogels were not followed by neither zero order nor Higuchi kinetic model. First-order release kinetic model was the best fit for the SNX release from HA and GO-SNX HA hydrogels (R^2 ~ 0.95-0.98). It refers that the SNX release rate depends on its concentration in the hydrogel scaffold. Korsmeyer-Peppas model was further used to confirm the exact release mechanism. This kinetic model is widely used for study the release mechanism from complex polymeric systems.[43] As shown in Eq (4), the mechanism of drug release from Korsmeyer-Peppas model is indicated by the release exponent (n). Namely, the case of $n \leq 0.45$ corresponds to a Fickian diffusion (diffusion-controlled drug release), $0.45 < n < 0.89$ corresponds to a non-Fickian transport (refers to the combination of diffusion and erosion controlled rate release), $n = 0.89$ corresponds to Case II transport (erosion-controlled drug release), and $n > 0.89$ corresponds to super case II transport mechanism. The relationship of the n values from fitting data of the SNX release from GO-SNX HA hydrogels and loading ratio of GO:SNX incorporated in the hydrogels was observed. The higher ratio of GO:SNX (more SNX loaded to GO) incorporated into hydrogels, the less n values observed from fitting data to Korsmeyer-Peppas model. Specifically, the n values from fitting data of the SNX release from GO-SNX HA (4:1) hydrogels were equal to 0.5445, which refers to the combination of diffusion and erosion controlled rate release mechanism. Meanwhile, the n values from the fitting data of the SNX release from GO-

المنارة للاستشارات
www.manaraa.com

SNX HA (1:1), and GO-SNX HA (1:3) hydrogels decreased to 0.3678, and 0.2764, respectively, matching to diffusion-controlled rate release mechanism.

Using these mathematical kinetic models, it could simplify that the SNX release were mainly driven by diffusion and erosion and depended on SNX concentration loaded to GO. Due to the fact that HA generally remains stable under physiological pH and temperature, and undergo dissolution in the aqueous medium due to solvent penetration effect, swelling, and polymer chain disentanglement and relaxation.[44] Thus, solute transport from HA-based material systems could be driven by diffusion and/or dissolution. Likewise, HA is a biodegradable polymer which can be degraded under extreme pH and temperature, various proteins, cells, and enzymes.[45] As a result, the drug release from HA systems could be also forced by erosion. More importantly, the SNX release rate is depended on drug loading concentration which refers to loading ratio of GO:SNX. Due to the interaction between the SNX and GO components, the SNX release rate could be retarded by GO from the material systems.

Table 5.2. Correlation coefficient (R^2), rate constant (K), and release exponent (n) values obtained by fitting the data of the release of SNX from different hydrogel formulations into PBS at pH 7.4.

Formulation	Zero order		First order		Higuchi		Korsmeyer-Peppas	
	K_0	R^2	K_1	R^2	K_h	R^2	n	R^2
SNX-HA	1.322	0.5094	0.389	0.9867	0.1162	0.7867	0.5461	0.9433
GO-SNX-HA (1:3)	1.435	0.5566	0.240	0.9722	0.1211	0.8169	0.2764	0.9455
GO-SNX-HA (1:1)	1.504	0.6493	0.237	0.9852	0.1223	0.8843	0.3678	0.9500
GO-SNX-HA (1:4)	1.5719	0.7615	0.228	0.9492	0.1223	0.9382	0.5445	0.9053

المنارة للاستشارات
www.manaraa.com

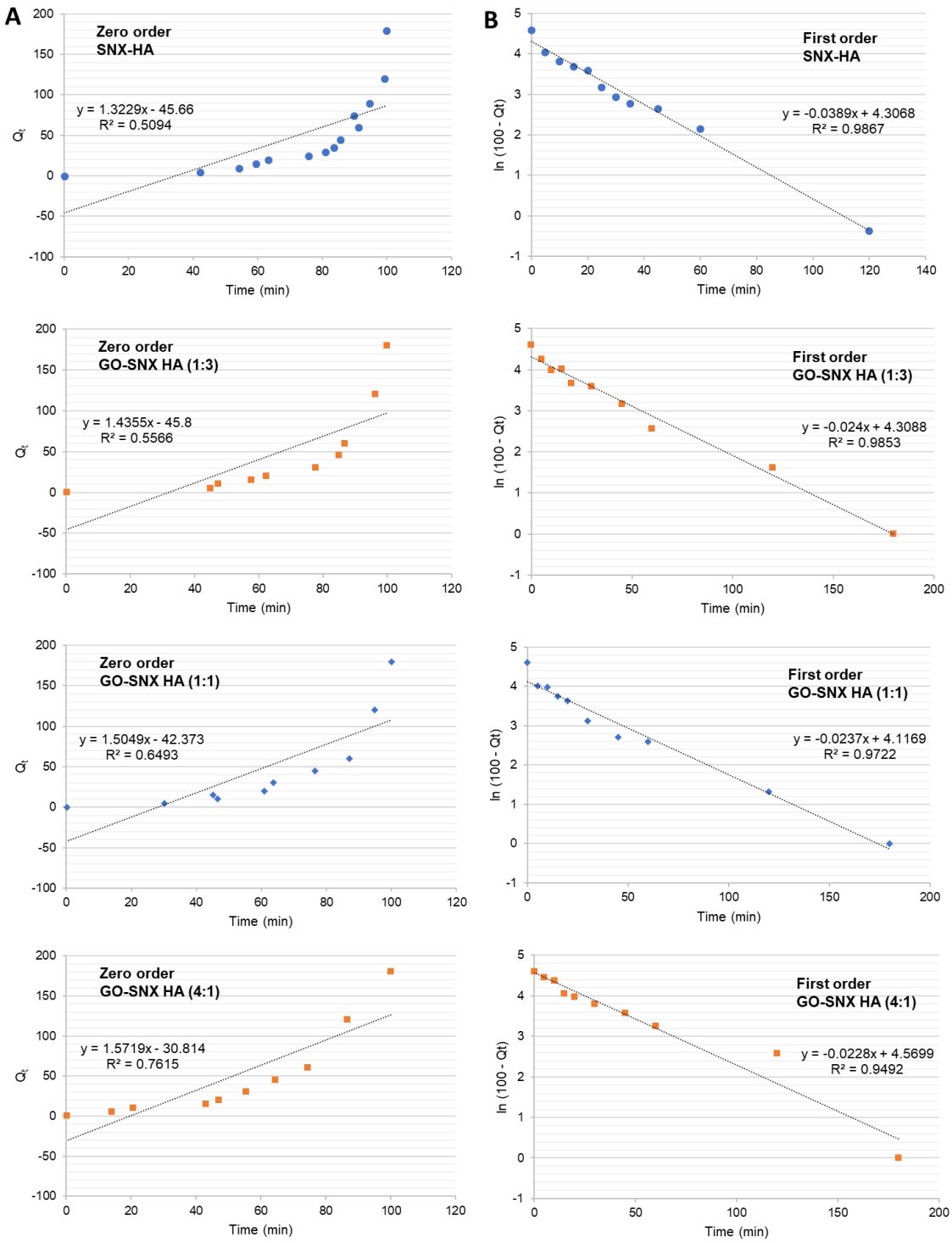

Figure 5.9. Fitting of the data for SNX release from the SNX loaded HA hydrogels (SNX-HA) and GO-SNX HA hydrogels having different loading ratio of GO:SNX (1:3, 1:1, and 4:1) into PBS (pH 7.4) to the zero order (A) and first order kinetics (B).

المنارة للاستشارات
www.manaraa.com

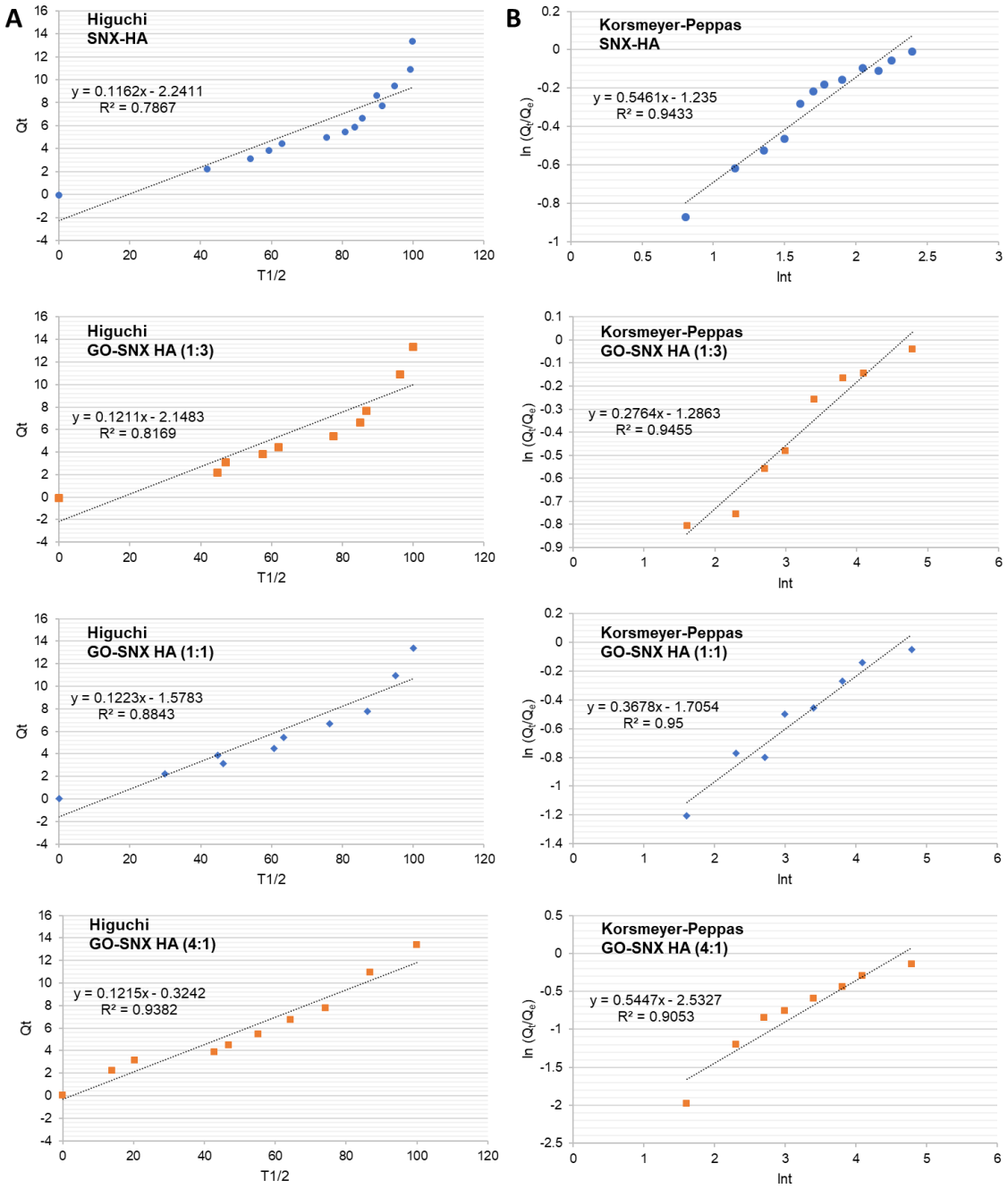

Figure 5.10. Fitting of the data for SNX release from the SNX loaded HA hydrogels (SNX-HA) and GO-SNX HA hydrogels having different loading ratio of GO:SNX (1:3, 1:1, and 4:1) into PBS (pH 7.4) to the Higuchi release model (A) and Korsmeyer-Peppas release model (B).

المنارة للاستشارات
www.manaraa.com

5.2.4 In Vitro Cytocompatibility and Efficacy of Senexin A-Loaded Graphene HA Hydrogels

Cytotoxicity is one of the most important properties of biomaterials for drug delivery, we thus investigated the cytotoxicity of our prepared SNX-GO HA hydrogels. It is satisfying to find that after incubation for 1 and 3 days, the incorporation of GO-SNX HA hydrogels showed no cytotoxicity compared to the control 2D cells based on Celltiter-Blue assays (Figure 5.11A, B). However, the *in vitro* long-term effects of the materials, particularly the effects of GO, should be considered in the future study. Previously, the interaction between dispersed graphene or GO sheets and lung epithelial cells, fibroblasts and neuronal cells has been studied in monolayer cultures. It was reported that single-layer GO sheets were internalized and sequestered in cytoplasmic, membrane bound vacuoles by human lung epithelial or fibroblast cells. and induced toxicity at doses above 20 μg/mL after 24 h. Additionally, GO and pristine graphene are both recognized to be ingested by macrophages, inducing cell activation and secretion of pro-inflammatory cytokines.[46-49] These effects were reported to be depended on the geometry of the used graphene. The larger flakes (approximately 2 μm) provoked a significantly increased secretion of inflammatory cytokines by macrophages *in vitro* compared to the smaller flakes (approximately 350 nm).[50] Therefore, the further optimization of GO lateral sizes for long term safety of GO-SNX HA hydrogels should be our next step of the development.

المنارة للاستشارات
www.manaraa.com

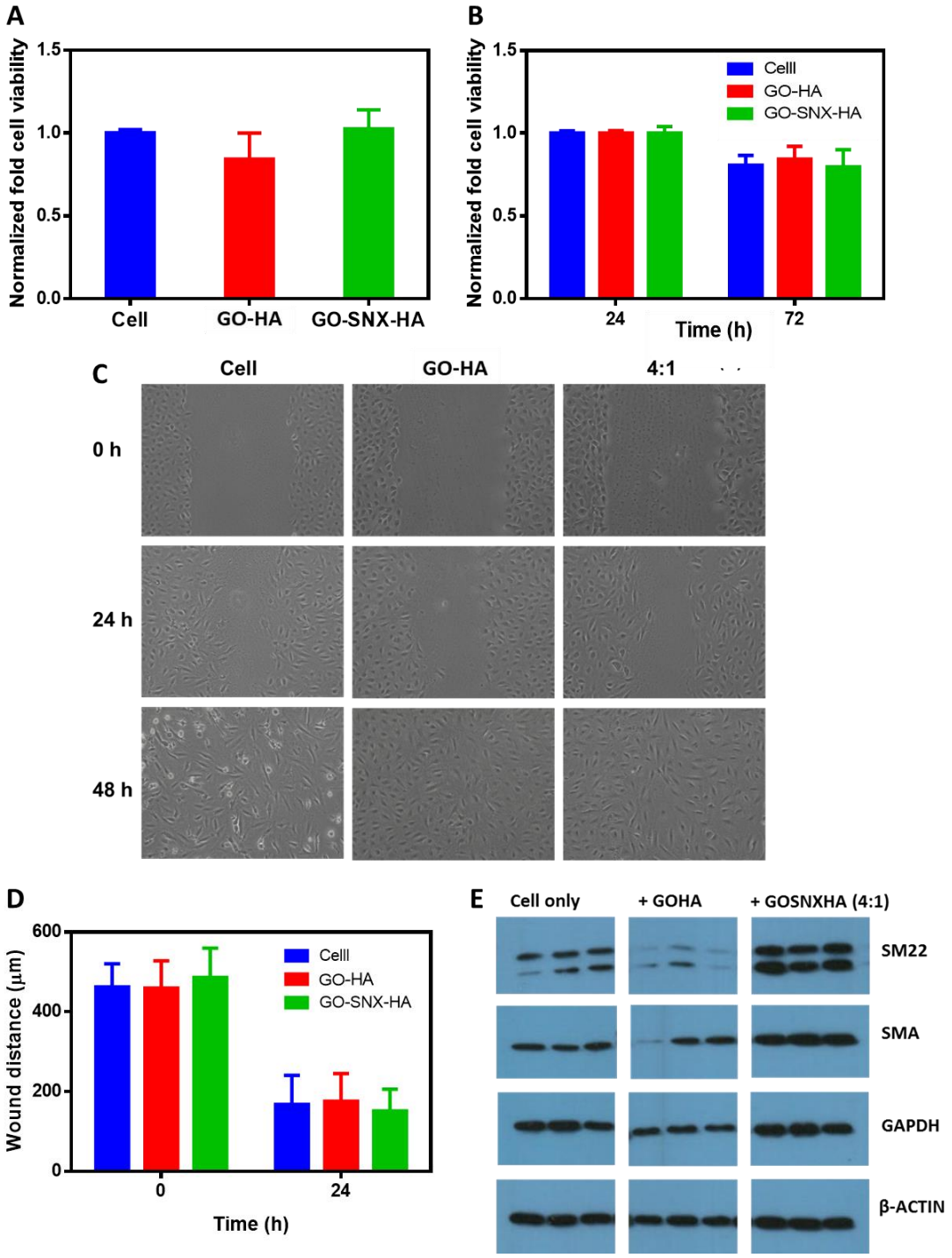

Figure 5.11. *In vitro* cytocompatibility and efficacy of Senexin A-loaded graphene HA hydrogels. (A) Cell viability of VSMCs after culturing in primary media with GO-HA hydrogels or GO-SNX HA hydrogels or without any hydrogel for 24 h using Celltiter-Blue assay. The data was normalized to the cell viability intensity of 2D cell culture (positive control). The values expressed are means ± SD, n = 3 with two repeated experiments. (B) Cell proliferation of VSMCs after culturing in DMEM media with 2% FBS for 24 and 72

المنارة للاستشارات
www.manaraa.com

h using Celltiter-Blue assay. The data was normalized to the cell viability intensity after 24 h culturing of each sample. The values expressed are means ± SD, $n = 3$ with two repeated experiments (C) Analysis of VSMC migration by *in vitro* scratch assay after culturing with GO-HA hydrogels or GO-SNX HA hydrogels or without any hydrogel until confluency. Images were acquired at 0, 24, and 48 h after incubation in DMEM media with 2% FBS using phase-contrast microscope. (D) Average wound distances of the scratch closures from (C) measured by Infinity Analyze software. The values expressed are means ± SD, $n = 4$, with 72 reading of distance for three repeated experiments. (E) Western blot analysis showed the expression of smooth muscle-specific SM22, alpha-smooth muscle actin (α-SMA) GAPDH and β-actin protein in VSMCs after treatment in serum-free medium for 48 h and later in complete medium with GO-HA hydrogels or GO-SNX HA hydrogels or without any hydrogel for 24 h, $n = 3$ with two repeated experiments.

The efficacy of GO-SNX HA hydrogels for suppression of neointima was evaluated by observing their impacts on proliferation, migration, dedifferentiation of VSMCs. Due to the fact that, during the graft occlusion process, VSMCs of "contractile" phenotype commonly migrate to the lumen of the graft and transform to a "synthetic" phenotype, proliferating and secreting ECM proteins to form a neointima.[51] The disappearance of SMC phenotype proteins is generally taken as characteristic of the synthetic phenotype of VSMCs, which could be observed in the dedifferentiation process of VMSCs.[52,53] Herein, we hypothesized that the GO-SNX HA hydrogels could suppress the neointima formation in the similar way to the treatment of SNX observed by Cui's research (data not was not shown). As expected, the materials (both GO-HA hydrogels and GO-SNX HA hydrogels) showed no significantly difference in the proliferation and migration of VSMCs compared to culturing without the materials (Figure 5.11A-D). More importantly, the GO-SNX HA hydrogels could successfully inhibit the dedifferentiation of VSMCs after the starvation for 48 h by maintaining the expression of smooth muscle-specific proteins, including SM22 and alpha-smooth muscle actin (α-SMA) (Figure 5.11E). In contrast, without the incorporation of GO-SNX HA hydrogels, the VSMCs expressed significantly lower

المنارة للاستشارات
www.manaraa.com

amount of smooth muscle-specific proteins as the starvation promotes VMSC dedifferentiation.[54,55] The GAPDH and β-actin protein used as the positive controls showed no significantly difference between VSMCs treated with or without the GO-SNX HA hydrogels. However, we observed that the VSMCs treated with GO-HA hydrogels after starvation revealed the lower amount of SM22 and GAPDH compared to the proteins expressed by VSMCs without the hydrogels. It is likely that the materials itself may impact on the dedifferentiation process. Hence, we further observed the impact of each component of the hydrogels, including HA, DTT, and GO, on the cellular protein expressions of the starved VSMCs. As shown in Figure 5.12, the expression of SM22, α-SMA, GAPDH and β-actin proteins significantly depleted only in the starved VSMCs treated with HA components. The result could be explained by the observation from Song *et al*., which found that the overexpression of hyaluronic acid by mouse SMCs promoted the progression of atherosclerosis by modulating SMC phenotypic towards the synthetic phenotype.[56]

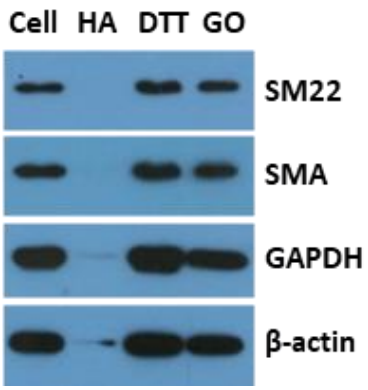

Figure 5.12. Western blot analysis showed the expression of smooth muscle-specific SM22, alpha-smooth muscle actin (α-SMA) GAPDH and β-actin protein in VSMCs after treatment in serum-free medium for 48 h and later in complete medium without or with HA (3 mg/mL) or 0.5M DTT (2μL/mL) or GO (1mg/mL) for 24 h, $n = 3$.

المنارة للاستشارات
www.manaraa.com

Taken together, we found that the hybridized GO-HA hydrogels could be used for prolonged delivery of SNX and provided well efficacy with high biocompatibility. However, in order to use GO-SNX HA hydrogels in real world clinical applications, there are several aspects should be further addressed; first, the *in vivo* efficacy and safety in long-term duration; second, whether the HA system is an ideal to serve as the polymeric system for vessel graft regeneration. Based on our *in vitro* dedifferentiation results, it also suggested us that other systems, such as fibrillar collagen type I, and collagen type IV, may be considered as an alternative for vessel graft regeneration application since they have been shown to promote the contractile phenotype of VSMCs.[57]

5.3 CONCLUSIONS

A GO hybridized HA hydrogel as a perivascular drug delivery wrap was created. The hydrogel could control the release of SNX over 21 days, could be tunable to provide different drug release rates by varying the amount of the loaded drug onto GO into a hydrogel, and was biocompatible and provided well efficacy *in vitro*. The GO hybridized HA construct was found to very flexible and highly attachable to decellularized scaffolds for *in vivo* placement. This study revealed a novel interaction of the of Senexin A with graphene oxide in HA based hydrogels, which could be used for prolonged delivery of aromatic small molecule drugs. The presented GO hybridized HA constructs provide an optimistic outlook for their successful use in perivascular drug delivery system for the local treatment of vascular graft neohyperplasia.

المنارة للاستشارات
www.manaraa.com

5.4 MATERIALS AND METHODS

5.4.1 Preparation of Graphene Oxide Nanosheets

Graphene oxide nanosheets were synthesized following the previous reports.[36,58] Briefly, 1 g of dried graphite flakes (Graphene Supermarket®) was dispersed in 50 mL of concentrated sulfuric acid while stirring at 0 ºC (ice bath). 3 g of potassium permanganate (>99%, Sigma Aldrich) was slowly added into the suspension. After that, the suspension was stirred at room temperature for 25 min and sonicated in ultrasonic bath for 5 min, repeating this stirring and sonication process for 12 cycles. 200 mL of distilled water was then added to quenched the reaction. The suspension was further sonicated for 2 h to obtain graphene oxide nanosheets (GO). Then, the GO was washed following a modified Hummers' method. Briefly, 20 mL of hydrogen peroxide (30%, Merck) was added into the GO suspension while stirring until released gas stopped. 1M hydrochloric acid was used for washing the GO precipitates by centrifugation for 3 times at 10000 rpm for 30 min, and followed by distilled water for 3 times with the same method. The final GO precipitates were dried in the oven at 40 ºC for several days.

5.4.2 Preparation of Drug-Loaded Graphene Oxide

Senexin A (SNX) (1, 2, 3 mg) and GO (1 mg) were added to 3 mL PBS (pH 7.4) (sonicated together for 1 h) and stirred for 20 h at room temperature in darkness. The product (SNX-GO) was collected by repeated centrifugation at 12000 rpm 5 min and washing with PBS until the supernatant became color free. The resulted SNX-GO was freeze-dried. The amount of unbound SNX was determined by measuring the absorbance

المنارة للاستشارات
www.manaraa.com

at 323 nm relative to a calibration curve recorded under identical conditions, allowing the drug loading efficiency to be estimated.

To quantify free SNX, the centrifuged solution was collected and diluted to 100 mL with deionized water in a flask. The amount of free SNX was determined by a UV–VIS spectrometer at wavelength of 323 nm. The SNX-loading efficiency was calculated as follows:

$$\text{SNX-loading efficiency \%} = 100\ (W_{feedSNX} - W_{freeSNX}) / W_{feedSNX}$$

5.4.3 Characterization of Graphene Oxide and Drug-Loaded Graphene Oxide.

GO and SNX-GO were characterized by UV−vis spectrophotometry (Nanodrop 2000), Fourier transform infrared (FTIR) (Spectrum-GX, PerkinElmer), Scanning Electron Microscope (Zeiss Ultraplus Thermal Field Emission SEM).

5.4.4 Formation of Drug-Loaded Graphene HA hydrogels

Prior to formation of the SNX-loaded GO HA hydrogels, methacrylated modified HA polymer at approximately 50% modification (50DM MeHA) was firstly synthesized following our previous reports.[59,60] The SNX-GO was dispersed in the medium (PBS or DMEM) at 0.1% w/v by sonication for 2 h. The 50DM MeHA was then added into the GO-SNX suspension at concentration of 3%. After the polymer completely dissolved in GO-SNX mixture, 0.5 M DTT was added into the mixture to form the hydrogel.

المنارة للاستشارات
www.manaraa.com

5.4.5 Gelation Test

The hydrogels were prepared previously described by using PBS as the medium. The gelation time was measured by the vial tilting method.[61] When the sample showed no flow within 20 s, it was considered as being completely formed hydrogel.

5.4.6 Mechanical Test

Complex modulus of the SNX-loaded GO HA hydrogels was performed using a DHR-3 rheometer (TA instrument) with 12 mm diameter parallel-plate geometry and temperature controlled Peltier plate. The hydrogels were prepared previously described by using DMEM as the medium. After gelation, the samples were cut into uniform cylinders and placed on a metal plate, where the tests were performed. Amplitude sweeps at constant frequency (1 rad/s) were performed to determine the linear viscoelastic range of deformation for each sample, after which frequency sweeps (0.1-10 rad/s) were performed at a strain amplitude within the linear range (1%). In amplitude and frequency sweeps measurement, the geometry gaps were conditioned by axial force at 0.2 N for every run.

5.4.7 Attachment of Senexin A-Loaded Graphene HA Hydrogels on Decellularized Scaffolds

The preformed GO HA or GO-SNX HA hydrogels (after preparation for 10 min) at 10 μL was used to coat around the decellularized vessel scaffolds. The images were taken after incubation in PBS for 20 min and 1 day at 4 ºC.

المنارة للاستشارات
www.manaraa.com

5.4.8 In Vitro Drug Release

Constructs were incubated at 37 °C with gentle shaking in 96-well plate with 100 μL of release DMEM medium. Sample medium was removed and replaced daily (every 24 h) at equal volume. The release profile of SNX from the GO-HA hydrogels was performed. The content of the released Senexin A in the withdrawn medium was determined by UV-vis spectra. The drug release was conducted for 21 days. Before performing UV-vis absorption experiments, a standard curve of Senexin A concentration versus absorption peak intensity (at 323 nm) will be established.

5.4.9 Release Kinetics of Senexin A from Drug-Loaded Graphene HA Hydrogels

Constructs were incubated at 25 °C in 96-well plate with 100 μL of PBS. Sample medium was collected at 5 μL for performing UV-vis, and replaced back to the well plate at different time points (5, 10 15, 20, 30, 45, 60, 90, 120, 180 min, and 24 h). The release kinetics of SNX from the systems were analyzed using different kinetic models for controlled drug delivery systems, including zero order, first order, Higuchi, and Korsmeyer-Peppas model equations:[42]

Zero-order release model:	$Q_t = K_0\, t$	Eq (1)
First-order release model:	$\ln (100 - Q_t) = \ln 100 - K_1 t$	Eq (2)
Higuchi release model:	$Q_t = K_h\, t^{1/2}$	Eq (3)
Korsmeyer-Peppas model:	$Q_t/Q_e = K\, t^n$	Eq (4)

where Q_t is the percentage of drug released at time t; Q_t/Q_e is the fraction of the SNX released at time t; K_0, K_1, K_h and K represent the zero-order release kinetic constant, the first-order release kinetic constant, the Higuchi release kinetic constant and the Korsmeyer-

المنارة للاستشارات
www.manaraa.com

Peppas kinetic constant incorporating structural and geometric characteristics of the hydrogel, respectively; and n is the release exponent, indicative of the mechanism of drug release. Namely, the case of $n \leq 0.45$ corresponds to a Fickian diffusion (diffusion-controlled drug release; the rate of release is independent of the drug concentration in the hydrogels.), $0.45 < n < 0.89$ to a non-Fickian transport, $n = 0.89$ to Case II transport (erosion-controlled drug release), and $n > 0.89$ to super case II transport mechanism. When determining the n exponent, only the portions of the release curve where $M_t \leq 60\%$ were used.

5.4.10 Vascular Smooth Muscle Cell (VSMC) Isolations and Cultures

Briefly, the aortic arch and root (1.5 cm in length) from male 8-week-old C57BL/6J mice were removed. After aortic isolation, vessel was cleaned of any connective tissue by gently scraping with forceps. After, the aorta was enzymatically digested for 10 min at 37 ^{o}C with 7.5 mg collagenase type 2 (Worthington) in 5.5 mL GibcoTM DMEM High Glucose containing 10% fetal bovine serum (FBS). Stopped digestion with cold 10% FBS DMEM High Glucose, then stripped the adventitia from the aorta under microscope. Cut the media into small pieces, digested with rocking, and filtered (for 70 min). Cells in the filtrate were pelleted at 300g for 8 minutes, then rinsed in DMEM High Glucose containing 20% FBS, penicillin (100 U/mL) and streptomycin (100 mg/mL). Cells were cultured and incubated for 6-7 days. Medium was changed every 2 days. After first passage, the mouse VSMCs were then maintained in DMEM High Glucose supplemented with 20% FBS, penicillin and streptomycin at 37 ^{o}C in a humidified atmosphere with 5% CO_2.

المنارة للاستشارات
www.manaraa.com

5.4.11 In Vitro Cytocompatibility for Senexin A-Loaded Graphene HA Hydrogels

CellTiter-Blue (CTB) cell viability assay (Promega) was performed after 1 day of culturing VSMCs on 96-well plate with SNX-Loaded GO HA Hydrogels or GO-HA hydrogels or without any hydrogels. The culture media in each well was replaced by 200 mL of prewarmed media containing 15% CTB and incubated for 2 h at 37 °C and 5% CO_2. The media containing CTB without cells was used as negative controls. The media containing metabolite of CTB was measured for fluorescence intensity at 560/590 nm (Ex/Em) using SpectraMax M2Multi-Mode microplate reader (Molecular Devices).

5.4.12 In Vitro Efficacy Test for Senexin A-Loaded Graphene HA Hydrogels

5.4.12.1 Proliferation of VSMCs

Proliferation of VSMCs was firstly performed to test the efficacy of the hydrogels by CTB cell viability assay after culturing with the hydrogels for 3 days in DMEM media with 2% FBS supplement. The proliferation of VSMCs was quantified by normalization their fluorescence intensities at 560/590 nm to their intensities after 24 h (n= *3* with two repeated experiments).

5.4.12.2 Migration of VSMCs

Migration of VSMCs was determined by *in vitro* scratch assay following the previous protocol.[62] Briefly, VSMCs were seeded on 24-well plate at 50,000 cells per well in 1 mL of complete growth medium with GO-HA hydrogels, or GO-SNX HA hydrogels, or without any hydrogels, and cultured them until confluency. The cells were then scrape in a straight line with a sterile p200 pipet tip. The debris was removed by washing the cells

المنارة للاستشارات
www.manaraa.com

once with 1 mL of the growth medium and them replace with 1 mL of DMEM with 2% FBS supplement. After 0, 24 and 48 h of incubation, the straight line was randomly imaged under phase-contrast microscope (Olympus CKX41) for 6 images per well (n= *4* with three repeated experiments). The images were further analyzed quantitatively by using Infinity Analyze software. Each image, the distances between one side of scratch and the other were measured at certain intervals (µm) for 3 readings.

5.4.12.3 Dedifferentiation of VSMCs

Dedifferentiation of VSMCs was also studied to access the efficacy of the hydrogels. VSMCs were seeded on 24-well plate at 10,000 cells per well in 1 mL of complete growth medium, and cultured until confluency. After that, the medium in each well was replaced with serum-free DMEM medium to starve the cells for 48 h. The starved VSMCs were then incubated in complete growth medium with GO-HA hydrogels, or GO-SNX HA hydrogels, or without any hydrogels for 24 h. Total protein extracted from different batches of cultured VSMCs were lysed with ice-cold RIPA lysis buffer (Alfa Aesar), agitated for 1 h on ice, then centrifuged at 14,000× g at 4 ºC for 15 min, and the supernatant was collected and aliquoted. The protein concentration was determined with a Lowry assay kit according to the manufacturer's instructions (Bio-rad). Equal amounts of total protein (30–50 µg) were subjected to SDS/PAGE under reducing conditions and then electrotransferred to polyvinylidene difluoride membrane (Millipore). The efficacy of protein loading and transfer to membranes was also assessed by Ponceau S staining. The membranes were blocked with 5% nonfat milk (Bio-rad) in Tris-Buffered Saline-0.05% Tween 20 (TBST) for 1 hour at room temperature and incubated with primary antibody against SM22, SMA, GAPDH, or β-actin overnight at 4 ºC, then incubated with a

المنارة للاستشارات
www.manaraa.com

horseradish peroxidase conjugated secondary antibody (1:5000) for 1h at room temperature. Blots were visualized using SuperSignal® West Femto Maximum Sensitivity Substrate (Pierce) and CL-XPosure™ Film (Pierce).

المنارة للاستشارات
www.manaraa.com

5.5 REFERENCES

(1) Luo, Y.; Kirker, K. R.; Prestwich, G. D. Cross-Linked Hyaluronic Acid Hydrogel Films: New Biomaterials for Drug Delivery. *J. Controlled Release* **2000,** *69*, 169-184.

(2) Hoare, T. R.; Kohane, D. S. Hydrogels in Drug Delivery: Progress and Challenges. *Polymer* **2008,** *49*, 1993-2007.

(3) Mayol, L.; Quaglia, F.; Borzacchiello, A.; Ambrosio, L.; La Rotonda, M. I. A Novel Poloxamers/Hyaluronic Acid in Situ Forming Hydrogel for Drug Delivery: Rheological, Mucoadhesive and in Vitro Release Properties. *Eur. J. Pharm. Biopharm.* **2008,** *70*, 199-206.

(4) Prestwich, G. D. Hyaluronic Acid-Based Clinical Biomaterials Derived for Cell and Molecule Delivery in Regenerative Medicine. *Journal of controlled release : official journal of the Controlled Release Society* **2011,** *155*, 193-199.

(5) Xu, X.; Jha, A. K.; Harrington, D. A.; Farach-Carson, M. C.; Jia, X. Hyaluronic Acid-Based Hydrogels: From a Natural Polysaccharide to Complex Networks. *Soft matter* **2012,** *8*, 3280-3294.

(6) Fu, S.; Xiao, X.; Dong, H.; Zhang, Z.; Zhang, X.; Zhong, Z.; Zhuo, R. An Injectable Hyaluronic Acid/Peg Hydrogel Produced Via Copper-Free Click Chemistry for Drug Delivery. *J. Controlled Release* **2017,** *259*, e123-e124.

(7) Singh, B. N.; Kim, K. H. Floating Drug Delivery Systems: An Approach to Oral Controlled Drug Delivery Via Gastric Retention. *J. Controlled Release* **2000,** *63*, 235-259.

(8) Nasongkla, N.; Bey, E.; Ren, J.; Ai, H.; Khemtong, C.; Guthi, J. S.; Chin, S.-F.; Sherry, A. D.; Boothman, D. A.; Gao, J. Multifunctional Polymeric Micelles as Cancer-Targeted, Mri-Ultrasensitive Drug Delivery Systems. *Nano Lett.* **2006,** *6*, 2427-2430.

المنارة للاستشارات
www.manaraa.com

(9) Wilczewska, A. Z.; Niemirowicz, K.; Markiewicz, K. H.; Car, H. Nanoparticles as Drug Delivery Systems. *Pharmacological Reports* **2012,** *64*, 1020-1037.

(10) Martin-Palma, R. J.; Hernandez-Montelongo, J.; Torres-Costa, V.; Manso-Silvan, M.; Munoz-Noval, A. Nanostructured Porous Silicon-Mediated Drug Delivery. *Expert Opin Drug Deliv* **2014,** *11*, 1273-1283.

(11) Barahuie, F.; Hussein, M. Z.; Fakurazi, S.; Zainal, Z. Development of Drug Delivery Systems Based on Layered Hydroxides for Nanomedicine. *International journal of molecular sciences* **2014,** *15*, 7750-7786.

(12) Langer, R. Drug Delivery. Drugs on Target. *Science* **2001,** *293*, 58-59.

(13) Geim, A. K.; Novoselov, K. S. The Rise of Graphene. *Nat Mater* **2007,** *6*, 183-191.

(14) Kim, K. S.; Zhao, Y.; Jang, H.; Lee, S. Y.; Kim, J. M.; Ahn, J. H.; Kim, P.; Choi, J. Y.; Hong, B. H. Large-Scale Pattern Growth of Graphene Films for Stretchable Transparent Electrodes. *Nature* **2009,** *457*, 706-710.

(15) Service, R. F. Materials Science. Carbon Sheets an Atom Thick Give Rise to Graphene Dreams. *Science* **2009,** *324*, 875-877.

(16) Zhou, X.; Liu, Z. A Scalable, Solution-Phase Processing Route to Graphene Oxide and Graphene Ultralarge Sheets. *Chem Commun (Camb)* **2010,** *46*, 2611-2613.

(17) Pandey, H.; Parashar, V.; Parashar, R.; Prakash, R.; Ramteke, P. W.; Pandey, A. C. Controlled Drug Release Characteristics and Enhanced Antibacterial Effect of Graphene Nanosheets Containing Gentamicin Sulfate. *Nanoscale* **2011,** *3*, 4104-4108.

(18) Miao, W.; Shim, G.; Lee, S.; Choe, Y. S.; Oh, Y. K. Safety and Tumor Tissue Accumulation of Pegylated Graphene Oxide Nanosheets for Co-Delivery of Anticancer Drug and Photosensitizer. *Biomaterials* **2013,** *34*, 3402-3410.

المنارة للاستشارات
www.manaraa.com

(19) Liu, Z.; Robinson, J. T.; Sun, X.; Dai, H. Pegylated Nanographene Oxide for Delivery of Water-Insoluble Cancer Drugs. *J. Am. Chem. Soc.* **2008,** *130*, 10876-10877.

(20) Yang, K.; Wan, J.; Zhang, S.; Zhang, Y.; Lee, S.-T.; Liu, Z. In Vivo Pharmacokinetics, Long-Term Biodistribution, and Toxicology of Pegylated Graphene in Mice. *ACS Nano* **2011,** *5*, 516-522.

(21) Yang, Y.; Zhang, Y.-M.; Chen, Y.; Zhao, D.; Chen, J.-T.; Liu, Y. Construction of a Graphene Oxide Based Noncovalent Multiple Nanosupramolecular Assembly as a Scaffold for Drug Delivery. *Chemistry – A European Journal* **2012,** *18*, 4208-4215.

(22) Zhang, L.; Wang, Z.; Xu, C.; Li, Y.; Gao, J.; Wang, W.; Liu, Y. High Strength Graphene Oxide/Polyvinyl Alcohol Composite Hydrogels. *J. Mater. Chem.* **2011,** *21*, 10399-10406.

(23) Hong, H.; Yang, K.; Zhang, Y.; Engle, J. W.; Feng, L.; Yang, Y.; Nayak, T. R.; Goel, S.; Bean, J.; Theuer, C. P.; Barnhart, T. E.; Liu, Z.; Cai, W. In Vivo Targeting and Imaging of Tumor Vasculature with Radiolabeled, Antibody-Conjugated Nanographene. *ACS Nano* **2012,** *6*, 2361-2370.

(24) Ma, X.; Tao, H.; Yang, K.; Feng, L.; Cheng, L.; Shi, X.; Li, Y.; Guo, L.; Liu, Z. A Functionalized Graphene Oxide-Iron Oxide Nanocomposite for Magnetically Targeted Drug Delivery, Photothermal Therapy, and Magnetic Resonance Imaging. *Nano Research* **2012,** *5*, 199-212.

(25) Harskamp, R. E.; Lopes, R. D.; Baisden, C. E.; de Winter, R. J.; Alexander, J. H. Saphenous Vein Graft Failure after Coronary Artery Bypass Surgery: Pathophysiology, Management, and Future Directions. *Ann. Surg.* **2013,** *257*, 824-833.

المنارة للاستشارات
www.manaraa.com

(26) Klinkert, P.; Post, P. N.; Breslau, P. J.; van Bockel, J. H. Saphenous Vein Versus Ptfe for above-Knee Femoropopliteal Bypass. A Review of the Literature. *Eur. J. Vasc. Endovasc. Surg.* **2004,** *27*, 357-362.

(27) Eslami, M. H.; Gangadharan, S. P.; Belkin, M.; Donaldson, M. C.; Whittemore, A. D.; Conte, M. S. Monocyte Adhesion to Human Vein Grafts: A Marker for Occult Intraoperative Injury? *J. Vasc. Surg.* **2001,** *34*, 923-929.

(28) Burkel, W. E.; Vinter, D. W.; Ford, J. W.; Kahn, R. H.; Graham, L. M.; Stanley, J. C. Sequential Studies of Healing in Endothelial Seeded Vascular Prostheses: Histologic and Ultrastructure Characteristics of Graft Incorporation. *J. Surg. Res.* **1981,** *30*, 305-324.

(29) Haruguchi, H.; Teraoka, S. Intimal Hyperplasia and Hemodynamic Factors in Arterial Bypass and Arteriovenous Grafts: A Review. *J. Artificial Organs* **2003,** *6*, 227-235.

(30) Lemson, M. S.; Tordoir, J. H. M.; Daemen, M. J. A. P.; Kitslaar, P. J. E. H. M. Intimal Hyperplasia in Vascular Grafts. *Eur. J. Vasc. Endovasc. Surg.* **2000,** *19*, 336-350.

(31) Davies, M. G.; Hagen, P. O. Reprinted Article "Pathophysiology of Vein Graft Failure: A Review". *Eur. J. Vasc. Endovasc. Surg.* **2011,** *42*, S19-S29.

(32) FitzGibbon, G. M.; Leach, A. J.; Kafka, H. P.; Keon, W. J. Coronary Bypass Graft Fate: Long-Term Angiographic Study. *J. Am. Coll. Cardiol.* **1991,** *17*, 1075-1080.

(33) Padberg, F. T.; Calligaro, K. D.; Sidawy, A. N. Complications of Arteriovenous Hemodialysis Access: Recognition and Management. *J. Vasc. Surg.* **2008,** *48*, S55-S80.

(34) Zetrenne, E.; McIntosh, B. C.; McRae, M. H.; Gusberg, R.; Evans, G. R. D.; Narayan, D. Prosthetic Vascular Graft Infection: A Multi-Center Review of Surgical Management. *The Yale Journal of Biology and Medicine* **2007,** *80*, 113-121.

المنارة للاستشارات
www.manaraa.com

(35) Akhavan, O. The Effect of Heat Treatment on Formation of Graphene Thin Films from Graphene Oxide Nanosheets. *Carbon* **2010,** *48*, 509-519.

(36) Marcano, D. C.; Kosynkin, D. V.; Berlin, J. M.; Sinitskii, A.; Sun, Z.; Slesarev, A.; Alemany, L. B.; Lu, W.; Tour, J. M. Improved Synthesis of Graphene Oxide. *ACS Nano* **2010,** *4*, 4806-4814.

(37) Gurunathan, S.; Han, J. W.; Kim, E. S.; Park, J. H.; Kim, J.-H. Reduction of Graphene Oxide by Resveratrol: A Novel and Simple Biological Method for the Synthesis of an Effective Anticancer Nanotherapeutic Molecule. *International Journal of Nanomedicine* **2015,** *10*, 2951-2969.

(38) Barahuie, F.; Saifullah, B.; Dorniani, D.; Fakurazi, S.; Karthivashan, G.; Hussein, M. Z.; Elfghi, F. M. Graphene Oxide as a Nanocarrier for Controlled Release and Targeted Delivery of an Anticancer Active Agent, Chlorogenic Acid. *Materials Science and Engineering: C* **2017,** *74*, 177-185.

(39) Wang, H.; Gu, W.; Xiao, N.; Ye, L.; Xu, Q. Chlorotoxin-Conjugated Graphene Oxide for Targeted Delivery of an Anticancer Drug. *International Journal of Nanomedicine* **2014,** *9*, 1433.

(40) Depan, D.; Shah, J.; Misra, R. Controlled Release of Drug from Folate-Decorated and Graphene Mediated Drug Delivery System: Synthesis, Loading Efficiency, and Drug Release Response. *Materials Science and Engineering: C* **2011,** *31*, 1305-1312.

(41) Lv, Y.; Tao, L.; Bligh, S. A.; Yang, H.; Pan, Q.; Zhu, L. Targeted Delivery and Controlled Release of Doxorubicin into Cancer Cells Using a Multifunctional Graphene Oxide. *Materials Science and Engineering: C* **2016,** *59*, 652-660.

المنارة للاستشارات
www.manaraa.com

(42) Dash, S.; Murthy, P. N.; Nath, L.; Chowdhury, P. Kinetic Modeling on Drug Release from Controlled Drug Delivery Systems. *Acta Pol. Pharm.* **2010,** *67*, 217-223.

(43) Korsmeyer, R. W.; Gurny, R.; Doelker, E.; Buri, P.; Peppas, N. A. Mechanisms of Solute Release from Porous Hydrophilic Polymers. *Int. J. Pharm.* **1983,** *15*, 25-35.

(44) Bonacucina, G.; Cespi, M.; Palmieri, G. F. Evaluation of Dissolution Kinetics of Hydrophilic Polymers by Use of Acoustic Spectroscopy. *Int. J. Pharm.* **2009,** *377*, 153-158.

(45) Siepmann, J.; Göpferich, A. Mathematical Modeling of Bioerodible, Polymeric Drug Delivery Systems. *Adv. Drug Del. Rev.* **2001,** *48*, 229-247.

(46) Girish, C. M.; Sasidharan, A.; Gowd, G. S.; Nair, S.; Koyakutty, M. Confocal Raman Imaging Study Showing Macrophage Mediated Biodegradation of Graphene in Vivo. *Advanced Healthcare Materials* **2013,** *2*, 1489-1500.

(47) Chen, G.-Y.; Yang, H.-J.; Lu, C.-H.; Chao, Y.-C.; Hwang, S.-M.; Chen, C.-L.; Lo, K.-W.; Sung, L.-Y.; Luo, W.-Y.; Tuan, H.-Y.; Hu, Y.-C. Simultaneous Induction of Autophagy and Toll-Like Receptor Signaling Pathways by Graphene Oxide. *Biomaterials* **2012,** *33*, 6559-6569.

(48) Zhou, H.; Zhao, K.; Li, W.; Yang, N.; Liu, Y.; Chen, C.; Wei, T. The Interactions between Pristine Graphene and Macrophages and the Production of Cytokines/Chemokines Via Tlr- and Nf-Kb-Related Signaling Pathways. *Biomaterials* **2012,** *33*, 6933-6942.

(49) Russier, J.; Treossi, E.; Scarsi, A.; Perrozzi, F.; Dumortier, H.; Ottaviano, L.; Meneghetti, M.; Palermo, V.; Bianco, A. Evidencing the Mask Effect of Graphene Oxide:

المنارة للاستشارات
www.manaraa.com

A Comparative Study on Primary Human and Murine Phagocytic Cells. *Nanoscale* **2013,** *5*, 11234-11247.

(50) Yue, H.; Wei, W.; Yue, Z.; Wang, B.; Luo, N.; Gao, Y.; Ma, D.; Ma, G.; Su, Z. The Role of the Lateral Dimension of Graphene Oxide in the Regulation of Cellular Responses. *Biomaterials* **2012,** *33*, 4013-4021.

(51) Tsui, J. C. S.; Dashwood, M. R. Recent Strategies to Reduce Vein Graft Occlusion: A Need to Limit the Effect of Vascular Damage. *Eur. J. Vasc. Endovasc. Surg.* **2002,** *23*, 202-208.

(52) Christen, T.; Bochaton-Piallat, M.-L.; Neuville, P.; Rensen, S.; Redard, M.; van Eys, G.; Gabbiani, G. Cultured Porcine Coronary Artery Smooth Muscle Cells. *A New Model With Advanced Differentiation* **1999,** *85*, 99-107.

(53) Rensen, S. S. M.; Doevendans, P.; van Eys, G. Regulation and Characteristics of Vascular Smooth Muscle Cell Phenotypic Diversity. *Netherlands Heart Journal* **2007,** *15*, 100-108.

(54) Wanjare, M.; Kuo, F.; Gerecht, S. Derivation and Maturation of Synthetic and Contractile Vascular Smooth Muscle Cells from Human Pluripotent Stem Cells. *Cardiovasc. Res.* **2013,** *97*, 321-330.

(55) Davis-Dusenbery, B. N.; Wu, C.; Hata, A. Micro-Managing Vascular Smooth Muscle Cell Differentiation and Phenotypic Modulation. *Arterioscler. Thromb. Vasc. Biol.* **2011,** *31*, 2370-2377.

(56) Chai, S.; Chai, Q.; Danielsen, C. C.; Hjorth, P.; Nyengaard, J. R.; Ledet, T.; Yamaguchi, Y.; Rasmussen, L. M.; Wogensen, L. Overexpression of Hyaluronan in the Tunica Media Promotes the Development of Atherosclerosis. *Circ. Res.* **2005,** *96*, 583-591.

المنارة للاستشارات
www.manaraa.com

(57) Thyberg, J.; Hultgardh-Nilsson, A. Fibronectin and the Basement Membrane Components Laminin and Collagen Type Iv Influence the Phenotypic Properties of Subcultured Rat Aortic Smooth Muscle Cells Differently. *Cell Tissue Res.* **1994,** *276*, 263-271.

(58) Yu, H.; Zhang, B.; Bulin, C.; Li, R.; Xing, R. High-Efficient Synthesis of Graphene Oxide Based on Improved Hummers Method. *Scientific reports* **2016,** *6*, 36143.

(59) Maturavongsadit, P.; Bi, X.; Metavarayuth, K.; Luckanagul, J. A.; Wang, Q. Influence of Cross-Linkers on the in Vitro Chondrogenesis of Mesenchymal Stem Cells in Hyaluronic Acid Hydrogels. *ACS applied materials & interfaces* **2016**.

(60) Maturavongsadit, P.; Luckanagul, J. A.; Metavarayuth, K.; Zhao, X.; Chen, L.; Lin, Y.; Wang, Q. Promotion of in Vitro Chondrogenesis of Mesenchymal Stem Cells Using in Situ Hyaluronic Hydrogel Functionalized with Rod-Like Viral Nanoparticles. *Biomacromolecules* **2016,** *17*, 1930-1938.

(61) Hiemstra, C.; Zhou, W.; Zhong, Z.; Wouters, M.; Feijen, J. Rapidly in Situ Forming Biodegradable Robust Hydrogels by Combining Stereocomplexation and Photopolymerization. *J. Am. Chem. Soc.* **2007,** *129*, 9918-9926.

(62) Liang, C.-C.; Park, A. Y.; Guan, J.-L. In Vitro Scratch Assay: A Convenient and Inexpensive Method for Analysis of Cell Migration in Vitro. *Nat. Protocols* **2007,** *2*, 329-333.

المنارة للاستشارات
www.manaraa.com

APPENDIX A – COPYRIGHT CLEARANCE FOR CHAPTER 1 AND 2

Copyright Clearance Center RightsLink®

Home | Account Info | Help

ACS Publications
Most Trusted. Most Cited. Most Read.

Title: Promotion of In Vitro Chondrogenesis of Mesenchymal Stem Cells Using In Situ Hyaluronic Hydrogel Functionalized with Rod-Like Viral Nanoparticles

Author: Panita Maturavongsadit, Jittima Amie Luckanagul, Kamolrat Metavarayuth, et al

Publication: Biomacromolecules

Publisher: American Chemical Society

Date: Jun 1, 2016

Copyright © 2016, American Chemical Society

Logged in as:
Panita Maturavongsadit
LOGOUT

PERMISSION/LICENSE IS GRANTED FOR YOUR ORDER AT NO CHARGE

This type of permission/license, instead of the standard Terms & Conditions, is sent to you because no fee is being charged for your order. Please note the following:

- Permission is granted for your request in both print and electronic formats, and translations.
- If figures and/or tables were requested, they may be adapted or used in part.
- Please print this page for your records and send a copy of it to your publisher/graduate school.
- Appropriate credit for the requested material should be given as follows: "Reprinted (adapted) with permission from (COMPLETE REFERENCE CITATION). Copyright (YEAR) American Chemical Society." Insert appropriate information in place of the capitalized words.
- One-time permission is granted only for the use specified in your request. No additional uses are granted (such as derivative works or other editions). For any other uses, please submit a new request.

المنارة للاستشارات
www.manaraa.com

APPENDIX B – COPYRIGHT CLEARANCE FOR FIGURE 1.2

Copyright Clearance Center RightsLink®

Home | Account Info | Help

Title: A plant virus substrate induces early upregulation of BMP2 for rapid bone formation
Author: Pongkwan Sitasuwan,L. Andrew Lee,Peng Bo,Erin N. Davis,Yuan Lin,Qian Wang
Publication: Integrative Biology
Publisher: Royal Society of Chemistry
Date: Mar 27, 2012
Copyright © 2012, Royal Society of Chemistry

Logged in as:
Panita Maturavongsadit
Account #:
3001168418
LOGOUT

Order Completed

Thank you for your order.

This Agreement between Ms. Panita Maturavongsadit ("You") and Royal Society of Chemistry ("Royal Society of Chemistry") consists of your license details and the terms and conditions provided by Royal Society of Chemistry and Copyright Clearance Center.

Your confirmation email will contain your order number for future reference.

Printable details.

License Number	4183171261545
License date	Sep 06, 2017
Licensed Content Publisher	Royal Society of Chemistry
Licensed Content Publication	Integrative Biology
Licensed Content Title	A plant virus substrate induces early upregulation of BMP2 for rapid bone formation
Licensed Content Author	Pongkwan Sitasuwan,L. Andrew Lee,Peng Bo,Erin N. Davis,Yuan Lin,Qian Wang
Licensed Content Date	Mar 27, 2012
Licensed Content Volume	4
Licensed Content Issue	6
Type of Use	Thesis/Dissertation
Requestor type	academic/educational
Portion	figures/tables/images
Number of figures/tables/images	2
Distribution quantity	4
Format	print and electronic
Will you be translating?	no
Order reference number	
Title of the thesis/dissertation	THE DEVELOPMENT OF NOVEL HYBRIDIZED BIOMATERIALS FOR APPLICATIONS IN TISSUE ENGINEERING AND TARGETED DRUG DELIVERY
Expected completion date	Dec 2017
Estimated size	170
Requestor Location	Ms. Panita Maturavongsadit 631 Sumter St. COLUMBIA, SC 29208 United States Attn: Ms. Panita Maturavongsadit
Billing Type	Invoice
Billing address	Ms. Panita Maturavongsadit 631 Sumter St. COLUMBIA, SC 29208 United States Attn: Ms. Panita Maturavongsadit
Total	0.00 USD

ORDER MORE | CLOSE WINDOW

Copyright © 2017 Copyright Clearance Center, Inc. All Rights Reserved. Privacy statement. Terms and Conditions.
Comments? We would like to hear from you. E-mail us at customercare@copyright.com

المنارة للاستشارات
www.manaraa.com

APPENDIX C – COPYRIGHT CLEARANCE FOR FIGURE 1.3

Copyright Clearance Center RightsLink®

Home | Account Info | Help

ACS Publications
Most Trusted. Most Cited. Most Read.

Title: Porous Alginate Hydrogel Functionalized with Virus as Three-Dimensional Scaffolds for Bone Differentiation
Author: Jittima Luckanagul, L. Andrew Lee, Quyen L. Nguyen, et al
Publication: Biomacromolecules
Publisher: American Chemical Society
Date: Dec 1, 2012
Copyright © 2012, American Chemical Society

Logged in as:
Panita Maturavongsadit
Account #:
3001168418
LOGOUT

PERMISSION/LICENSE IS GRANTED FOR YOUR ORDER AT NO CHARGE

This type of permission/license, instead of the standard Terms & Conditions, is sent to you because no fee is being charged for your order. Please note the following:

- Permission is granted for your request in both print and electronic formats, and translations.
- If figures and/or tables were requested, they may be adapted or used in part.
- Please print this page for your records and send a copy of it to your publisher/graduate school.
- Appropriate credit for the requested material should be given as follows: "Reprinted (adapted) with permission from (COMPLETE REFERENCE CITATION). Copyright (YEAR) American Chemical Society." Insert appropriate information in place of the capitalized words.
- One-time permission is granted only for the use specified in your request. No additional uses are granted (such as derivative works or other editions). For any other uses, please submit a new request.

Copyright Clearance Center RightsLink®

Home | Account Info | Help

ACS Publications
Most Trusted. Most Cited. Most Read.

Title: Tobacco Mosaic Virus Functionalized Alginate Hydrogel Scaffolds for Bone Regeneration in Rats with Cranial Defect
Author: Jittima Amie Luckanagul, Kamolrat Metavarayuth, Sheng Feng, et al
Publication: ACS Biomaterials Science & Engineering
Publisher: American Chemical Society
Date: Apr 1, 2016
Copyright © 2016, American Chemical Society

Logged in as:
Panita Maturavongsadit
Account #:
3001168418
LOGOUT

PERMISSION/LICENSE IS GRANTED FOR YOUR ORDER AT NO CHARGE

This type of permission/license, instead of the standard Terms & Conditions, is sent to you because no fee is being charged for your order. Please note the following:

- Permission is granted for your request in both print and electronic formats, and translations.
- If figures and/or tables were requested, they may be adapted or used in part.
- Please print this page for your records and send a copy of it to your publisher/graduate school.
- Appropriate credit for the requested material should be given as follows: "Reprinted (adapted) with permission from (COMPLETE REFERENCE CITATION). Copyright (YEAR) American Chemical Society." Insert appropriate information in place of the capitalized words.
- One-time permission is granted only for the use specified in your request. No additional uses are granted (such as derivative works or other editions). For any other uses, please submit a new request.

المنارة للاستشارات
www.manaraa.com

APPENDIX D – COPYRIGHT CLEARANCE FOR CHAPTER 3 AND 4

Copyright Clearance Center RightsLink®

Home | Account Info | Help

ACS Publications
Most Trusted. Most Cited. Most Read.

Title: Influence of Cross-Linkers on the in Vitro Chondrogenesis of Mesenchymal Stem Cells in Hyaluronic Acid Hydrogels

Author: Panita Maturavongsadit, Xiangdong Bi, Kamolrat Metavarayuth, et al

Publication: Applied Materials

Publisher: American Chemical Society

Date: Feb 1, 2017

Copyright © 2017, American Chemical Society

Logged in as:
Panita Maturavongsadit
LOGOUT

PERMISSION/LICENSE IS GRANTED FOR YOUR ORDER AT NO CHARGE

This type of permission/license, instead of the standard Terms & Conditions, is sent to you because no fee is being charged for your order. Please note the following:

- Permission is granted for your request in both print and electronic formats, and translations.
- If figures and/or tables were requested, they may be adapted or used in part.
- Please print this page for your records and send a copy of it to your publisher/graduate school.
- Appropriate credit for the requested material should be given as follows: "Reprinted (adapted) with permission from (COMPLETE REFERENCE CITATION). Copyright (YEAR) American Chemical Society." Insert appropriate information in place of the capitalized words.
- One-time permission is granted only for the use specified in your request. No additional uses are granted (such as derivative works or other editions). For any other uses, please submit a new request.

المنارة للاستشارات
www.manaraa.com

APPENDIX E – COPYRIGHT CLEARANCE FOR FIGURE 3.2

Copyright Clearance Center RightsLink®

Home | Account Info | Help

Title: Adhesive peptides conjugated PAMAM dendrimer as a coating polymeric material enhancing cell responses

Author: Panita Maturavongsadit,Xiangdong Bi,Togor A. Gado,Yu-Zhe Nie,Qian Wang

Publication: Chinese Chemical Letters

Publisher: Elsevier

Date: September 2016

© 2016 Qian Wang. Published by Elsevier B.V. on behalf of Chinese Chemical Society and Institute of Materia Medica, Chinese Academy of Medical Sciences. All rights reserved.

Logged in as:
Panita Maturavongsadit
Account #:
3001168418
LOGOUT

Order Completed

Thank you for your order.

This Agreement between Ms. Panita Maturavongsadit ("You") and Elsevier ("Elsevier") consists of your license details and the terms and conditions provided by Elsevier and Copyright Clearance Center.

Your confirmation email will contain your order number for future reference.

Printable details.

License Number	4165950860599
License date	Aug 11, 2017
Licensed Content Publisher	Elsevier
Licensed Content Publication	Chinese Chemical Letters
Licensed Content Title	Adhesive peptides conjugated PAMAM dendrimer as a coating polymeric material enhancing cell responses
Licensed Content Author	Panita Maturavongsadit,Xiangdong Bi,Togor A. Gado,Yu-Zhe Nie,Qian Wang
Licensed Content Date	Sep 1, 2016
Licensed Content Volume	27
Licensed Content Issue	9
Licensed Content Pages	6
Type of Use	reuse in a thesis/dissertation
Portion	figures/tables/illustrations
Number of figures/tables/illustrations	4
Format	both print and electronic
Are you the author of this Elsevier article?	Yes
Will you be translating?	No
Original figure numbers	figure 1, 2, 3, scheme 1
Title of your thesis/dissertation	THE DEVELOPMENT OF NOVEL HYBRIDIZED BIOMATERIALS FOR APPLICATIONS IN TISSUE ENGINEERING AND TARGETED DRUG DELIVERY
Expected completion date	Dec 2017
Estimated size (number of pages)	170
Requestor Location	Ms. Panita Maturavongsadit 631 Sumter St. COLUMBIA, SC 29208 United States Attn: Ms. Panita Maturavongsadit
Publisher Tax ID	98-0397604
Total	0.00 USD

ORDER MORE | CLOSE WINDOW

Copyright © 2017 Copyright Clearance Center, Inc. All Rights Reserved. Privacy statement. Terms and Conditions.
Comments? We would like to hear from you. E-mail us at customercare@copyright.com

المنارة للاستشارات
www.manaraa.com

APPENDIX F – THE DEVELOPMENT OF GRAPHENE-FET NANOSENSOR FOR SMALL-MOLECULE DETECTION

This present work was a part of collaborive research with Dr. Qiao Lin, Columbia University (New York), Department of Mechanical Engineering.

1.1 INTRODUCTION

Single layer graphene (SLG), a layer of carbon atoms bonded together in a hexagonal honeycomb lattice, is emerging as an attractive functional nanomaterial in chemical and biological sensors. Previously, we have functionalized SLG bonded on a field effect transistor (FET) nanosensor with a boronic acid-derivatized pyrene via π-π interaction for glucose recognition. The sensors could effectively measure glucose concentration in a practically relevant range of 2 μM to 25 mM through the changes in the electric conductance of graphene which observed by the shifts of transfer characteristics.[1] Inspired by this work, we hypothesized that the change in electronic transfer properties of graphene is strongly related to the types and sizes of functional groups, density of modification, and the pH of the environment. Modification of graphene with the appropiate functional groups at high density will create a higher sentivity of graphene-FET nanosensors for glucose and other small molecule detection.

Herein, two strategies for molecular functionalization of SLG, including non-covalent and covalent modification, were applied to understand the effect of functionalized molecules and their densities on charge transfer characteristics, which is the key

المنارة للاستشارات
www.manaraa.com

consideration for improving the sensitivity of FET devices. For the non-covalent strategy, we used pyrene derivatives carrying different electron withdrawing/donating functional groups to interact with the graphene via π-π interaction. The different length sizes of functional groups of pyrene derivatives were also used to interact with the graphene in order to study the effect of functional group sizes on the sensitivity of charge transfer characteristics (Figure 1) The different electron withdrawing/donating aryl radicals was also colvantly functionalized on the SLG by electrografting method. The different controllable densities of functional aryl groups were also created by varying the amount of electro-reaction cycles (Figure 2). The shifts of charge transfer characteristics from these different modified functional group SLG on FET devices will be observed.

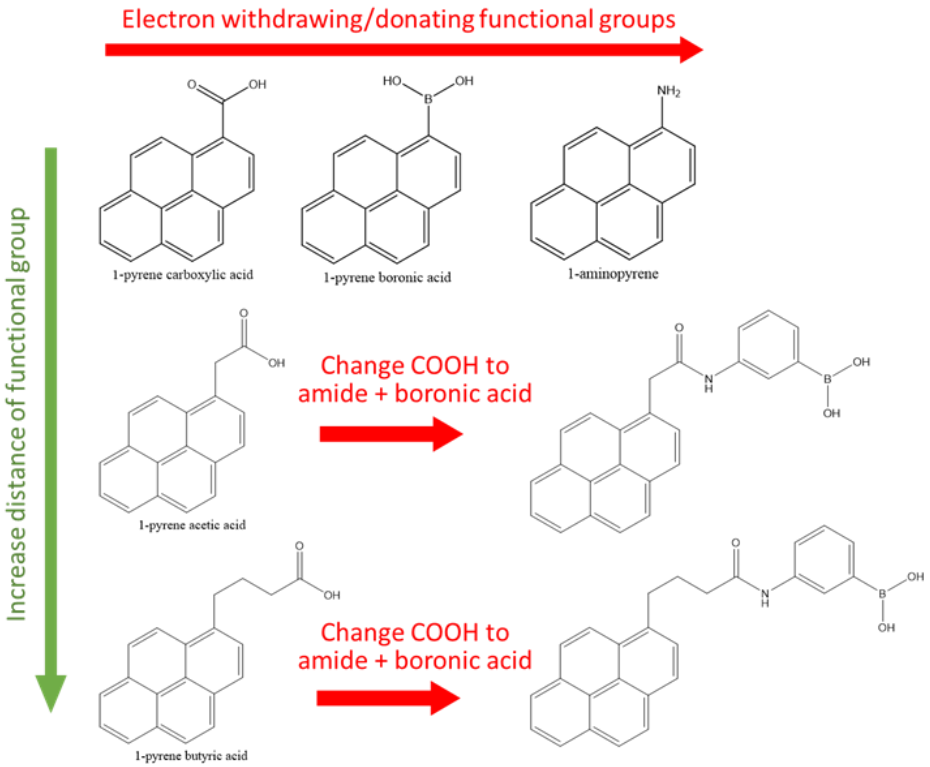

Figure F.1. The schematic illustration of the non-covalent strategy to functionalize single layer graphene to improve the sensitivity of the detection. The pyrene derivatives carrying different electron withdrawing/donating functional groups and different length sizes were interacted to the graphene via π-π interaction.

المنارة للاستشارات
www.manaraa.com

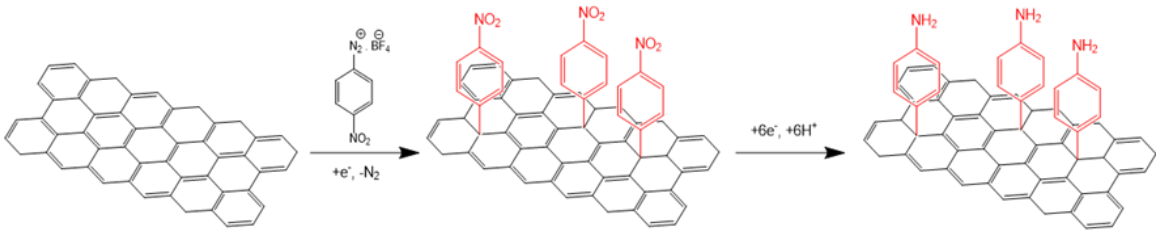

Figure F.2. The schematic illustration of the covalent strategy to functionalize single layer graphene to improve the sensitivity of the detection. The electrografting of different functionalized aryl radicals at different densities was used to covalently modify the single layer graphene.

1.2 RESULTS AND DISCUSSION

Based on our previous report, the recognition of glucose by a graphene-based affinity nanosensor was due to the formation of glucose-boronate ester, which could reduce the boronic acid-induced p-type doping in the graphene.[1] In particular, at pH 7.4, most of the pyrene boronic acid motifs remain neutral as a sp^2 hybridized electron configuration (the pK_a of pyrene boronic acid ($pK_{a\text{-}acid}$) was reported approximately 8.8.[2]). Upon anchoring on the surface of graphene, the empty *p*-orbital of boron will offer a strong electron withdrawing effect to deprive the electrons from graphene, resulting in a strong *p*-doping effect. When glucose molecules are introduced in the system, pyrene boronate esters will be formed which favors the equilibrium towards a sp^3 hybridization (Figure 3B).[3,4] As such, the boron atom no longer exhibits an empty *p*-orbital; instead, it becomes an electron rich sp^3 configuration, leading to a profound *n*-doping effect on the graphene upon glucose binding. We believe that the sensitivity of doping effect alteration on this graphene devices can be improved or modified by changing the functional motifs. Specifically, introduction of strongly electron withdrawing/donating groups at high density on graphene-FET devices, creating a strongly *p*-doping/*n*-doping effects, may enhance the

المنارة للاستشارات
www.manaraa.com

responsiveness after binding to the detected molecules compared to introduction of weaky or neutral functional groups at low density.

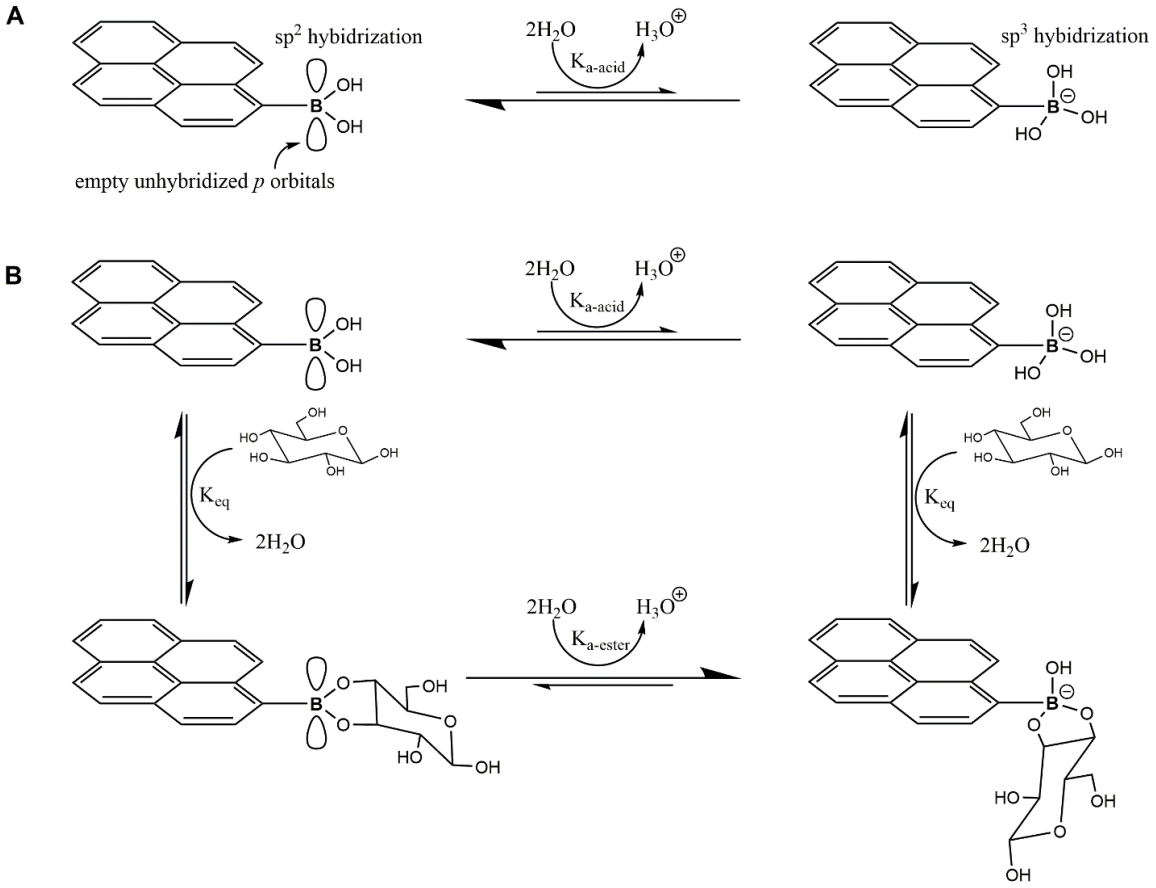

Figure F.3. (A) The relationships between sp^2 and sp^3 pyrene boronic acid in 0.10 M phosphate buffer (pH 7.4). $K_{a\text{-}acid}$ is the dissociation constant of pyrene boronic acid. (B) Boronate ester formation and the relationships between pyrene boronic acids and their boronate esters in 0.10 M phosphate buffer (pH 7.4) with glucose. K_{eq} is the association constant of boronate ester. $K_{a\text{-}ester}$ is the dissociation constant of pyrene boronate-glucose ester.

Here we report the sucessfully modification of strong electron withdrawing and donating aryls (nitro- and amino- aryls, repectively) onto SLG via electrografting method. First, SLGs grown via a chemical vapor deposition (CVD) process were transferred onto silicon substrates using a nondestructive polymer-mediated (PMMA) transfer technique.[5]

المنارة للاستشارات
www.manaraa.com

Cyclic voltammetry (CV) experiments were performed in an electrolytic cell containing 2 mM of (4-nitrophenyl) diazonium tetrafluoroborate (NDTB) in 0.1 M H_2SO_4 solution by using SLGs as the working electrode with the aid of Cu metal (as shown in Figure 4). A broad irreversible wave located at − 0.2 V (vs. Ag/AgCl) was observed at a scan rate of 0.2 V/s which indicated that nitrophenyl groups were grafted to the surface of SLGs. When the CV performed at range of 1 V – (-1)V, the additional broad irriversible wave at − 0.5 V (vs. Ag/AgCl) was observed. This wave corresponds to the reduction of nitro group to amino groups which confirmed that aminophenyl groups were created to the surface of SLGs.. The atomic force microscopy (AFM) was further used to prove the formation of a compact nitro-/ amino-phenyl layer. The AFM image revealed an obvious differences between pristine and modified SLGs (Figure 6A). The surface modification was calculated based on Faraday's law. By integration of the electrochemical current from data in Figure 5A and B, a surface concentration of grafted nitrophenyl and aminophenyl groups was approximately 2-4 × 10^{-8} mol/cm^2 (Figure 5C, D).

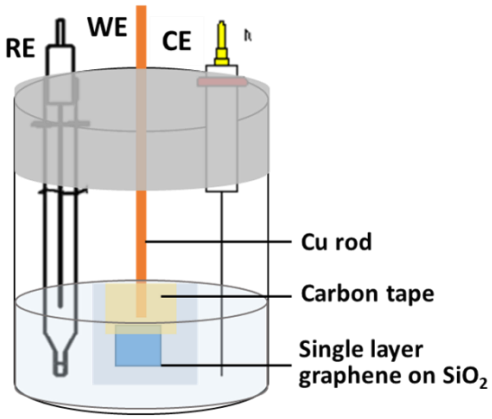

Figure F.4. The electrolytic cell used for diazonium electrografting of graphenes. WE represents working electrode (SLG) ; CE represents counter electrode (Pt) ; RE represents reference electrode (Ag/AgCl).

المنارة للاستشارات
www.manaraa.com

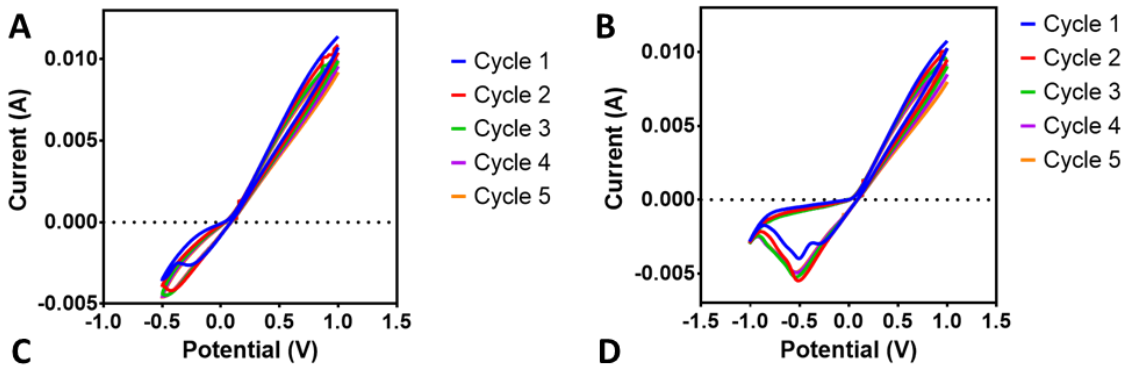

Gr-NO_2(-0.5V)	Cycle 1	Cycle 2	Cycle 3	Cycle 4	Cycle 5
q	0.0009238	0.00115	0.001196	0.001211	0.00122
n	7	7	7	7	7
F	96485.33	96485.33	96485.33	96485.33	96485.33
A	0.30	0.30	0.30	0.30	0.30
Γ	4.5593E-09	5.68E-09	5.9E-09	5.98E-09	6.02E-09
total Γ	2.8136E-08 mol/cm²				

Gr-NH_2(-1V)	Cycle 1	Cycle 2	Cycle 3	Cycle 4	Cycle 5
q	0.001605	0.002055	0.002129	0.002058	0.002026
n	7	7	7	7	7
F	96485.33	96485.33	96485.33	96485.33	96485.33
A	0.35	0.35	0.35	0.35	0.35
Γ	6.78965E-09	8.69E-09	9.01E-09	8.71E-09	8.57E-09
total Γ	4.17659E-08 mol/cm²				

Figure F.5. Characterization of the modification of the functional groups on single layer graphene. A, C) The cyclic voltammogram and surface coverage calculation of nitro aryl modified graphene. B, D) The cyclic voltammogram and surface coverage calculation of amino aryl modified graphene.

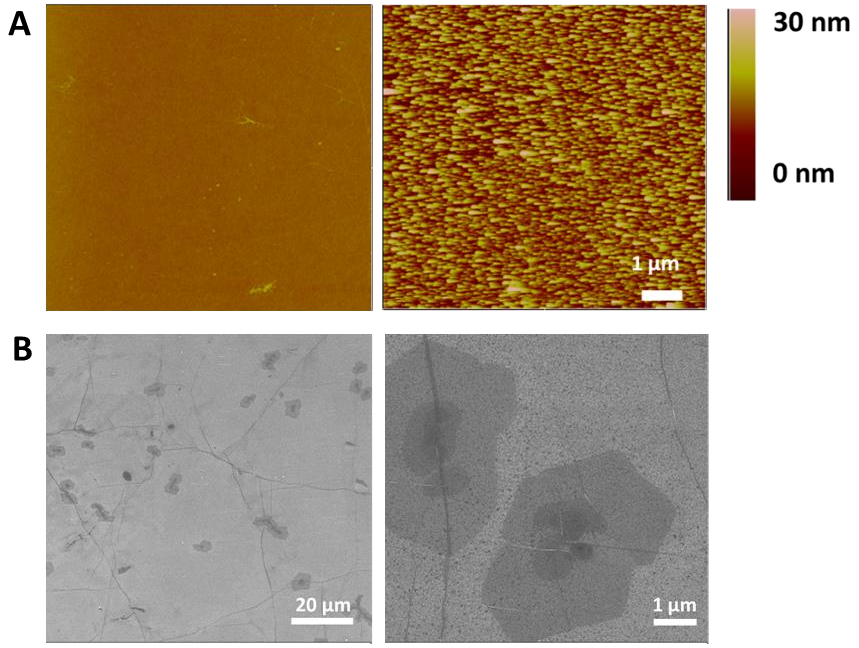

Figure F.6. Surface characterization of the modified single layer graphene (right) compared to the non-modified single layer graphene (left) by AFM (A) and SEM (B).

المنارة للاستشارات
www.manaraa.com

1.3 FUTURE DIRECTIONS

To further confirm the successful diazonium electrografting of graphenes, raman spectroscopy and X-ray photoelectron spectroscopy (XPS) studies should be used to characterize the modified graphene surfaces. The study of the doping effect and responsiveness of the resulted graphene-based affinity nanosensors will be the next step of the experiments. We expect that the *p*- and *n*-doping effect will be observed from -0.5V samples (NO_2 group) and -1V samples (NH_2 group), repectively. The higher surface coverage of the modifed aryls will provide higher sensitity of the detection.

1.4 MATERIALS AND METHODS

1.4.1 Modification of Single Layer Graphene by Electrografting Method

The graphene sheets (0.5 × 0.5 cm) on SiO_2 wafer as the working electrode was immersed into the electrochemical cell. The platinum (Pt) was used as a counter electrode, and Ag/AgCl was used as a reference electrode. The electrolyte solution containing 2 mM of (4-nitrophenyl) diazonium tetrafluoroborate (NDTB) in 0.1 M H_2SO_4 solution was added in the cell at volume of 15 cm^3. Prior to performing the electrochemical reactions, the system was purged by a stream of nitrogen gas for 10 min to remove any trace of air or oxygen in the cell. Voltammetric measurements were performed using CHI 660A electrochemical workstation ll. The cyclic voltammograms (1V – (-1)V and 1V – (-0.5V)) were observed at a scan rate of 0.2 V/s and room temperature.

المنارة للاستشارات
www.manaraa.com

1.4.2 Characterization of the Modified Single Layer Graphene

After the electrochemical reactions, the modified SLGs were prepared for characterization by rinsing with abundant amounts of de-ionized (DI) water three times to completely remove diazonium salts that had been physically absorbed onto the graphene surface. After that, atomic force microscopic (AFM) images were performed using a Nanoscope IIIA Scanning Probe Microscope with silicon cantilevers in the tapping mode. Scanning Electron microscope (SEM) images of the modified SLGs were also obtained by Zeiss Ultraplus Thermal Field Emission SEM at 5 kV.

1.4.3 Calculation for the Modified Surface Concentration

The surface concentration was calculated following this equation;

$$\Gamma = q/nFA$$

Where q = charge of the peak [C], n = number of electrons involved in the redox process, F = Faraday constant [C/mol], A = area of the electrode [cm^2], Γ = surface concentration on the electrode [mol/cm^2].[6]

1.5 REFERENCES

(1) Zhu, Y.; Hao, Y.; Adogla, E. A.; Yan, J.; Li, D.; Xu, K.; Wang, Q.; Hone, J.; Lin, Q. A Graphene-Based Affinity Nanosensor for Detection of Low-Charge and Low-Molecular-Weight Molecules. *Nanoscale* **2016,** *8*, 5815-5819.

(2) Lerner, M. B.; Kybert, N.; Mendoza, R.; Villechenon, R.; Lopez, M. A. B.; Johnson, A. T. C. Scalable, Non-Invasive Glucose Sensor Based on Boronic Acid Functionalized Carbon Nanotube Transistors. *Appl. Phys. Lett.* **2013,** *102*, 183113.

المنارة للاستشارات
www.manaraa.com

(3) Springsteen, G.; Wang, B. A Detailed Examination of Boronic Acid–Diol Complexation. *Tetrahedron* **2002,** *58*, 5291-5300.

(4) Yan, J.; Springsteen, G.; Deeter, S.; Wang, B. The Relationship among Pka, Ph, and Binding Constants in the Interactions between Boronic Acids and Diols—It Is Not as Simple as It Appears. *Tetrahedron* **2004,** *60*, 11205-11209.

(5) Wang, Q.; Guo, X.; Cai, L.; Cao, Y.; Gan, L.; Liu, S.; Wang, Z.; Zhang, H.; Li, L. Tio2-Decorated Graphenes as Efficient Photoswitches with High Oxygen Sensitivity. *Chemical Science* **2011,** *2*, 1860-1864.

(6) Kondo, T.; Kanai, T.; Uosaki, K. Control of the Charge-Transfer Rate at a Gold Electrode Modified with a Self-Assembled Monolayer Containing Ferrocene and Azobenzene by Electro- and Photochemical Structural Conversion of Cis and Trans Forms of the Azobenzene Moiety. *Langmuir* **2001,** *17*, 6317-6324.

المنارة للاستشارات
www.manaraa.com